NASA Technical Paper 1008

Acoustic Performance of Two 1.83-Meter-Diameter Fans Designed for a Wind-Tunnel Drive System

Paul R. Soderman and V. Robert Page

AUGUST 1977

NASA

NASA Technical Paper 1008

Acoustic Performance of Two 1.83-Meter-Diameter Fans Designed for a Wind-Tunnel Drive System

Paul R. Soderman and V. Robert Page

Ames Research Center
and
Ames Directorate,
U.S. Army Air Mobility R&D Laboratory
Moffett Field, California

National Aeronautics
and Space Administration

Scientific and Technical Information Office

1977

SYMBOLS

A	fan area, m^2 (ft^2)
B	number of rotor blades
c	blade chord, m (ft)
D	fan diameter, m (ft)
dBA	A-weighted sound power or sound pressure level
F_n	number of fans
f	frequency, Hz
Δf	analyzer bandwidth, Hz
$\dot{m}$	mass flow rate, kg/sec
N	rotor rotational speed, revolutions per minute (rpm)
$OAPWL$	overall sound power level, dB
PR	fan pressure ratio (total pressure aft of stator divided by atmospheric pressure)
PWL	sound power level relative to 10^{-12} watt, dB
Q	$1 - R^3$
q	dynamic pressure, N/m^2 (lb/ft^2)
R	hub-tip ratio
r	observer distance, m (ft)
SPL	sound pressure level relative to 2×10^{-5} N/m^2, dB
St	Strouhal number
T	fan thrust, N (lbf)
t	blade thickness, m (ft)
V	air speed, m/sec (ft/sec)
W	acoustic power, watts
x	Qf/N

α	angle of attack at 3/4 radius, deg (see fig. 2)
ξ	stagger angle at 3/4 radius, deg (see fig. 2)
ϕ	swirl angle behind rotor, deg (see fig. 2)

Subscripts

1	small scale or initial speed
2	large scale or final speed
ℓ	local condition in duct
m	mean condition over duct cross section
sb	standard blade
tip	blade tip

ACOUSTIC PERFORMANCE OF TWO 1.83-METER-DIAMETER FANS DESIGNED FOR A WIND-TUNNEL DRIVE SYSTEM

Paul T. Soderman and V. Robert Page

Ames Research Center
and
Ames Directorate, USAAMRDL

SUMMARY

A parametric study was made of the noise generated by two 1.83-m (6-ft) diameter fans operating up to a maximum pressure ratio of 1.03. One fan had 15 rotor blades, 23 stator blades, and a maximum rotational speed of 1200 rpm. The other fan had 9 rotor blades, 13 stator blades, and a maximum speed of 2000 rpm. The fans were approximately 1/7-scale models of the 12.2-m (40-ft) diameter fans proposed for repowering the NASA-Ames 40- by 80-Foot Wind Tunnel. The fans were operated individually in a 23.8-m (78-ft) long duct. Sound pressure levels in the duct were used to determine radiated acoustic power as fan speed, blade angle, and mass flow were varied. Appropriate pressures were measured for the computation of fan thrust, mass-flow rate, and steady-state velocity distributions. Inflow conditions were altered by various flow distortion devices and honeycomb.

Results showed that the low-speed fan was slightly quieter than the high-speed fan and, when scaled to full scale, would be 16 dB quieter than the present wind-tunnel fans. The fan noise varied directly with thrust regardless of whether thrust was varied by rotational speed or blade setting for the ranges studied.

INTRODUCTION

Plans have been made to modify the NASA-Ames 40- by 80-Foot Wind Tunnel (refs. 1,2). A major part of that modification is the replacement of the six 12.2-m (40-ft) diameter fans. The new drive system will have more power than the present system, a total of 1.01×10^5 kW (135,000 hp) compared to 0.27×10^5 kW (36,000 hp), for higher test-section air speeds. The opportunity exists to reduce the fan noise despite the increased power of the new system, because the present fans have several bad features, acoustically (high tip speed; close, upstream struts). Reduced noise levels benefit the community adjacent to the wind tunnel (ref. 2) and acoustic research conducted in the test section (ref. 3). Consequently, considerable effort has been made to design

a quiet fan system. A 1/7-scale test facility was built to study the aerodynamic and acoustic performance of candidate fans for the modified wind tunnel. This report describes the results of parametric studies of the noise of two 1/7-scale fans. Other fans will be evaluated in the future.

MODELS AND APPARATUS

High-Speed Fan

A 1.83-m (6-ft) diameter fan with a maximum tip speed of 192 m/sec (628 ft/sec), which is comparable to the tip speed of the present wind tunnel fans, is described in table 1. The fan had 9 rotor blades and 13 stator blades. Rotor-stator spacing was two rotor chords. Maximum total pressure ratio was 1.028 (total pressure aft of stator divided by atmospheric pressure). The rotor geometry is illustrated in figures 1(a) and (b).

Low-Speed Fan

A 1.83-m (6-ft) diameter fan with a maximum tip speed of 115 m/sec (377 ft/sec) is described in table 1 and figures 1(c) and (d). The fan had 15 rotor blades and 23 stator blades. Rotor-stator spacing was two rotor chords. The maximum pressure ratio was 1.027. Figure 1(e) is a photograph of the fan. Pertinent blade angles for both fans are defined on figure 2.

Both the high-speed and low-speed fan rotor airfoils had the same thickness distribution as listed in table 2.

Fan Duct

The fan-in-duct test facility is shown in figures 3(a) and (b). The duct was square upstream and rectangular downstream of the fan, with transitions that contracted to the circular fan section. The motor center body was supported by two struts, each 76-mm (3-in.) thick and with 0.91-m (3-ft) chords. The motor support strut leading edges were 1.9 m (6.1 ft) aft of the rotor. The mass flow was regulated by varying the exhaust opening (fig. 3(c)). The inlet had a bellmouth. The duct wall construction was 12.7-mm (0.5-in.) plywood at the rectangular sections, 3-mm (0.125-in.) steel at the transitions, and 12.7-mm (0.5-in.) steel at the fan section. The inlet transition from square to circular section is shown in figure 4.

Honeycomb

Aluminum honeycomb material was placed in the inlet between the microphones and fan as shown in figure 3(b). The honeycomb cell structure is shown in figure 5. A wire screen was placed in front of the honeycomb to

protect the fan from foreign-object damage, as shown in figure 6. The honeycomb was removed during selected runs to determine its effect on the fan performance and noise.

Flow Distortion Generators

In addition to the protective screen, multilayers of screen were temporarily placed upstream of the fan, as shown in figure 6. The screens covered the lower half of the duct. An alternate means of distorting the flow was to block 40 percent of the duct area with a wooden barrier, also shown in figure 6.

Acoustic Instrumentation

Four microphones were located in the duct upstream of the fan and four were located downstream at the duct stations shown in figure 3(b). The microphones were mounted on traversing struts. Data samples between 30 and 60 sec long were taken at each of the 36 points in the duct cross sections shown in figure 7(a). Figures 7(b) and (c) are photographs of the microphone/strut configurations in the inlet and exhaust, respectively. B&K 4133, 12.7-mm (0.5-in.) microphones with UA 0386 nose cones were used. The data were recorded on magnetic tape for laboratory spectral analysis.

Aerodynamic Instrumentation

The fan performance was determined from fluid mechanic measurements. Total and static pressure measurements in the duct were used to calculate fan thrust, velocity distortion profile, and mass-flow rate. Directional cobra probes were used to determine flow swirl ahead and behind the fan. No measurements were made of the flow turbulence intensities or scale. Only the pressure rakes (fig. 8) affected fan noise; these rakes were placed directly in front of the fan during certain runs. The rake wakes intersected the fan, causing a substantial noise increase. Details of the aerodynamic data are described in reference 4.

TESTING AND PROCEDURES

With a fan operating at a fixed rotational speed, blade pitch, and mass-flow rate, noise levels were recorded at 36 positions upstream and 36 positions downstream of the fan. In some cases, only 12 positions were sampled at the duct mid-height. The data were analyzed in third-octave bands and integrated over the duct cross section to give sound power levels. Narrowband spectra of sound pressure were generated for selected microphone positions.

Mass-flow rate is given in percent of the design or optimum mass-flow rate for a particular stagger angle. At a stagger angle of 35.4° and a

rotational speed of 1200 rpm, the design mass-flow rate was 163 kg/sec (359 lbm/sec). The data are presented for 100 percent mass-flow rate and 1200 rpm fan speed unless noted otherwise on the figures.

Accuracy

The accuracy of a single sound pressure measurement was estimated to be ±0.5 dB. However, the accuracy of the computed sound power levels depended on (1) the variability of the noise levels with time, (2) the variability of noise over the duct cross section, (3) the possibility of nonradiating duct modes influencing the data, (4) the possibility of duct end reflections, (5) the possible masking of fan noise by microphone wind noise, (6) the possible masking of fan noise by throttle noise, and (7) the loss of acoustic power through the duct walls.

A definitive evaluation of each of the above potential effects was not possible. However, the following observations were made for each of the respective effects:

1. The greatest variation of sound pressure tones with time was ±4 dB (inlet honeycomb removed) and ±3 dB (inlet honeycomb installed).

2. The sound power level variation with microphone position was ±3 dB for tones and ±2 dB for broadband noise.

3. Doak (ref. 5) showed that nonpropagating (cutoff) acoustic modes in a duct contribute significantly to integrated mean-square pressures measured within two to four duct radii from the source. Within that distance, there is no simple relationship between the measured sound pressure and the acoustic power propagating away from the fan. However, the implication from Doak's work is that the nonpropagating modes have sufficiently decayed at distances beyond four duct radii to be insignificant compared to the propagating modes. Since the microphones in this study were located seven fan radii upstream and ten radii downstream, it is concluded that the measured sound pressures were direcly related to the propagating acoustic energy.

4. To check the accuracy of the sound power calculations based on sound pressure measurements, a calibrated noise source (ILG Industries fan described in ref. 6) was operated in the fan section. Figure 9 shows that the power calculations were quite accurate above 200 Hz. Below that frequency, the measured power was greater than the free-field levels, probably because of duct end reflections. Therefore, data below 125 Hz were omitted from the results. The lowest frequency of interest, the blade-passage frequency of the fans, varied from 150 Hz to 300 Hz for rotational speeds of 50 percent to 100 percent maximum. (Both fans had the same blade-passage frequency.) Figure 9 also shows that the duct did not inhibit the acoustic power output of the ILG fan. It is assumed that the duct did not inhibit acoustic sources on the 1.8-m (6-ft) fans, although certain spinning modes were cut off, as discussed later.

5. Microphone wind noise is estimated to be over 20 dB below the measured noise levels, as shown in figure 10(a)(inlet) and figure 10(b)(exhaust). The microphone wind noise levels were taken from reference 7, which contains data for a microphone in smooth flow and a microphone in the wake of an aerodynamic body. The smooth flow condition corresponds to the duct inlet microphones; the wake flow corresponds to the exhaust microphones, which were in the wake of the fan-motor center body.

6. The throttle noise can be attributed to the turbulent boundary layer flowing past the trailing edge of the throttle doors. However, estimation of the noise, based on the method of reference 8, indicated that the resulting sound power was much below the measured levels.

7. The loss of acoustic power through the duct walls was negligible compared to the power flowing along the duct axis, as can be inferred from the results of figure 9.

In summary, the time-averaged sound pressure levels integrated over the duct cross sections gave the following sound power accuracies as a function of frequency.

Frequency, Hz	PWL accuracy, dB
125	+4, -0
160 to 200	+3, -1
250 to 400	± 2
500 to 8000	± 1
10,000 to 12,500	± 2

The time-averaged sound pressure levels varied ± 3 dB with microphone position.

RESULTS AND DISCUSSION

High-Speed Fan vs Low-Speed Fan

At equal-thrust operating conditions, the low-speed fan generated less sound power than the high-speed fan did at the fundamental and second harmonic of the blade-passage frequency and at frequencies above 1600 Hz, as shown in figure 11(a). Both fans had the same blade-passage frequency ($f = BN/60$) of 300 Hz. The low-speed fan was noisier at frequencies below 250 Hz.

Also shown on figure 11(a) are predicted sound power levels of these fans (private communication from R. Wells, General Electric Co., Schenectady, N.Y.).

The prediction scheme was based on the following empirical fit to axial fan noise data accumulated from previous studies.

$$PWL(f) = -48.2 - 10 \log[1 + (4.4x)^2] + 10 \log f + 40 \log N + 70 \log D + 10 \log Q + 10 \log F_n \quad (1)$$

(D measured in meters)

Figure 11(a) shows that the predictions bracketed the data of the present study, being too low for the low-speed fan and too high for the high-speed fan.

Figures 11(b) and (c) are typical narrowband spectra of sound pressure levels measured with microphone 3 (inlet) and 7 (exhaust), respectively. The data show that, over most of the spectrum, the low-speed fan generated less tonal noise and less broadband noise than the high-speed fan.

Large-Scale Fan Noise

The data of figure 11(a) were scaled to represent the acoustic power of the six 12.2-m (40-ft) diameter fans described in table 3, which would drive the 40- by 80-foot wind tunnel. The full-scale fans will be housed in circular ducts whose inlets will be 11 m (36 ft) from the rotor and whose exhaust will be 37 m (122 ft) from the rotor. Thus, the acoustic end reflections should have no effect on source sound power. To make the aerodynamic conditions of the large-scale fans similar to the small-scale test conditions, the blade tip speed, angle of attack, and airfoil section must not change. In addition, the size of the small-scale fans was chosen so that the Reynolds number change due to scaling would have no significant effect on the aerodynamic performance of the fan blades. Under those conditions, the acoustic power can be written

$$W = \text{const } V_{tip}^{5.5} D^2 F_n \quad (2)$$

Equation 2 is based on data discussed in a later section, which shows fan noise dependence on $V_{tip}^{5.5}$. The D^2 term comes from the premise that doubling the fan blade area by increasing the span and/or chord doubles the number of acoustic sources and, therefore, the radiated sound power. The term F_n accounts for the number of fans.

To scale from one 1.83-m (6-ft) fan to six 12.2-m (40-ft) fans at the same tip speed, the sound power level increases as follows:

$$\Delta \text{dB} = PWL_2 - PWL_1$$

$$= 10 \log \left(\frac{D_2^2}{D_1^2} F_n \right) = 24.3 \text{ dB} \quad (3)$$

Many empirical prediction schemes lead to the same result given by equation 3 (ref. 2 describes four such empirical formulas). Equation 3 is also valid for scaling the third-octave band levels of the small-scale fan to full-scale as long as the frequencies are shifted.[1] As a first approximation, the frequency ratio f_1/f_2 can be assumed proportional to fan rotational speed. For example, both turbulence-generated broadband noise frequency and vortex shedding rate depend on the Strouhal frequency, $f = StV/\text{chord} = \text{const } ND/\text{chord} = \text{const } N$ (refs. 9,10). Blade-passage noise occurs at frequencies proportional to rotational speed. Thus, the acoustic frequencies of the small-scale and large-scale fans are related as follows:

$$\frac{f_2}{f_1} = \frac{N_2}{N_1} = \frac{V_{tip_2} D_1}{V_{tip_1} D_2} = \frac{D_1}{D_2} = 0.15 \tag{4}$$

Equation 1, which contains several empirical terms necessary for approximating the acoustic spectrum shape, reduces to the same scaling relationship of equation 3 if the above assumptions about frequency dependence are made.

Figure 12 shows small-scale fan data scaled to full scale, using equation 3. The thrust levels on figure 12 were scaled from measured small-scale fan thrust.

$$T_2 = T_1 \frac{A_2}{A_1} \tag{5}$$

The variation of fan noise with operating condition has been determined. Because the high-speed fan model test was limited to only one blade angle and rotational speed, the effect of operating condition is discussed with respect to the low-speed fan only. The present 40- by 80-foot wind tunnel fans have fixed-pitch blades, so test-section speed is varied by changing fan rotational speed. During the study described in reference 11, the fan sound power varied as 50 log N_2/N_1 dB. The replacement fans will be operated by varying blade pitch and rotational speed as shown in figure 13 for the low-speed fans. There will be no restriction on the choice of fan speed or stagger angle to achieve a given test-section speed as long as the power and blade pitch limits are not exceeded. For example, the following sequence could be used: increase fan speed to 10 percent maximum at 105° stagger angle; decrease stagger angle to 65.5° (increases angle of attack); increase fan speed to 100 percent maximum; decrease stagger angle to 43.6°, achieving top speed in the test section. At fixed pitch, the wind-tunnel speed is directly proportional to blade tip speed. Note that above 58 percent maximum test-section speed, the fan must be at 100 percent maximum speed.

[1]No correction for bandwidth is required to shift from one third-octave band to another. A correction is necessary if the data is shifted to say, an octave-band spectrum.

Figure 14(a) shows the resulting noise variation with test-section speed of the present fans and the low-speed fans (full scale). Based on results described in a later section, a low-speed fan noise variation of either 55 log N_2/N_1 dB or -0.5 dB/deg increase in stagger angle was used depending on the mode of operation. The low-speed fans are estimated to be 7 dB quieter than the present fans, with both systems operating at top speed, despite the increase in maximum test-section speed from 100 m/sec to 155 m/sec (328 ft/sec to 509 ft/sec) expected from the new fan system. The acoustic power level of the present 40- by 80-foot wind tunnel fans is quite high because two large, 5.1-m (16.75-ft) chord struts are located immediately upstream of each rotor. The intersection of the strut wakes by the rotor blades is a very effective, but undesirable, source of noise. The low-speed fans will have relatively small stators (0.74-m (2.4 ft) chord when scaled to full scale) located two rotor chords downstream of the rotor.

Figure 14(a) shows that the predicted low-speed fan noise is almost insensitive to the manner in which the fan is operated, whether it be along the 65.5° stagger angle line or along the power and blade pitch limits (see fig. 13). That follows from the fact that the noise decrease due to rpm decrease (55 log N_2/N_1) is almost offset by the noise increase due to pitch change (0.5 dB/deg) necessary to maintain test-section speed. In other words, the low-speed fan noise depends only on test-section speed (approximately) at a rate given by

$$\Delta dB = 55 \log \frac{V_2}{V_1} \tag{6}$$

Figure 14(b) illustrates the noise variation described by equation 6. Note that figure 14(b) is not quite as accurate as figure 14(a) because the noise variation with rpm is not precisely equivalent to the noise variation with pitch change.

Because fan thrust is approximately proportional to test-section speed squared (ref. 12), equation 6 can be written

$$\Delta dB = 27.5 \log \frac{T_2}{T_1} \tag{7}$$

Thus, the wind-tunnel fan noise will vary (approximately) with thrust, irrespective of how that thrust is obtained.

Equation 7 is based on fan operation in a fixed duct system. An attempt was made to investigate the effect of variable duct losses on fan noise. The duct mass-flow rate was throttled 30 percent with the fan rotational speed and stagger angle fixed. However, the noise change was insignificant because the reduction of mass flow caused the blades to begin to stall; and, as discussed in a later section, once the blades begin to stall, the noise remains fairly constant even if the angle of attack increases.

At a given test-section speed, the low-speed fans will be approximately 16 dB quieter than the current fans. Figure 14(c) shows the third-octave band spectra for the two fan systems operating to give a test-section speed of 100 m/sec (q = 6128 N/m^2 (128 lb/ft^2)), which is the maximum speed generated by the present fans. Figure 14(c) represents an equal thrust-operating condition for the two fan systems.

The estimated noise levels of the scaled-up fans shown in figures 12 and 14 are accurate if (a) the acoustic source mechanisms scale with fan size at the rate assumed, and (b) no new sources develop in the full-scale installation. With respect to item (a), it was assumed that the number of uncorrelated acoustic sources would increase directly with an increase in blade area. That should be valid for the broadband noise, which is characteristic of blade interaction with small-scale random turbulence. Doubling the blade span and chord would quadruple the number of sources and quadruple the square of the acoustic pressure, resulting in a 6 dB noise increase (24.3 dB when scaling one 1.8-m fan to six 12.2-m fans). However, certain discrete noise sources, such as rotor-stator interaction, could conceivably increase in size rather than in number, causing the acoustic pressure to increase rather than the square of acoustic pressure. Wright (ref. 9) cites some fan noise data that increased 9 dB with the doubling of blade span and chord. If applicable to the low-speed fan, that would cause the peaks at 50 and 100 Hz on figure 12(a) to increase 8 dB (the higher harmonics of blade-passage frequency would still be dominated by broadband noise). The overall power level would increase 4 dB.

With respect to item (b) above, the acoustic source could change if the scale of turbulence relative to the fan chord is significantly different in the full-scale installation as compared to the small-scale test. Because neither the small-scale test turbulence levels nor the full-scale fan turbulence levels are precisely known, there is a corresponding element of uncertainty in the prediction of the large-scale fan noise. A rough estimate of the uncertainty can be made by comparing the noise levels measured with and without the eight pressure survey rakes placed immediately in front of the fan (fig. 8). Figures 15(a) through (c) show that the blade-wake interaction generated considerable discrete noise — up to 9 dB in third-octave bands and a 4-dB increase in overall power level. It is improbable that the full-scale wind tunnel would generate a vortex or turbulence structure more intense or with more axial length than the wake defects of the pressure rakes. Hence, +4,-0 dB is the estimated error in source noise, and +4,-0 dB is the estimated error in scaling for a total sound power prediction accuracy of +8,-0 dB.

Sound Propagation Upstream vs Downstream

Figure 16 shows that the acoustic power radiating downstream of the fan dominated the total fan sound power. This happened despite the fact that an omnidirectional noise source (ILG fan) in the bottom of the fan section, wind off, radiated 2 to 4 dB more sound power upstream than downstream (the downstream propagation was impeded by the fan-motor center body). Because blade-generated noise has a predominantly dipole directivity (ref. 9), it is

proposed that downstream convection of fan noise by wind accounted for the relatively large levels of noise downstream of the fan. Reference 13 reported that mean flow causes acoustic power at frequencies well above cutoff to be multiplied by $(1 + M)^2$ for downstream waves, and by $(1 - M)^2$ for upstream waves (M = Mach number). The mean flow speed for figure 16 was 70.4 m/sec (231 ft/sec) which corresponds to a Mach number of 0.2. The convection factor

$$\Delta dB = 10 \log \frac{(1 + 0.2)^2}{(1 - 0.2)^2} = 3.5 \text{ dB} \tag{10}$$

is the predicted difference between upstream and downstream sound power. The convection factor accounts for much of the mid- and high-frequency noise differences in figure 16, upstream and downstream. The reason for the dominance of downstream noise at low frequencies is unknown.

The dip in the upstream data from 2 kHz to 3.15 kHz was due to inlet honeycomb sound attenuation. Sound measurements of broadband noise (ILG noise source) with the honeycomb in and out showed 1 to 4 dB insertion loss from 2 kHz to 3.15 kHz with negligible effect at other frequencies.

Figures 17(a) and (b) illustrate the sound power spectra compared to typical sound pressure level spectra in the intake and exhaust, respectively.

Relative Importance of Noise Sources

Tones — Inspection of the low-speed fan data of figures 11(a) to (c) indicates that the broadband noise dominated the third-octave band spectra except at 300 and 600 Hz, which are the fundamental and second harmonics of blade-passage frequency. All the other tones in the narrowband spectra were masked by broadband noise when converted to third-octave bands. Hence, any aeroacoustic mechanisms that generated tones, such as rotor steady-lift rotation or rotor stator interaction, were generally less important than those mechanisms that generated broadband noise.

Estimation of rotor-stator interaction tone noise is difficult to make without some knowledge of the rotor-blade wakes at the stator. An attempt was made to estimate the interaction noise using a postulated wake profile, but the computed sound power levels were 15 dB above the measured levels at the second and fourth harmonic of the blade-passage frequency. In any case, rotor-stator interaction cannot be discarded as a possible source of the relatively weak tones generated by the fan.

Evaluation of duct modes using the method of Tyler and Sofrin (ref. 14) indicated that low-speed fan rotor-stator modes generated at the fundamental blade-passage frequency would not propagate in the duct; this result is inconsistent with the weak tone in the data at 300 Hz (see figs. 11(b) and (c)). However, tones generated by rotor intersection of large-scale turbulence could propagate at all blade-passage frequencies. Thus, rotor-turbulence interaction is probably responsible for the 300 Hz tone. A

potential source of the turbulence was the duct discontinuity 1 m (3.3 ft) ahead of the fan (see fig. 4).

Broadband noise— The more important broadband noise can be classified as rotor-alone-noise and excess noise. Rotor-alone-noise is that minimum rotor noise generated in smooth flow by blade boundary-layer turbulence and vortex shedding. Excess noise is that noise caused by all other sources, such as rotor blade interaction with inflow turbulence (ref. 15), stator interaction with nonperiodic flow (ref. 16), and rotor tip-clearance noise (ref. 17).

Wright (ref. 9) has developed an empirical method for estimating minimum broadband noise of rotors. He considered only the turbulent boundary-layer noise and assumed that coherent vortex shedding could be avoided by tripping the boundary layer. The resulting peak rotor self-noise at the Strouhal frequency, from reference 9, is

$$SPL = SPL_{sb} + 10 \log \left(\frac{D}{D_{sb}}\right)^2 \frac{B}{B_{sb}} \frac{c}{c_{sb}} + 10 \log \left(\frac{r}{r_{sb}}\right)^2 \frac{\Delta f}{\Delta f_{sb}} + 2\alpha \qquad (11)$$

where

SPL_{sb} = 2 dB (fig. 7.2, ref. 9)

D_{sb} = 0.3 m

B_{sb} = 1

c_{sb} = 0.1 m

r_{sb} = 30 m

Δf_{sb} = 1 Hz

Strouhal frequency = 0.9 V_{tip}/c

Figure 18 shows that the mid-frequency noise of the low-speed fan extrapolated to 30.5 m (100 ft) is approaching the minimum possible according to reference 9. The noise below 800 Hz and above 2500 Hz would be excess noise due to other sources.

Effect of Honeycomb

Inflow turbulence was not measured during the investigation. However, inflow conditions were altered by placing honeycomb and various flow distortion generators in the inlet. Changes in fan noise were then monitored.

The inlet honeycomb of figure 5 had only a minor effect on third-octave band noise levels as shown in figure 19(a). Narrowband spectra of figures 19(b) and (c) also show very little effect due to honeycomb. The small reductions of inlet noise may have been partially due to sound transmission loss through the honeycomb.

Examination of fan noise time histories, figures 20(a) through (f), show that the honeycomb reduced the unsteadiness of the blade-passage tones, especially in the inlet. However, the effect on the downstream microphones was so slight that the time-averaged sound power was little affected by the honeycomb. Hodder (ref. 18) has shown that honeycomb in a fan inlet broke up turbulence length scale in the flow direction, reduced tone unsteadiness, and reduced the time-averaged sound pressure level. Because these effects did not occur in the study described here (see, e.g., the 600 Hz tone in fig. 19(b)), it is possible that the fan excess noise was caused by (1) small-scale turbulence that passed through the honeycomb, or (2) some flow disturbance between the honeycomb and rotor (probably turbulence from the discontinuity in the transition between the square duct and circular fan section).

Effect of Flow Distortion

Steady-state measurements of pressures and flow angularity 23 mm (9 in.) ahead of the rotor showed that the inflow had considerable radial and azimuthal variation of swirl (fig. 21(a)), which was reduced by the inlet honeycomb (fig. 21(b)). Note the difference in scale of figures 21(a) and (b). The reduction of swirl by the honeycomb had little effect on the radiated sound power, as was shown in figure 19.

To introduce a flow velocity distortion, a multilayer screen was installed in the inlet, as shown in figure 6. However, the resulting flow distortion at the fan was small and the fan noise was unchanged, as shown in figure 22. Next, a wooden barrier was installed, which blocked the lower half of the duct (fig. 6). The massive flow distortion shown in figure 23 resulted in noise increases of 2 to 7 dB in the third-octave band power spectrum of figure 24. If the flow distortion had been confined to smaller portions of the fan disc, rapid changes in blade loading would have resulted in even greater noise increases (ref. 19).

Effect of Fan Rotational Speed

Figures 25(a) and (b) illustrate the noise variation with fan speed at a fixed stagger angle. The curves, though nonlinear, follow approximately a 55 log N_2/N_1 variation except at 88.4° stagger angle, where the variation is 50 log N_2/N_1. Because the boundary-layer rakes were installed in front of the fans, the noise was predominately narrowband in nature and, therefore, not representative of the basic fan noise. However, a plot of the variation of broadband noise on figure 25(b) ($f > 1.0$ kHz) also showed a 55 log N_2/N_1 variation. This variation is consistent with reference 19 for several fans operating in a range of tip speeds similar to that of the low-speed fan.

Effect of Blade Stagger Angle and Angle of Attack

Figure 26(a) shows that the variation of overall acoustic power level with stagger angle at constant rotational speed was -0.5 dB/deg. However, the mass flow and, therefore, the blade angle of attack were varying also.

Figure 26(b) shows the variation of acoustic power with estimated[2] angle of attack at 3/4 radius. Above 10° the angle of attack change had no effect on the noise. A possible explanation is that the rotor blade sections stall between 10° and 12° angle of attack, the noise peaks as part of the blade stalls, and then the noise remains constant as the entire blade moves into the stall regime.

CONCLUDING REMARKS

An experimental investigation has been made of two 1.8-m (6 ft) diameter fans. Acoustic power measurements of the fans in a 23.8-m (78 ft) duct showed that the low-speed fan (15 rotor blades, 1200 rpm) generated slightly less noise than did the high-speed fan (9 rotor blades, 2000 rpm).

The acoustic data were scaled to represent the noise of six 12.2-m diam fans that would drive the Ames 40- by 80-Foot Wind Tunnel. The resulting noise of the low-speed fans would be 16 dB less than the noise of the present wind-tunnel fan system at equal test-section speeds. That noise reduction can be attributed primarily to elimination of the motor support struts upstream of the present fan rotors and to a decrease of maximum rotational speed from 290 rpm (present fans) to 180 rpm (low-speed fans, full scale). Lack of flow-turbulence data puts some uncertainty in the predicted noise of the full-scale low-speed fans.

The low-speed fan was operated by varying both blade pitch and rotational speed. The noise varied -0.5 dB per degree change in stagger angle and, though nonlinear, varied approximately by $55 \log N_2/N_1$. Those two rates were approximately equal but opposite. Thus, the fan noise depended only on thrust level (or test-section speed) and did not depend on the particular rpm or stagger angle combination chosen to reach that thrust level. This does not mean that different fans generating the same thrust would make the same noise. The above conclusions apply only to the following ranges for which data were obtained: 50 to 100 percent maximum rpm and 35° to 53° stagger angle (4.5° to 19.5° blade angle of attack).

The sound power radiated downstream of the fan was 4 to 6 dB greater than the upstream levels at frequencies above 250 Hz. Below that frequency, the difference was as much as 17 dB.

The fan noise sources were not identified explicitly. However, the following observations were made concerning the low-speed fan:

1. Broadband noise dominated the spectrum, except at the first and second harmonics of blade-passage frequency.

[2]The estimation was based on the vector summation of blade speed, mean flow velocity, and one-half swirl velocity behind the fan (fig. 2). The swirl angle was measured.

2. At mid-frequencies (800 Hz to 2 kHz), the noise matched levels predicted for rotor-alone broadband noise (i.e, self-noise of rotor in smooth flow).

3. Because inlet honeycomb had little effect, the broadband noise at other frequencies was probably caused by rotor interaction with small-scale turbulence or with turbulence created at the duct transition/contraction ahead of the fan.

Ames Research Center
National Aeronautics and Space Administration
Moffett Field, Calif., 94035, April 5, 1977

REFERENCES

1. Mort, K. W.; Kelly, M. W.; and Hickey, D. H.: The Rationale and Design Features for the 40 by 80/80 by 120-Foot Wind Tunnel. Symposium on Wind Tunnel Design and Testing Techniques, AGARD CP-174, AGARD Fluid Dynamics Panel, London, U.K., Oct. 6-8, 1975.

2. Scharton, T. D.; Sawley, R. J.; and Wilby, E. G.: An Acoustic Study for the Modified 40- by 80-Foot Wind Tunnel. BBN Report 2765, 1975.

3. Soderman, P. T.: Instrumentation and Techniques for Acoustic Research in Wind Tunnels. ICIASF '75 RECORD, pp. 270-276, 6th Inter. Cong. on Instrumentation in Aerospace Simulation Facilities, Ottawa, Canada, Sept. 22-24, 1975, IEEE Publication 75 CHO 993-6AES.

4. Page, V. R.; Eckert, W. T.; and Mort, K. W.: An Aerodynamic Investigation of Two 1.83 Meter Diameter Fan Systems Designed to Drive a Subsonic Wind Tunnel. NASA TM X-73,175, 1977.

5. Doak, P. E.: Excitation, Transmission and Radiation of Sound from Source Distributions in Hard-Walled Ducts of Finite Length (I): The Effects of Duct Cross-Section Geometry and Source Distribution Space-Time Pattern. J. of Sound and Vibration, vol. 31, no. 1, Nov. 1973, pp. 1-72.

6. Beranek, L. L., ed.: Noise and Vibration Control. Ch. 6, McGraw-Hill Book Co., Inc., 1971.

7. Noiseux, D. U.; Noiseux, N. B.; and Kadman, Y.: Study of a Porous Microphone Sensor in an Aerofoil. NASA CR-137652, 1975.

8. Hayden, R. E.: Noise from Interaction of Flow with Rigid Surfaces: A Review of Current Status of Prediction Techniques. NASA CR-2126, 1972.

9. Wright, S. E.: The Acoustic Spectrum of Axial Flow Machines. U. of Southhampton ISVR Report No. 69, April 1975 and J. of Sound and Vibration, vol. 45, no. 2, Mar. 1976, pp. 165-223.

10. Arndt, R. E. and Nagel, R. T.: Effect of Leading Edge Serrations on Noise Radiation from a Model Rotor. AIAA Paper No. 72-655, June 1972.

11. Bies, D. A.: Investigation of the Feasibility of Making Model Acoustic Measurements in the NASA Ames 40- by 80-Foot Wind Tunnel. NASA CR 114352, 1971.

12. Pankhurst, R. C.; and Holder, D. W.: Wind-Tunnel Technique. Sir Isaac Pitman & Sons Ltd., 1952, pp. 62-63.

13. Morfey, C. L.: Sharland, I. J.; and Yeow, K. W.: Fan Noise. Ch. 10 in Noise and Acoustic Fatigue in Aeronautics, ed. by E. J. Richards and D. J. Mead, John Wiley & Sons, N. Y., 1968.

14. Tyler, J. M.; and Sofrin, T. G.: Axial Flow Compressor Noise Studies. S.A.E. Trans., vol. 70, 1962, pp. 309-332.

15. Sharland, I. J.: Sources of Noise in Axial Flow Fans. J. of Sound and Vibration, vol. 1, no. 3, 1964, pp. 302-322.

16. Hanson, D. B.: Unified Analysis of Fan Stator Noise. J. Acoust. Soc. America, vol. 54, no. 6, Dec. 1973, pp. 1571-1591.

17. Mugridge, B. D.; and Morfey, C. L.: Sources of Noise in Axial Flow Fans. J. Acoust. Soc. America, vol. 51, no. 5 (Part 1), May 1972, pp. 1411-1426.

18. Hodder, B. K.: Investigation of the Effect of Inlet Turbulence Length Scale on Fan Discrete Tone Noise. NASA TM X-62,300, 1973.

19. Wright, S. E.: Discrete Radiation from Rotating Periodic Sources. J. of Sound and Vibration, vol. 17, no. 4, 1971, pp. 437-498.

20. Wallis, R. A.: Axial Flow Fans. Academic Press, N. Y., 1961.

TABLE 1.— 1/7TH SCALE FAN GEOMETRY AND PERFORMANCE PARAMETERS

Rotor	Low-speed fan	High-speed fan
Number of blades	15	9
Radius, m (ft)	0.914 (3.0)	0.914 (3.0)
Hub-tip ratio	0.5	0.5
Root chord, mm (ft)	183 (0.602)	136 (0.445)
Tip chord, mm (ft)	135 (0.442)	87 (0.284)
Blade area per blade, m^2 (ft^2)	0.073 (0.783)	0.051 (0.547)
Maximum rpm	1200	2000
Maximum tip speed, m/s (ft/sec)	115 (377)	192 (628)
Design thrust, N (lb)	5022 (1129)	5022 (1129)
Maximum pressure ratio	1.027	1.028
Solidity, hub	0.958	0.425
tip	0.352	0.136
Stator		
Number of blades	23	13
Location relative to rotor	Downstream	Downstream
Spacing from rotor in rotor chords	2	2
Chord, mm (ft)	111 (0.365)	157 (0.515)

TABLE 2.— ROTOR AIRFOIL THICKNESS DISTRIBUTION:
LOW-SPEED AND HIGH-SPEED FANS

Distance from leading edge, percent chord	Distance to upper or lower* surface from camber line† at 3/4 radius, percent chord
1.25	1.65
2.5	2.27
5.0	3.08
7.5	3.62
10	4.02
15	4.55
20	4.83
30	5.00
40	4.875
50	4.512
60	3.921
70	3.148
80	2.205
90	1.137
95	0.523

*Nominal thickness distribution of a 10% thick *C*-4 airfoil (ref. 20). The airfoil shape changes from root to tip. The thickness coordinates at 3/4 radius (in percent chord) grow linearly up to 20% at the root and decrease linearly up to 20% at the tip. Thus, the root airfoil has a maximum thickness of 12% chord and the tip airfoil has a maximum thickness of 8% chord (see figs 1(a) and (c).

†The camber line is a circular arc.

TABLE 3.— FULL SCALE FAN GEOMETRY AND PERFORMANCE PARAMETERS FOR THE 40- BY 80-FOOT WIND TUNNEL

Rotor	Current fans	Scaled up low-speed fan
Number of blades	6	15
Radius, m (ft)	6.1 (20)	6.1 (20)
Hub-tip ratio	0.35	0.50
Root chord, m (ft)	0.91 (3.00)	1.22 (4.01)
Tip chord, m (ft)	0.41 (1.33)	0.9 (2.95)
Blade area (per blade), m^2 (ft^2)	2.62 (28.17)	3.23 (34.8)
Maximum rpm	290	180
Maximum tip speed, m/s (ft/sec)	185 (607)	115 (377)
Maximum thrust (each), N (lb)	94,742 (21300)	213,300 (47950)
Maximum speed in 40- by 80-test section, m/s (ft/sec)	100 (328)	155 (507)
Stator		
Number of blades	2 (struts)	23
Location relative to rotor	Upstream	Downstream
Spacing from rotor in rotor chords	1	2
Chord, m (ft)	5.1 (16.75)	0.74 (2.43)

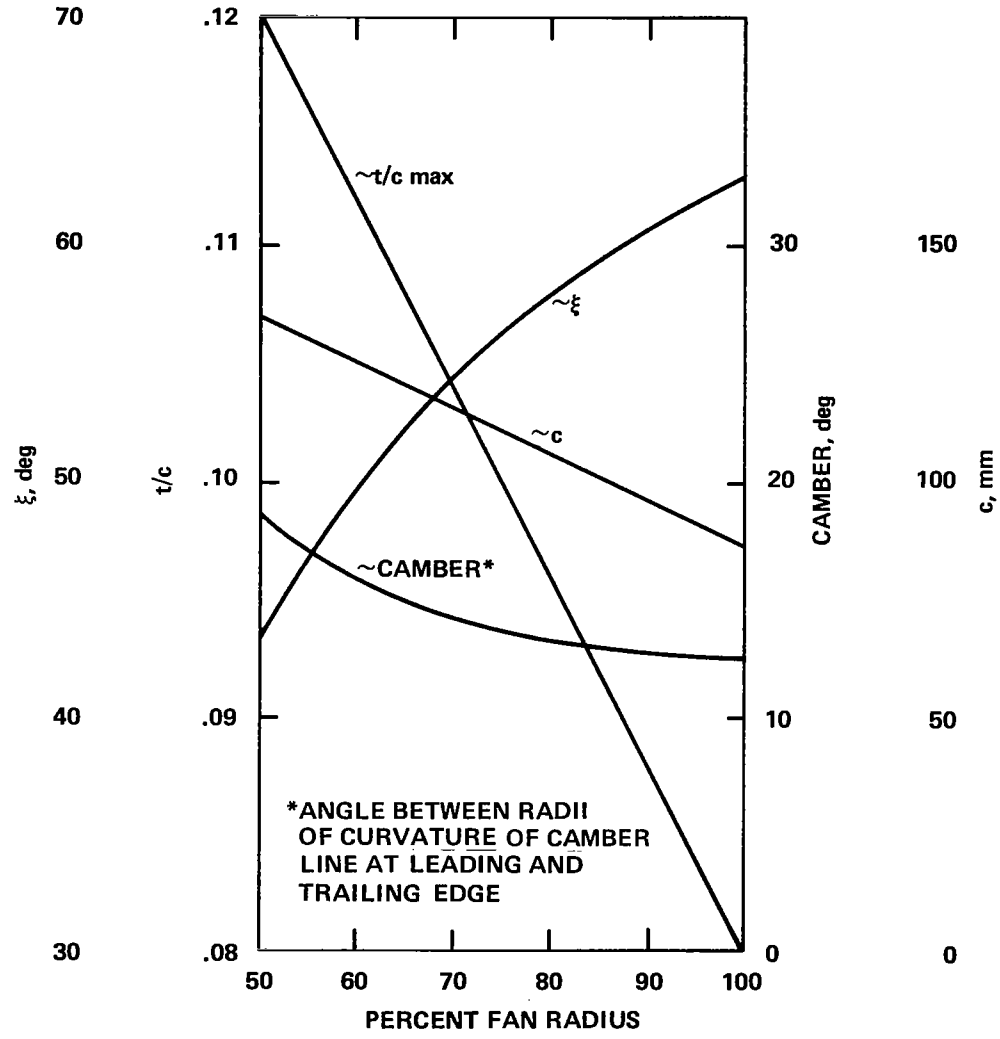

(a) High-speed fan rotor geometry versus radius; stagger angle, thickness-to-chord ratio, camber angle and chord.

Figure 1.- Fan-rotor geometry.

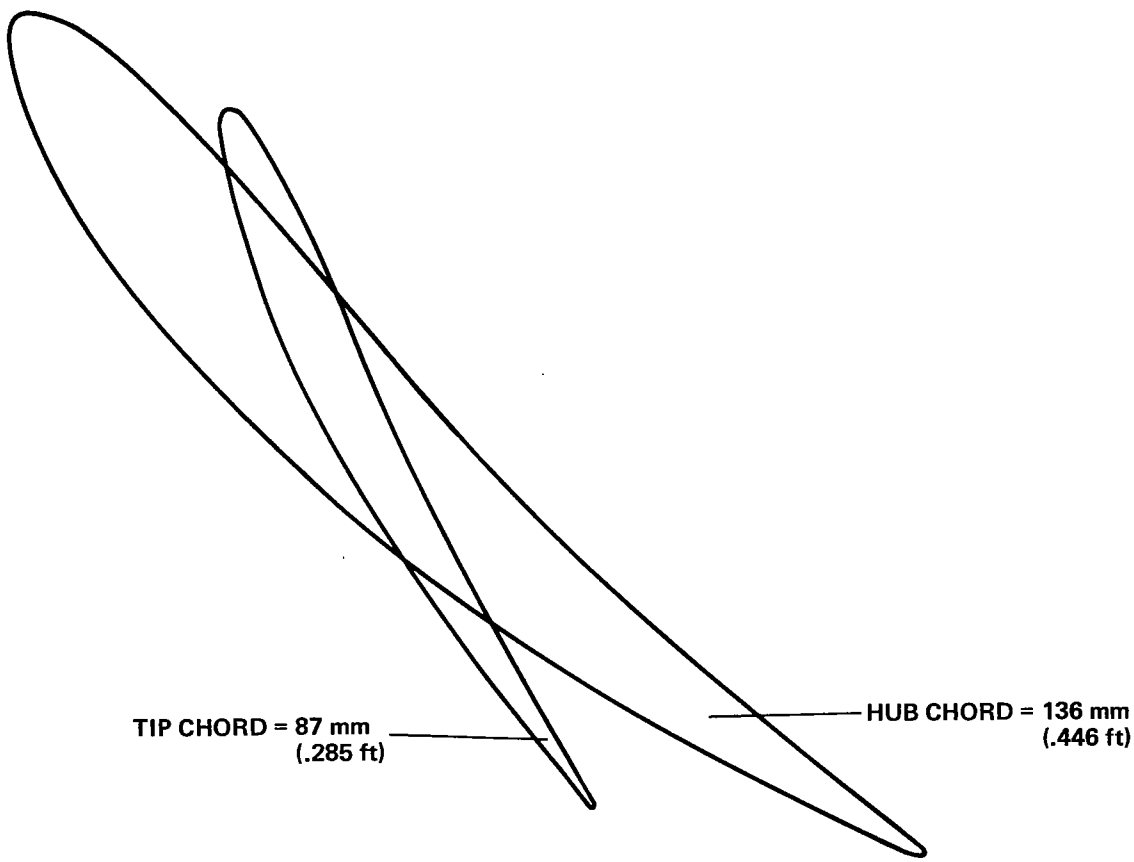

(b) High-speed rotor airfoil sections.

Figure 1.- Continued.

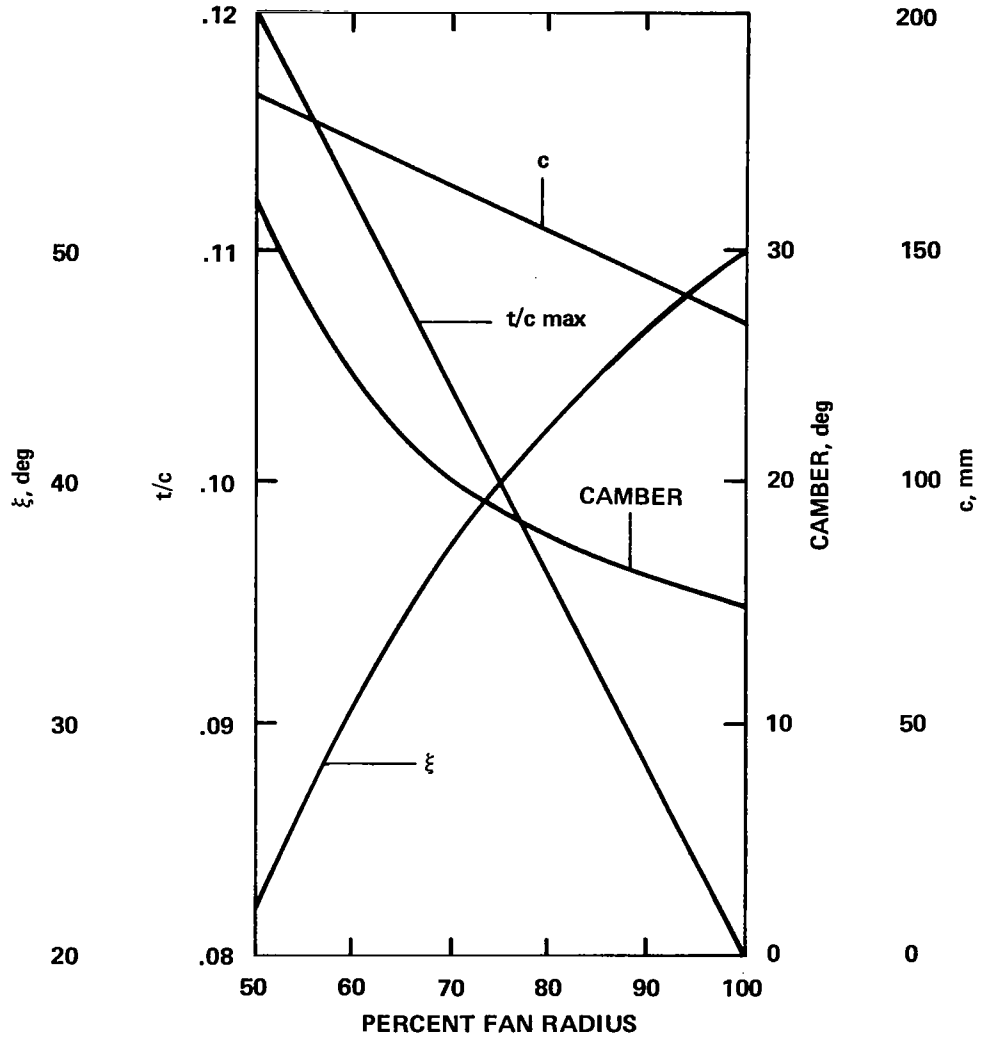

(c) Low-speed fan rotor geometry versus radius; stagger angle, thickness-to-chord ratio, camber angle and chord.

Figure 1.- Continued.

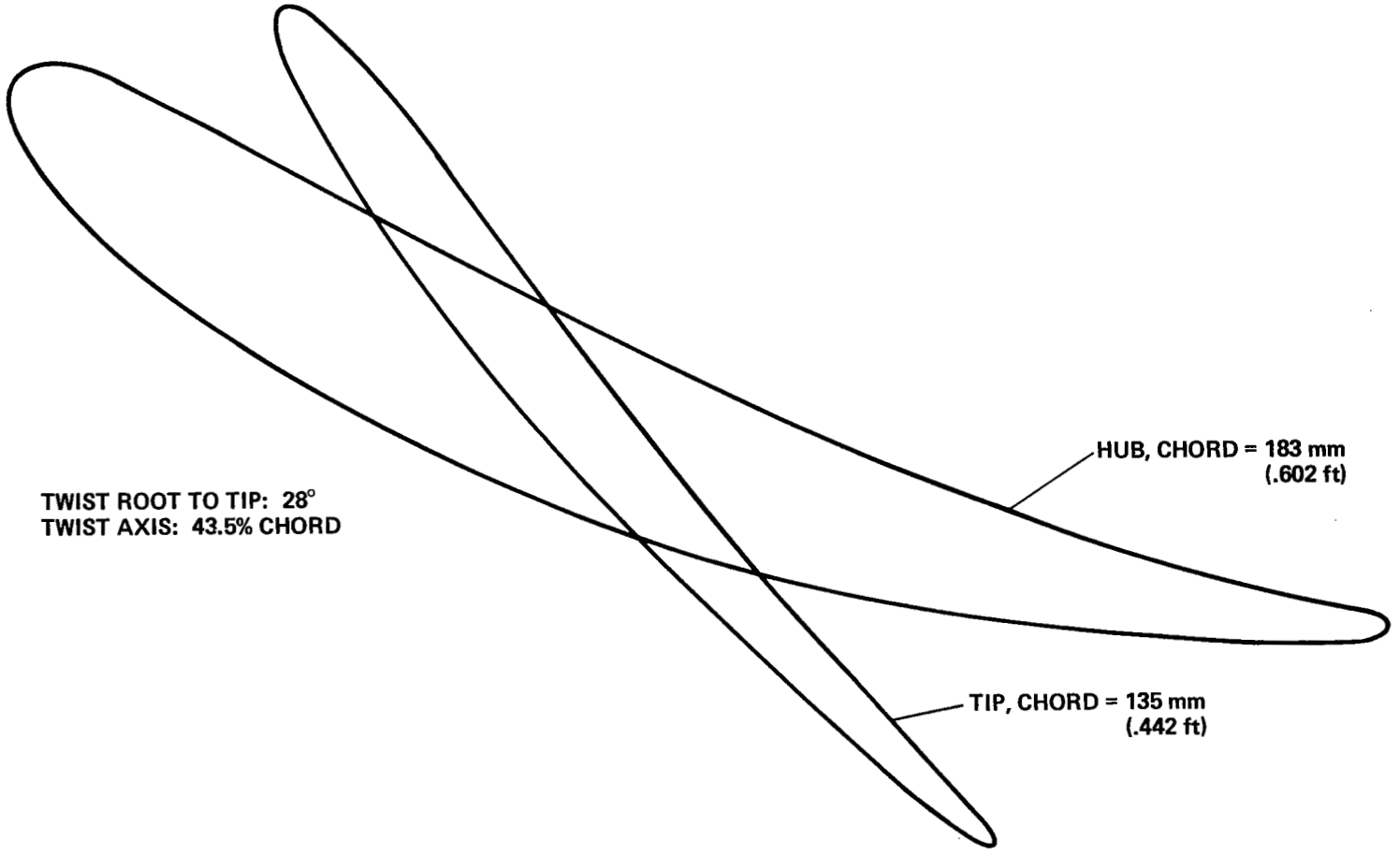

(d) Low-speed rotor airfoil sections.

Figure 1.- Continued.

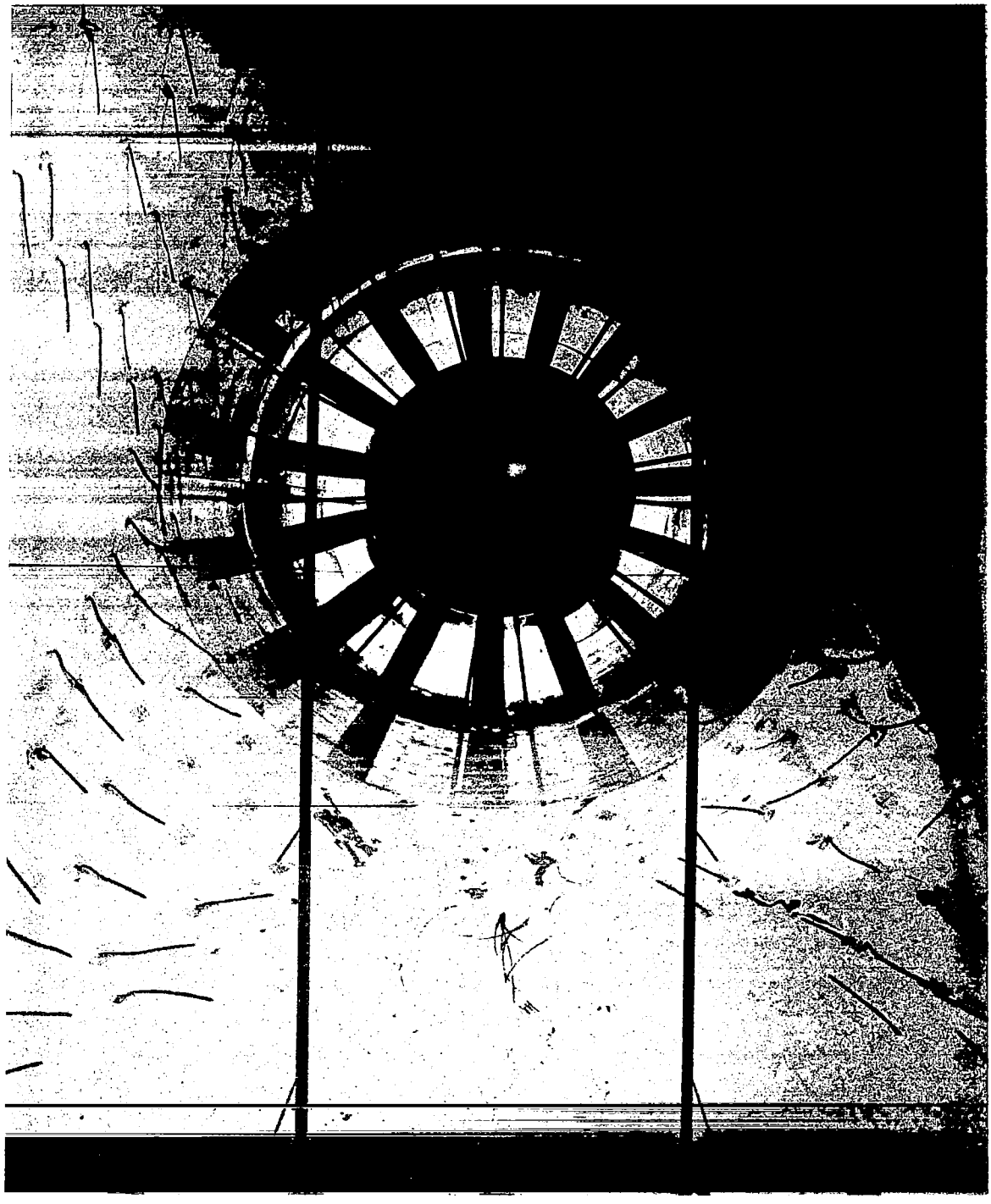

(e) Low-speed fan.

Figure 1.- Concluded.

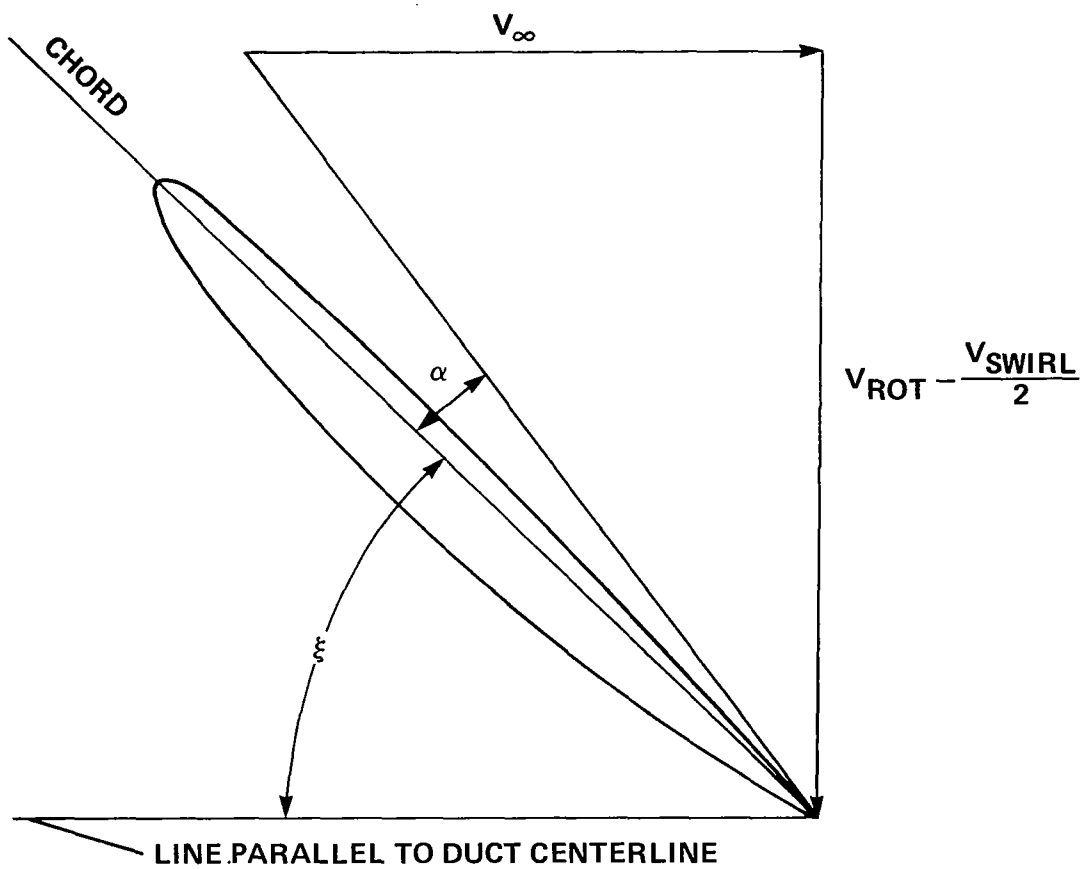

α = ANGLE OF ATTACK
ξ = STAGGER ANGLE (MEASURED AT 3/4 RADIUS)
V_∞ = FREE-STREAM VELOCITY AT FAN
V_{ROT} = BLADE ROTATIONAL SPEED AT 3/4 RADIUS
V_{SWIRL} = SWIRL OR DOWNWASH VELOCITY = V_∞ TAN ϕ
ϕ = SWIRL ANGLE MEASURED BETWEEN ROTOR AND STATOR

Figure 2.- Rotor stagger angle and angle of attack.

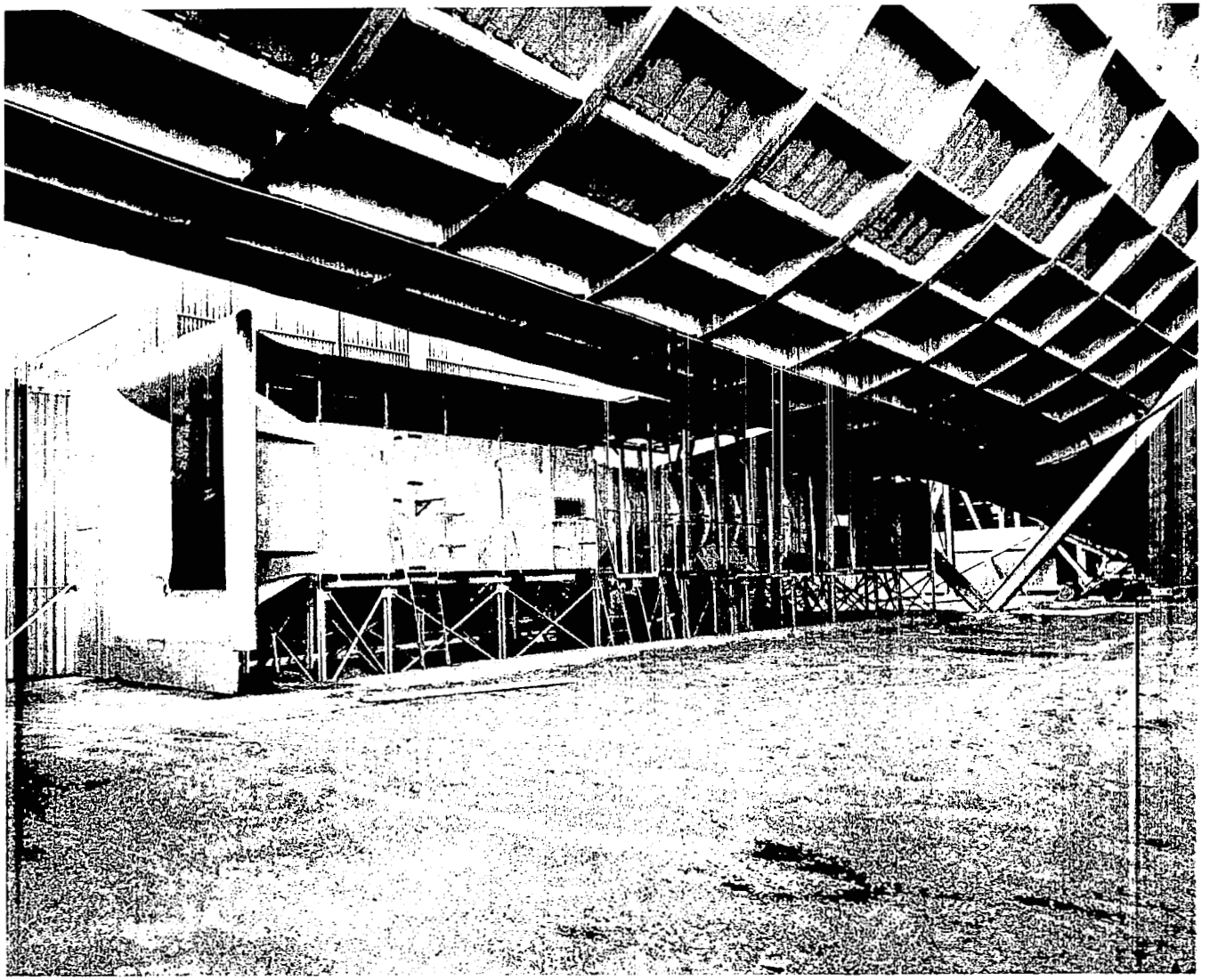

(a) Exterior view.

Figure 3.- Fan-duct facility.

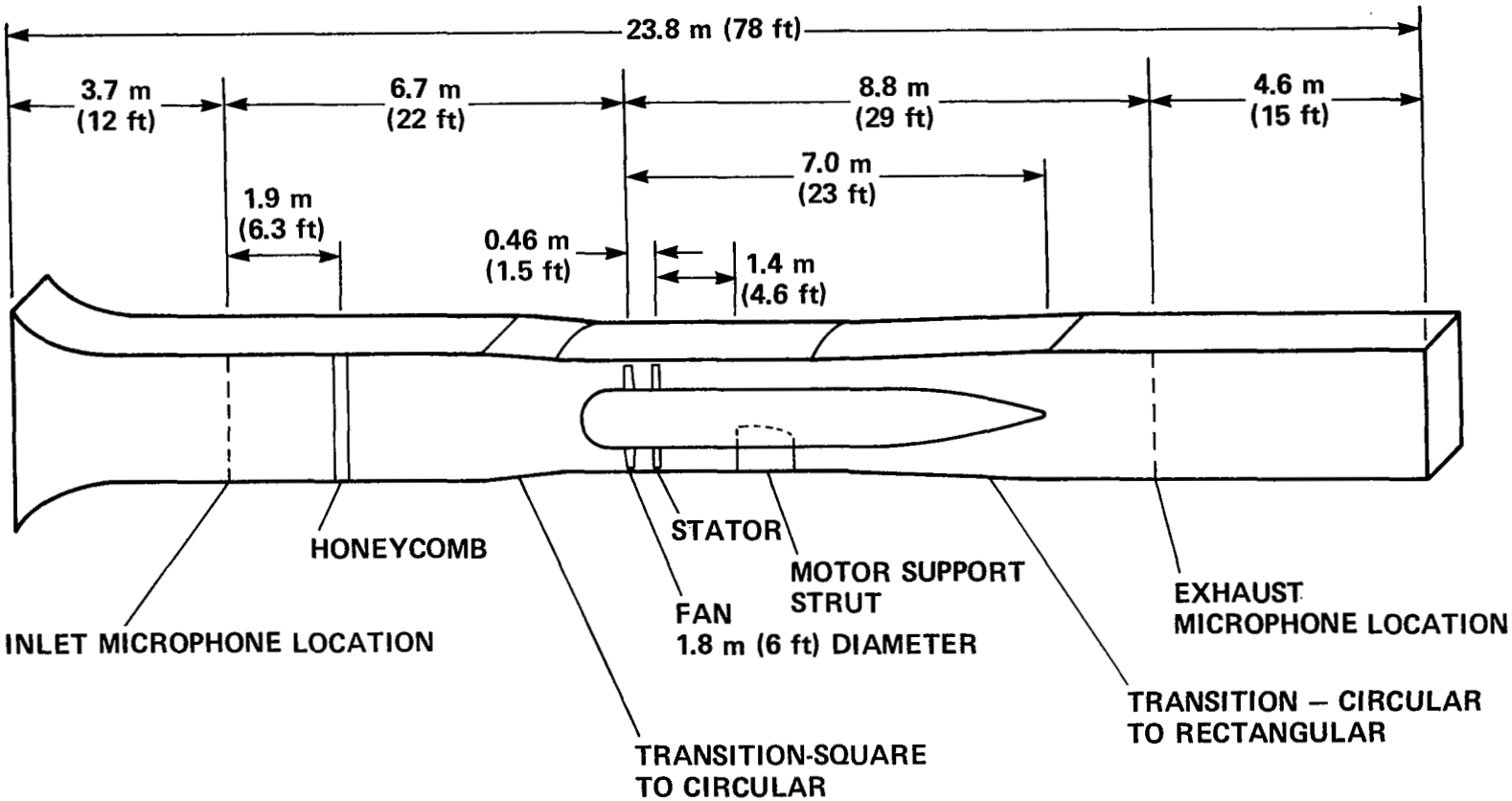

(b) View through center plane of duct.

Figure 3.- Continued.

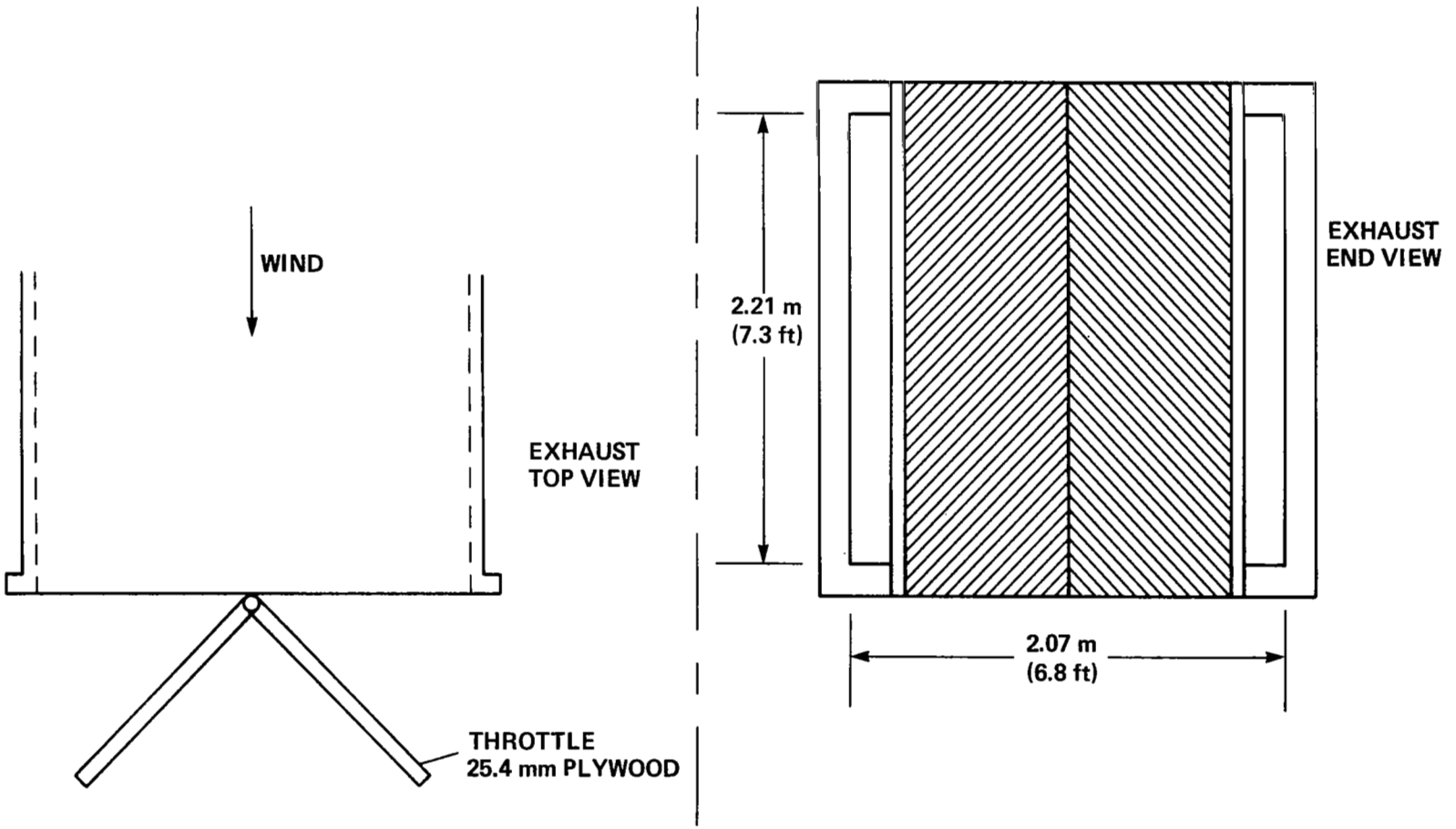

(c) Exhaust throttle.

Figure 3.- Concluded.

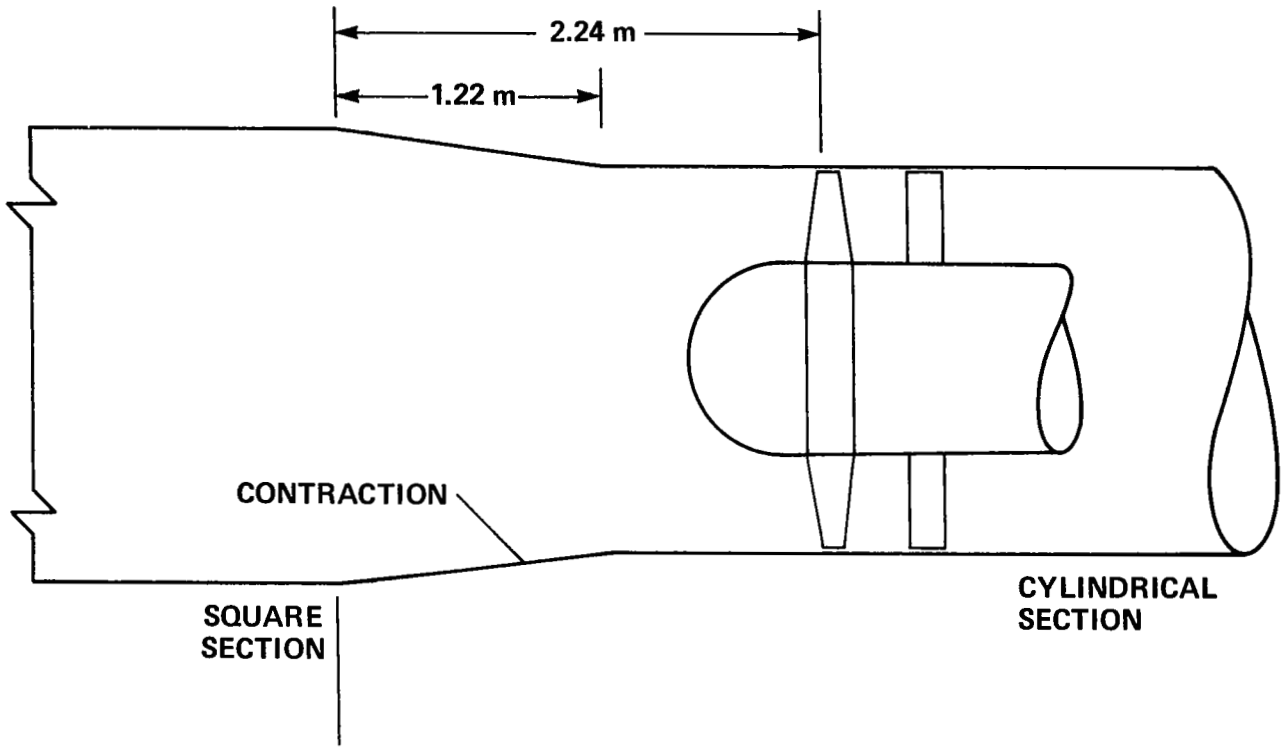

Figure 4.- Inlet contraction from square to cylindrical duct.

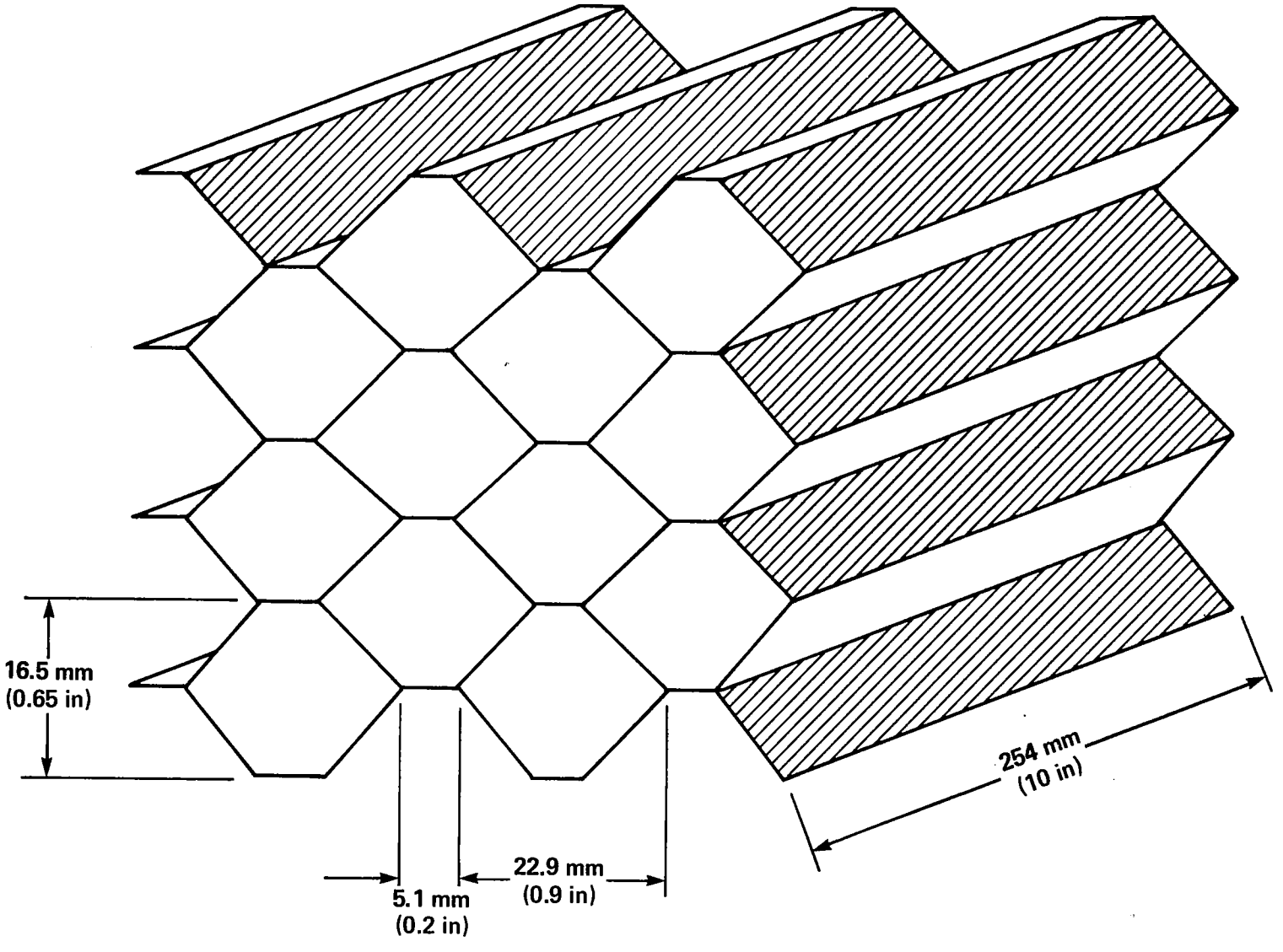

Figure 5.- Inlet honeycomb cell geometry.

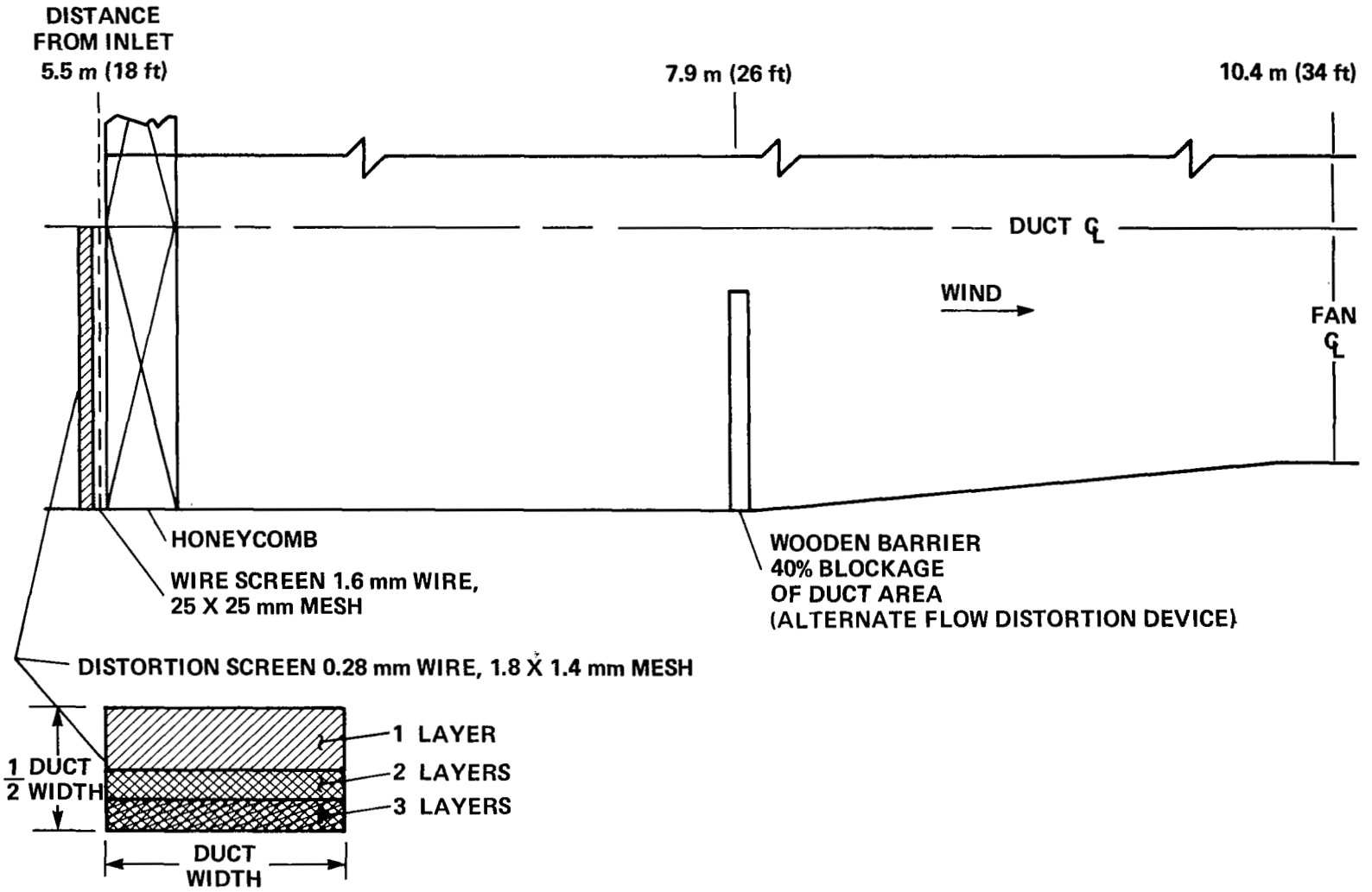

Figure 6.- Location and geometry of distortion screen and flow-blockage barrier.

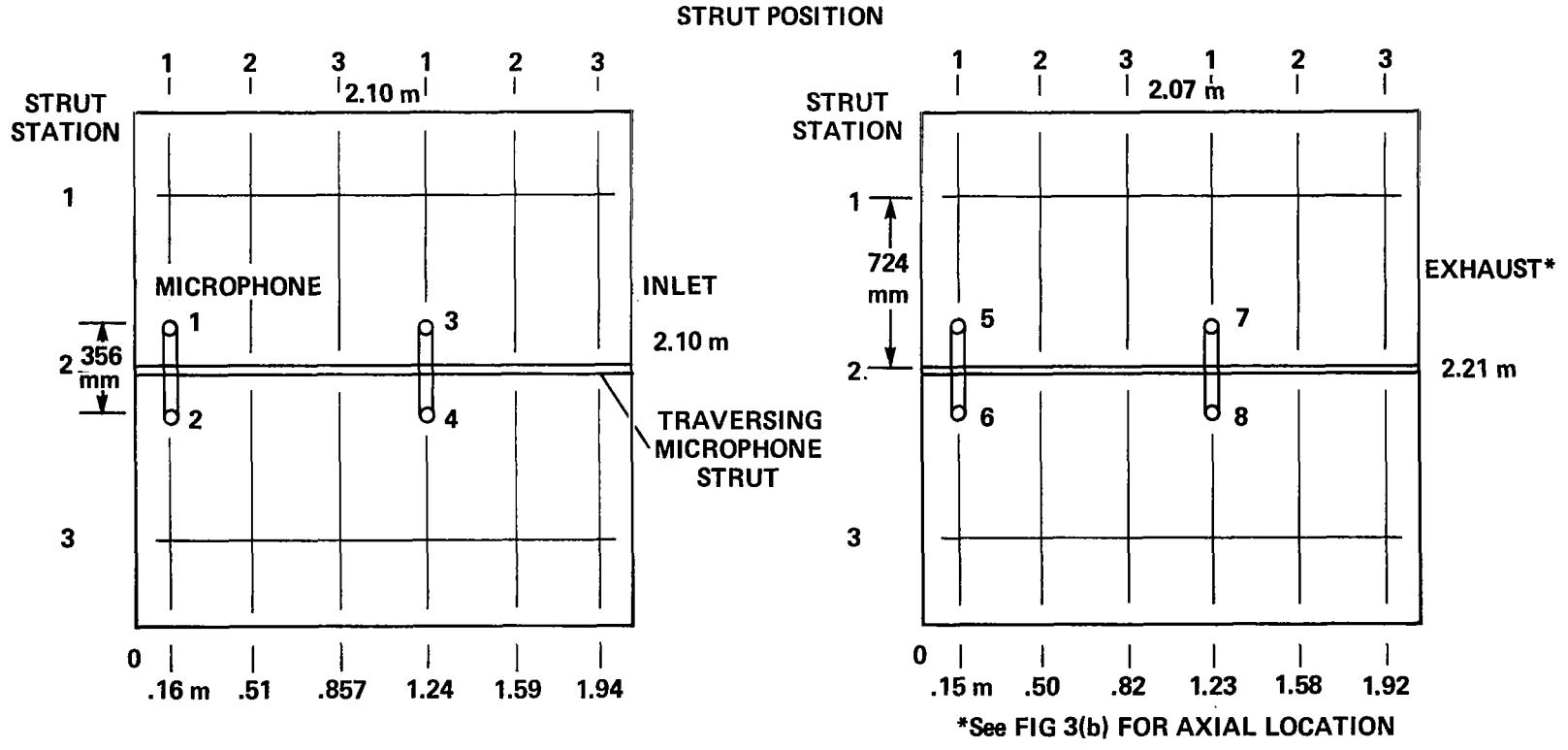

(a) Locations in duct cross sections looking upstream.

Figure 7.- Microphones.

(b) Inlet microphones and support strut.

Figure 7.- Continued.

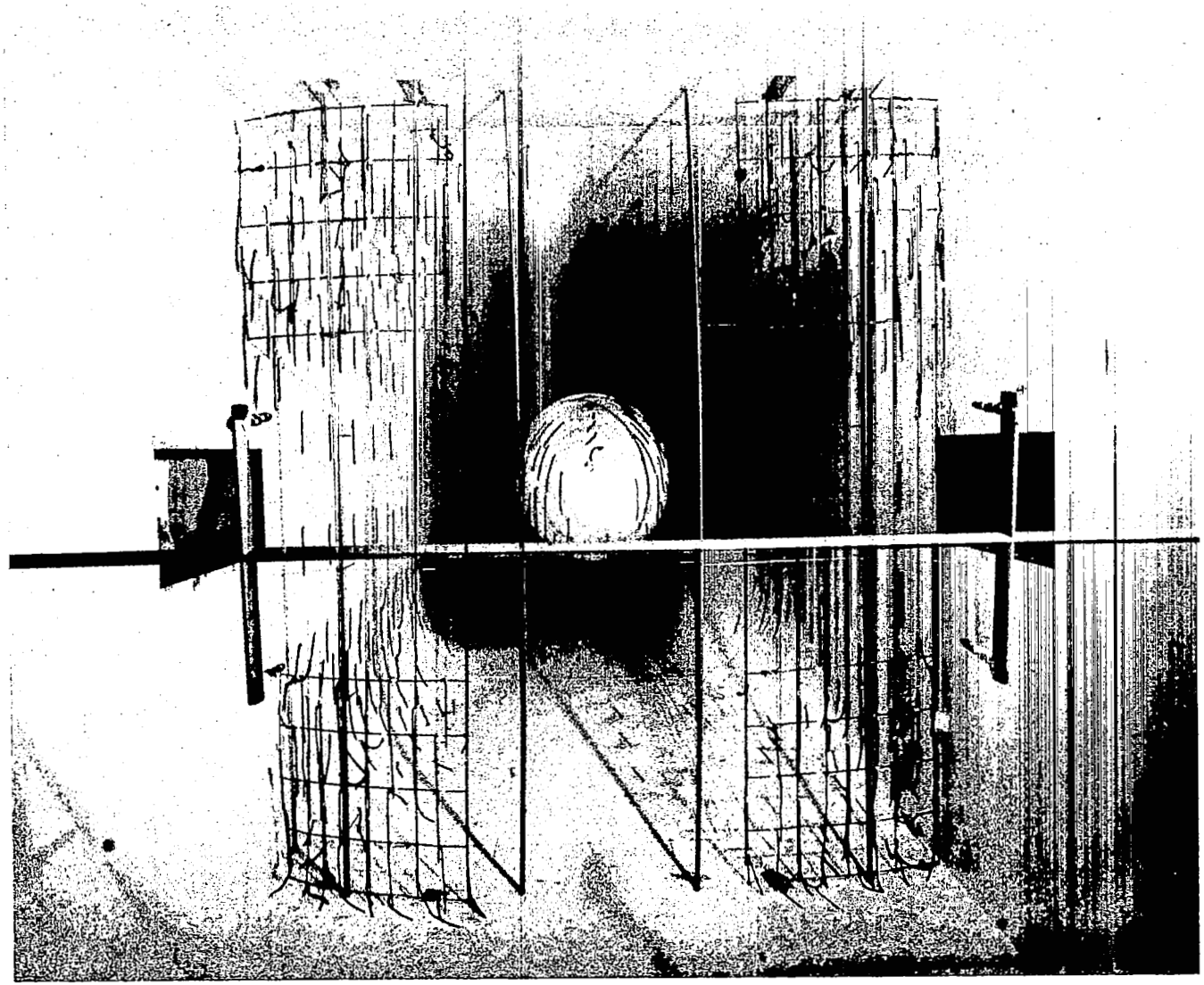

(c) Exhaust microphones and support strut.

Figure 7.- Concluded.

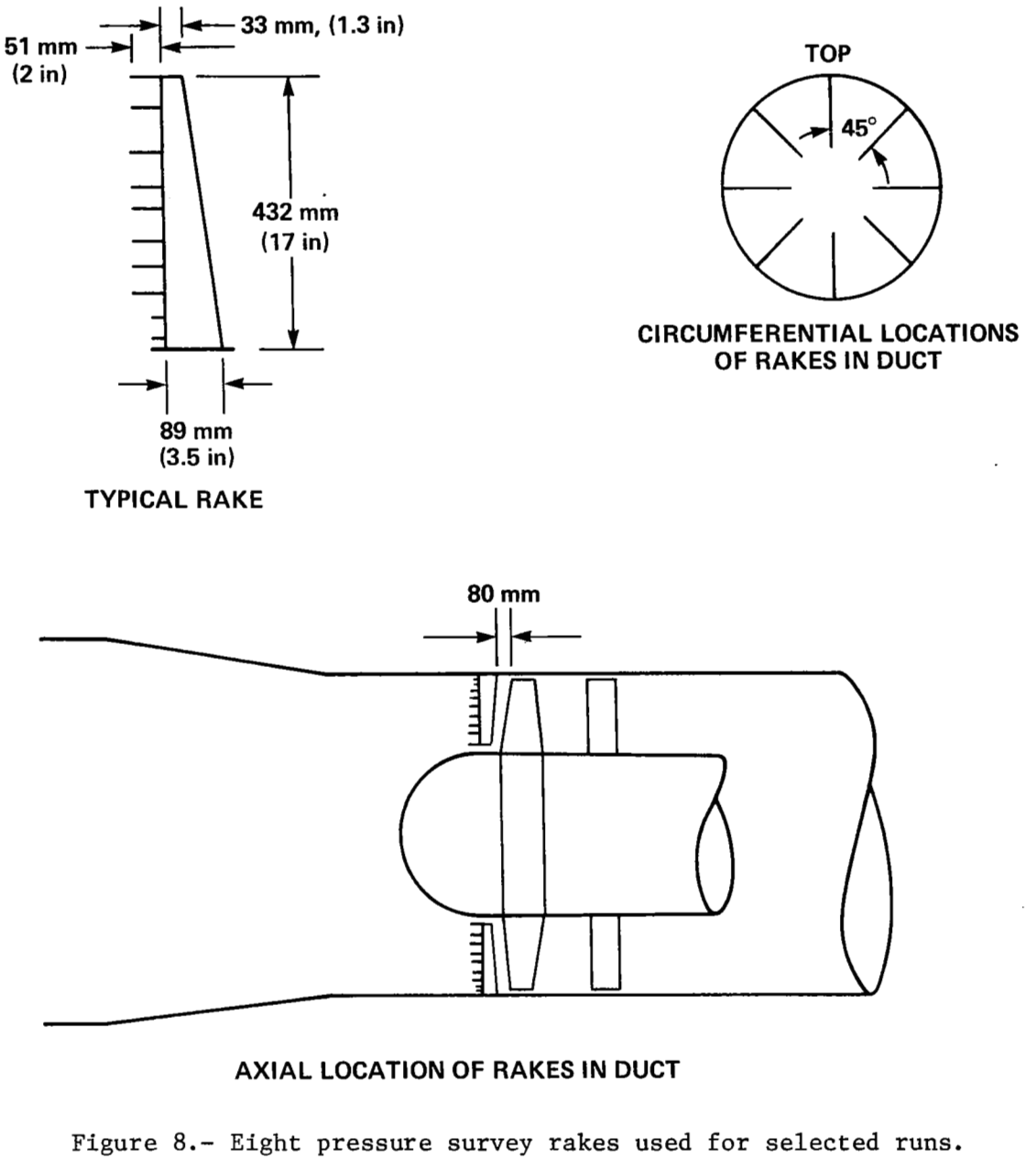

Figure 8.- Eight pressure survey rakes used for selected runs.

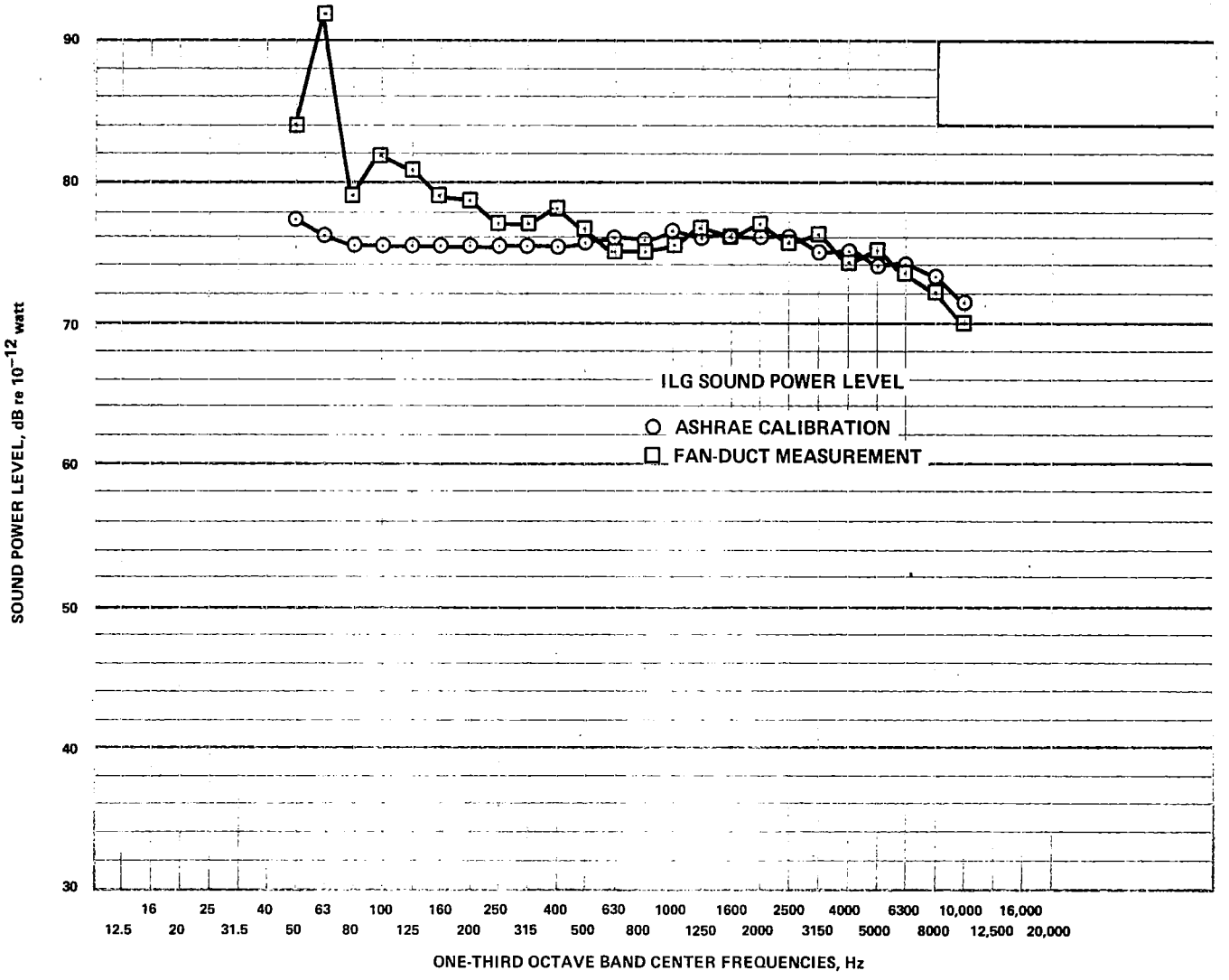

Figure 9.- Sound power levels of ILG Industries noise source determined by free-field calibration and by fan-duct sound pressure measurements.

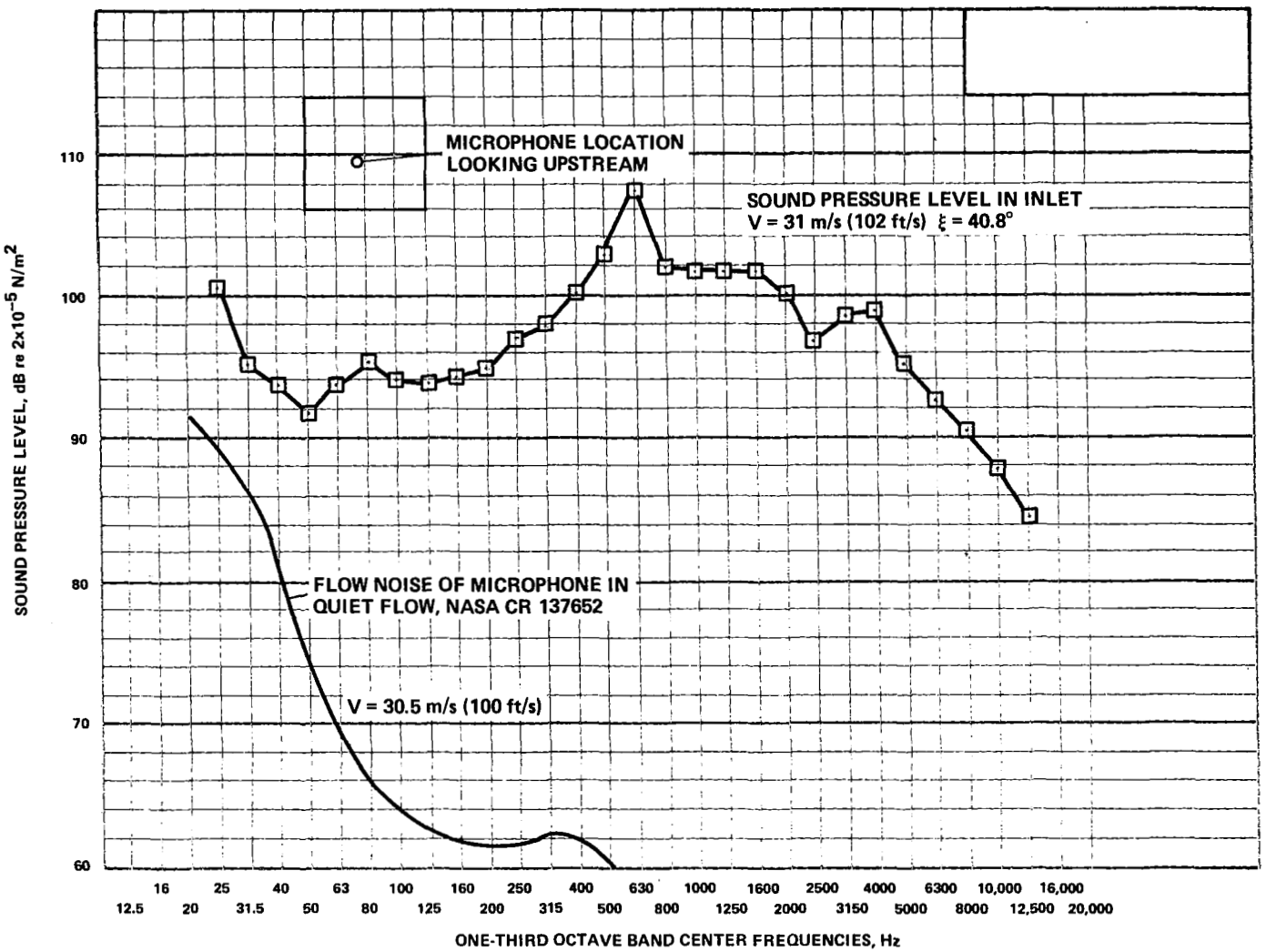

(a) Inlet.

Figure 10.- Typical sound pressure levels of low-speed fan operating at top speed compared with flow noise reported in reference 7.

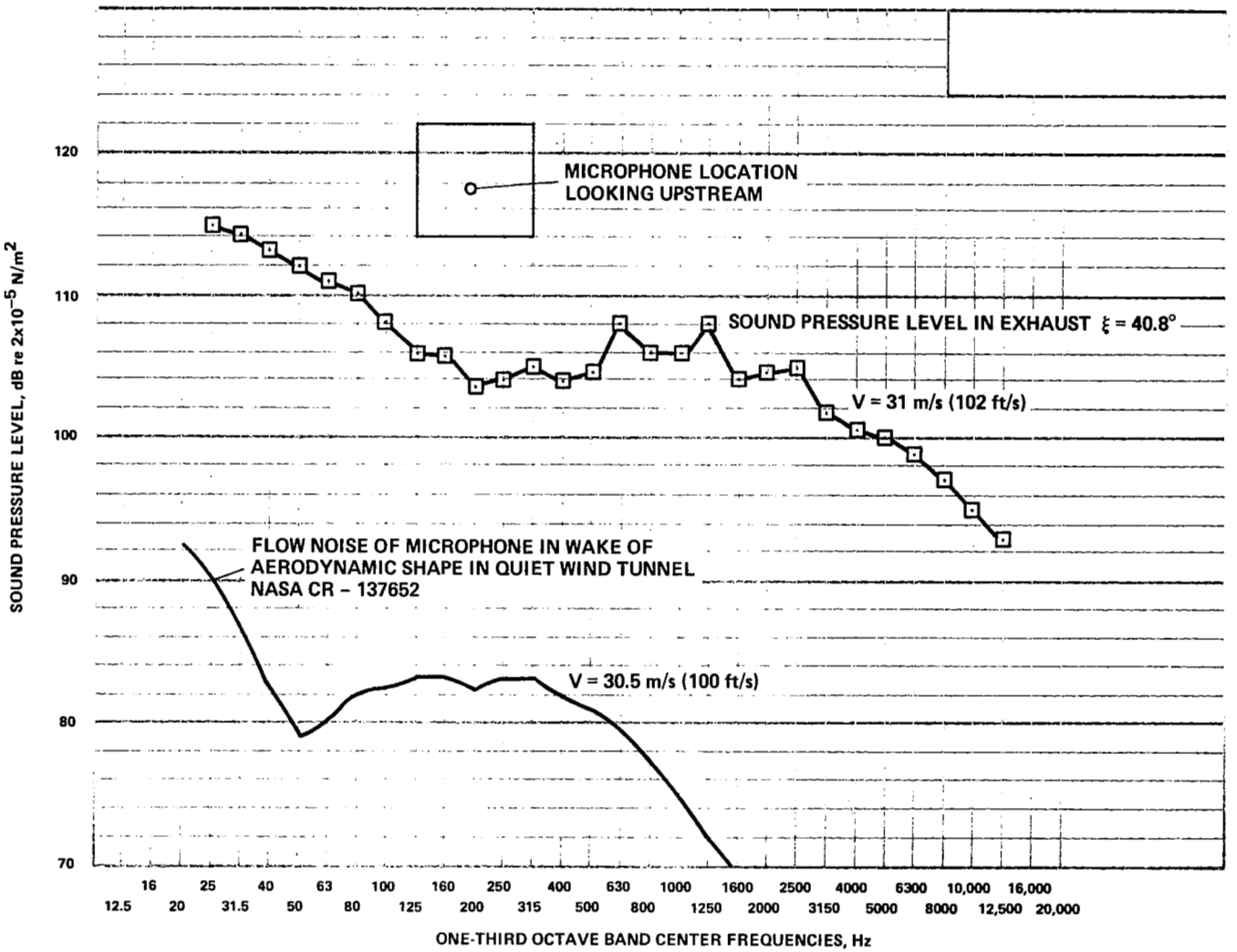

(b) Exhaust.

Figure 10.- Concluded.

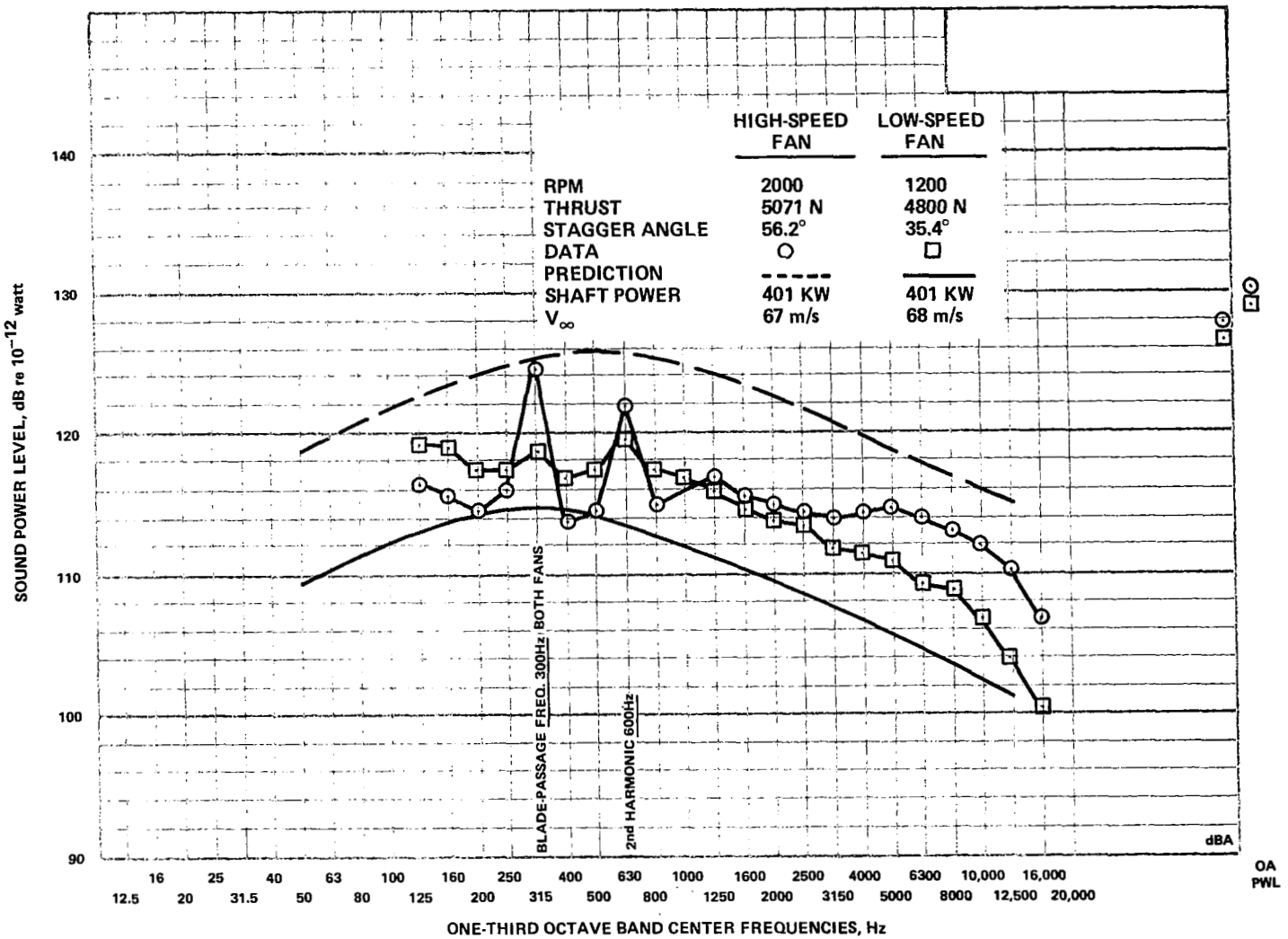

(a) Third-octave spectra of sound power.

Figure 11.- Measured and predicted noise of the high-speed and low-speed fans.

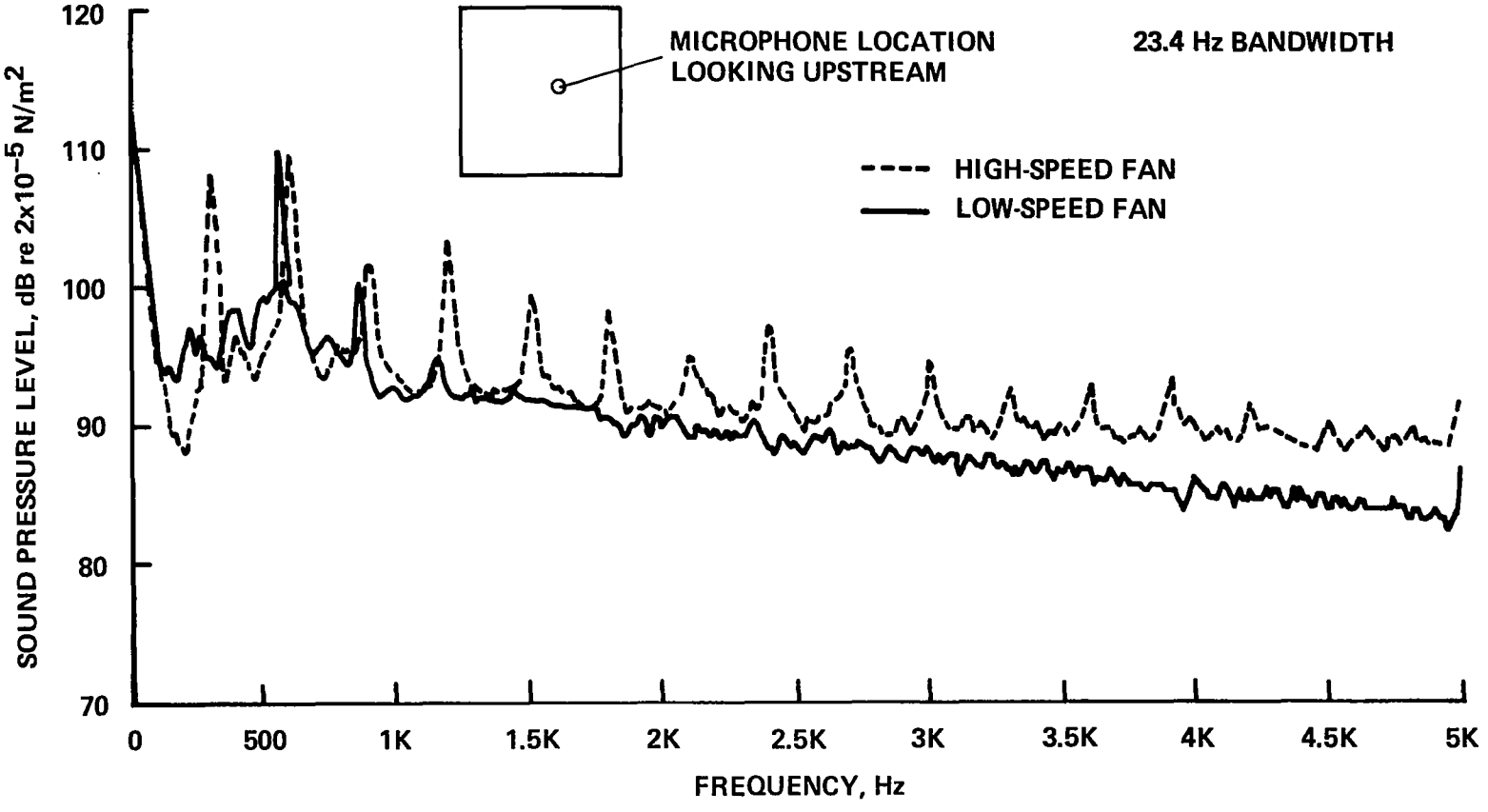

(b) Narrow-band spectra of sound pressure in inlet.

Figure 11.- Continued.

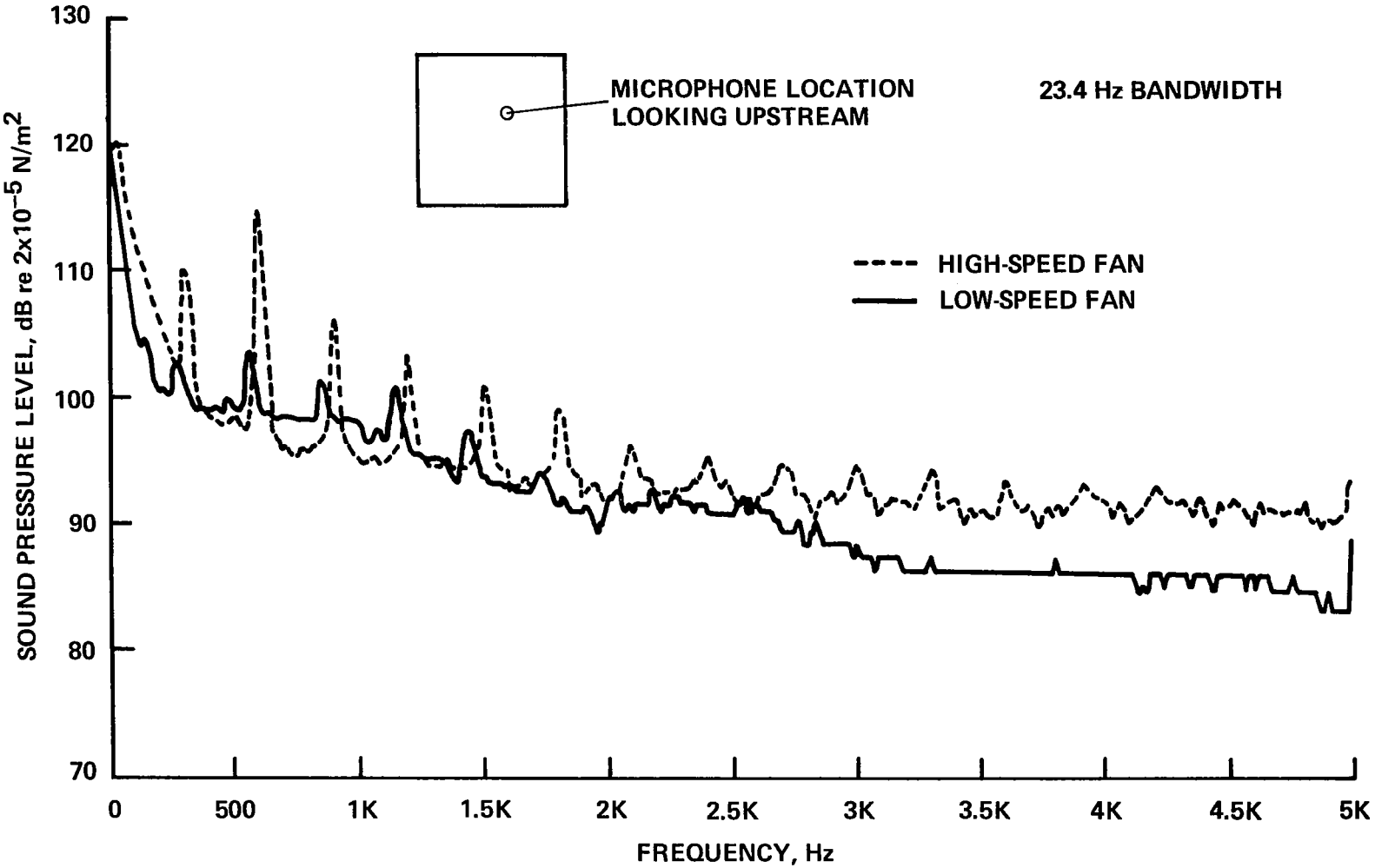

(c) Narrow-band spectra of sound pressure in exhaust.

Figure 11.- Concluded.

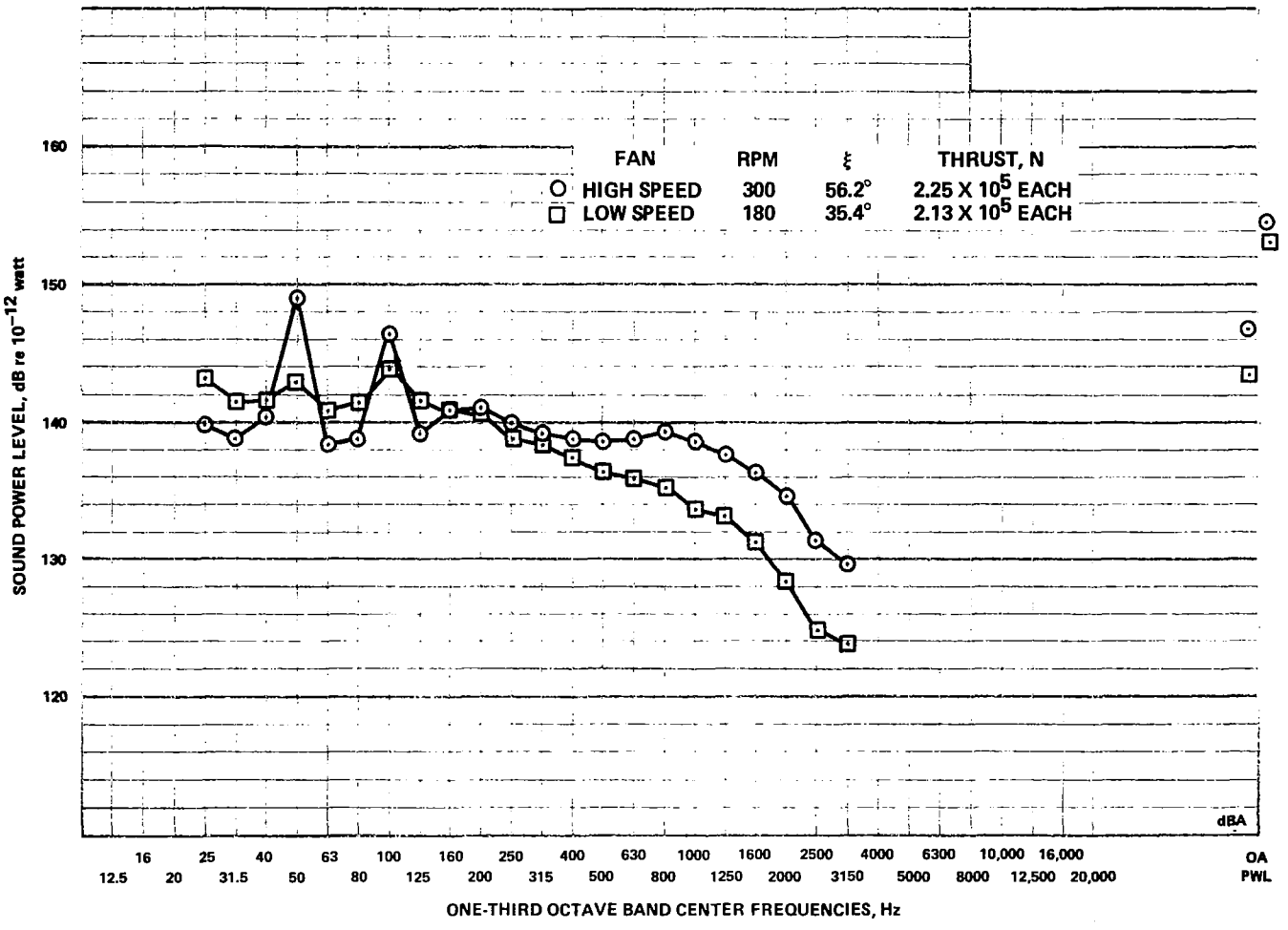

Figure 12.- Sound power of six high-speed and low-speed fans scaled to 12.2 m (40 ft) diameter.

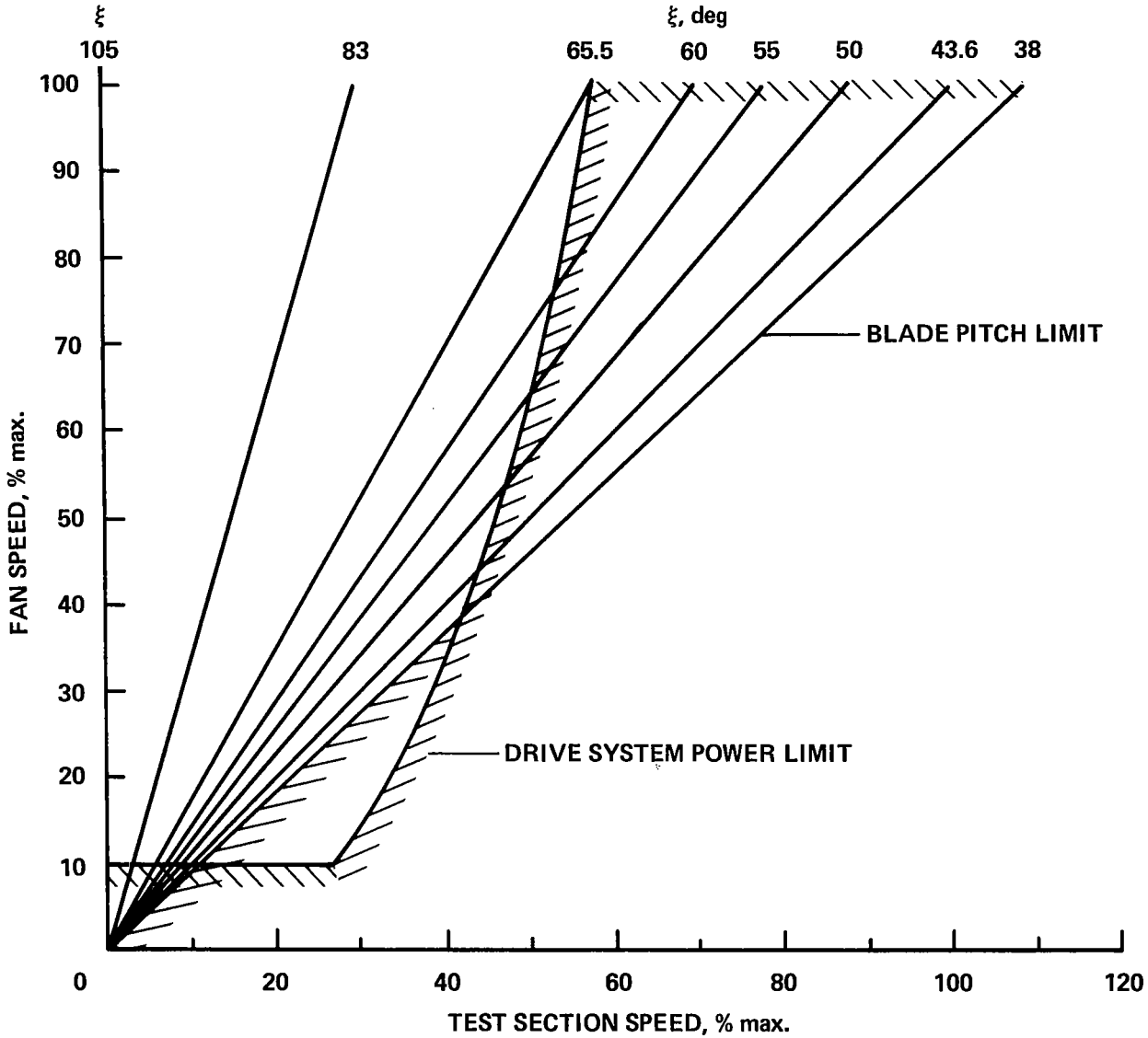

Figure 13.- Operating map for the full-scale low-speed fans driving the 40- by 80-foot wind tunnel.

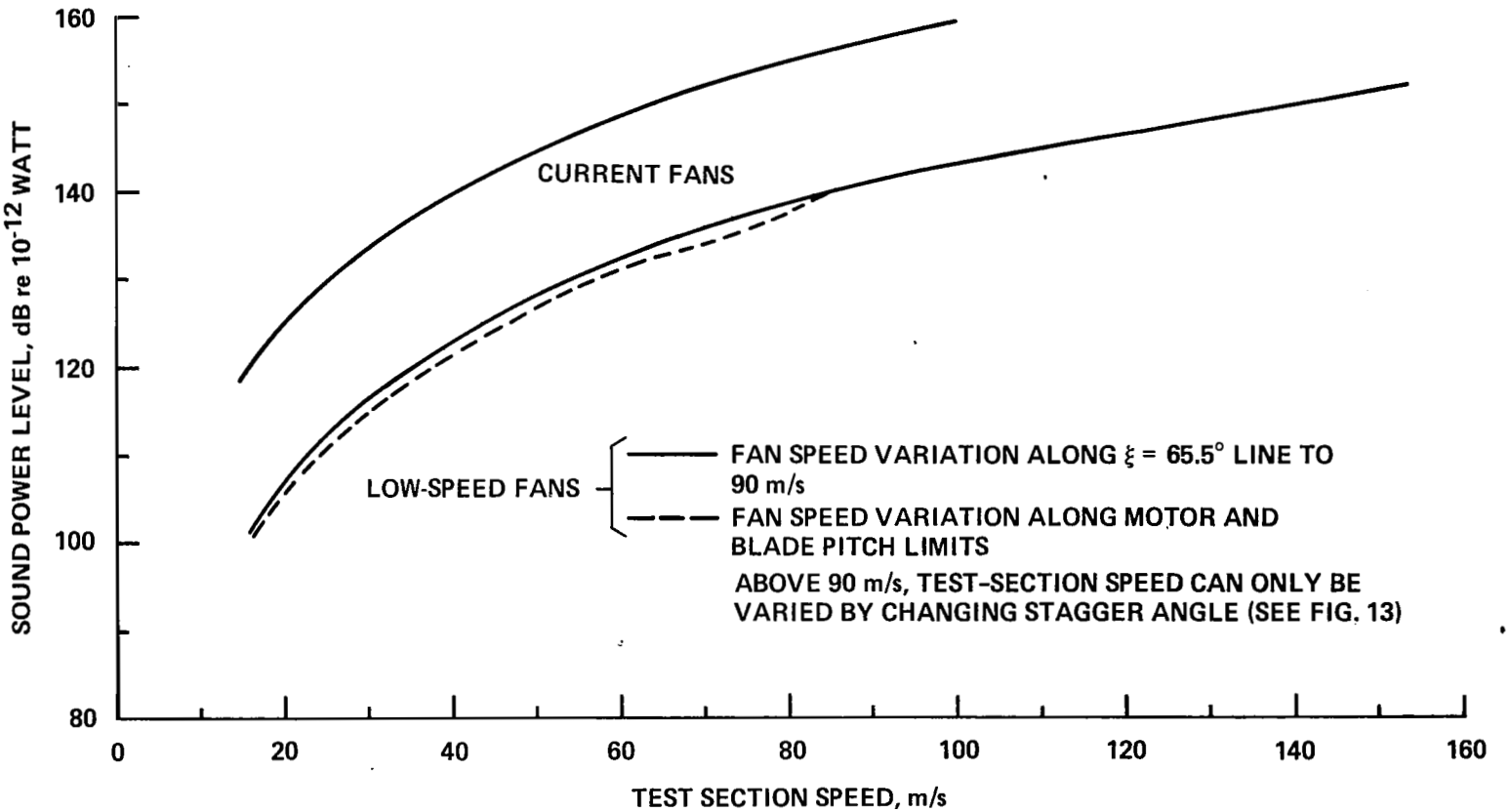

(a) Overall sound power level.

Figure 14.- Comparison of the noise of six full-scale low-speed fans with the noise of the current six 40- by 80-foot wind-tunnel fans as a function of test-section speed.

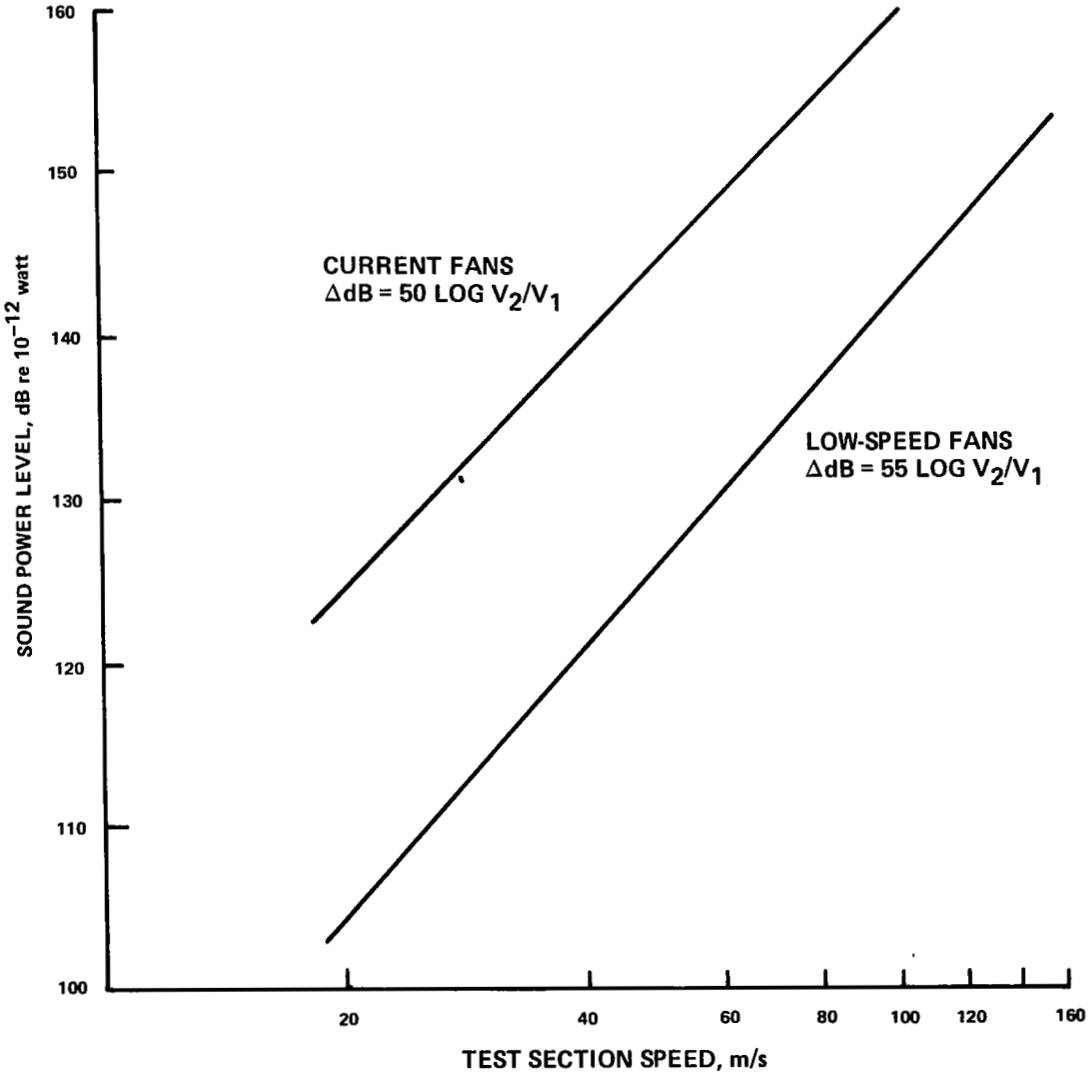

(b) Approximation of fan noise using $W \alpha V^5$ (present fans) and $W \alpha V^{5.5}$ (low-speed fans), V = test-section speed.

Figure 14.- Continued.

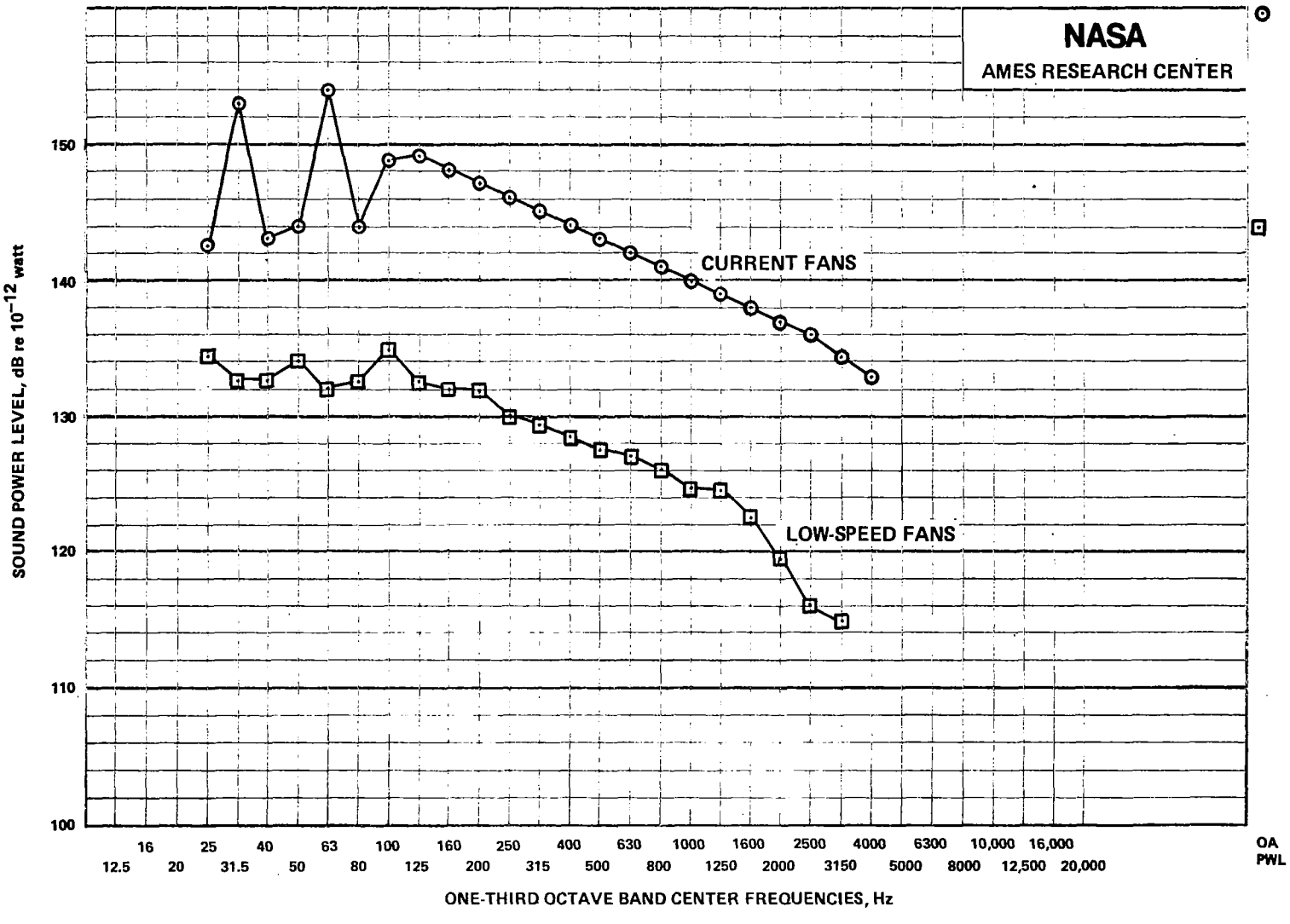

(c) Third-octave spectra at test-section speed V_{TS} = 100 m/s.

Figure 14.- Concluded.

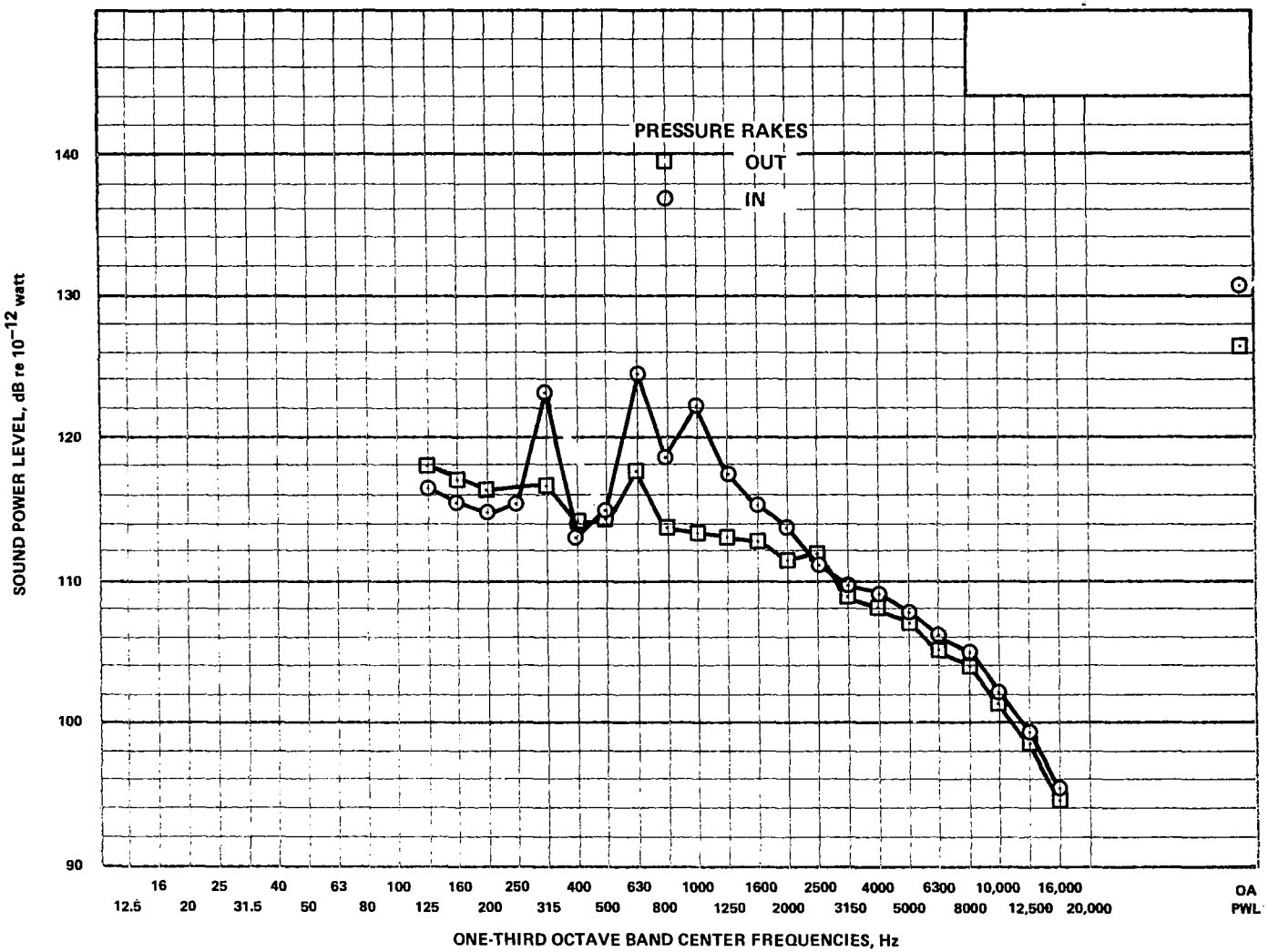

(a) Third-octave band spectra.

Figure 15.- Effect of pressure survey rake installation (fig. 8) on low-speed fan sound power, ξ = 40.8°.

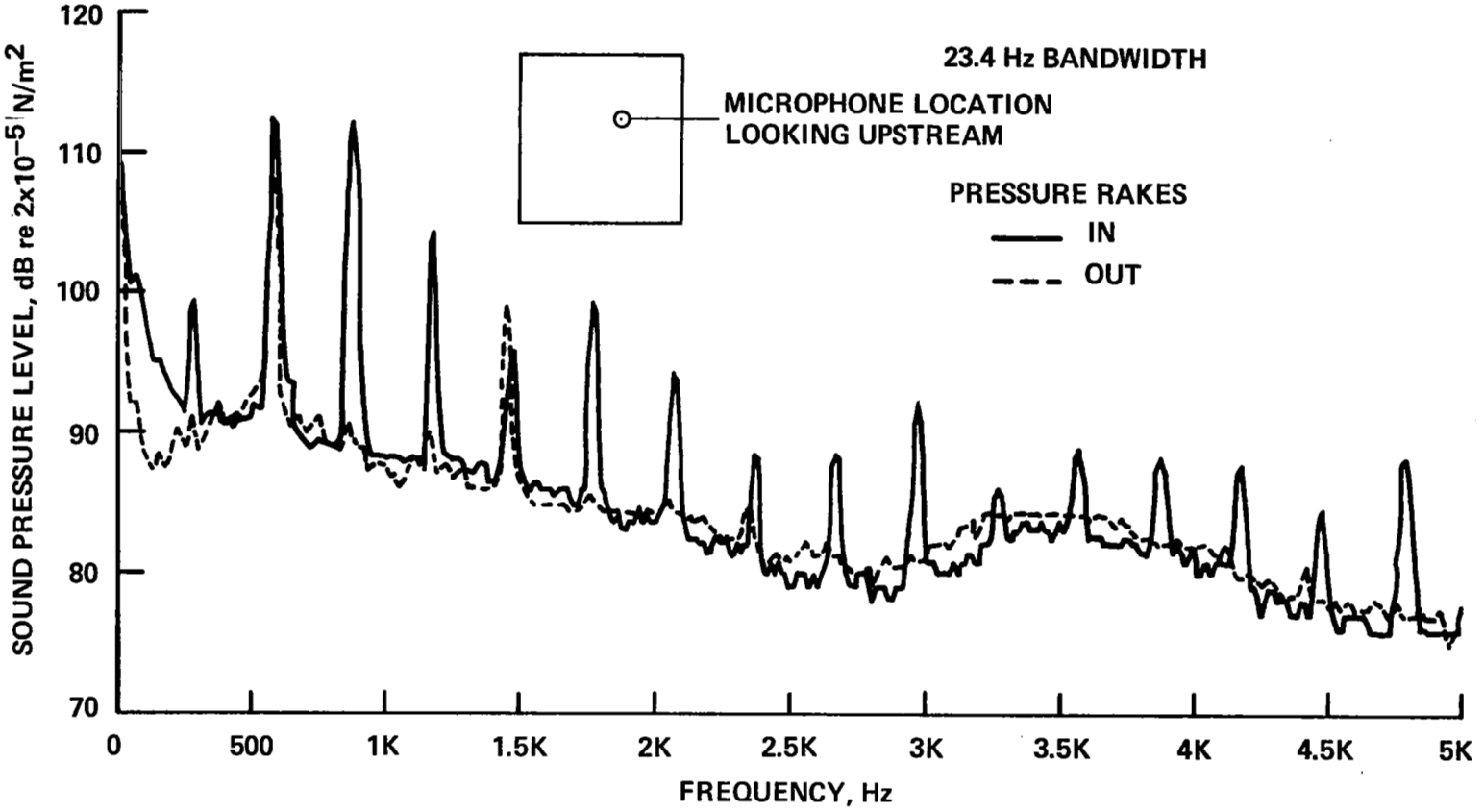

(b) Narrow-band spectra of sound pressure in inlet.

Figure 15.- Continued.

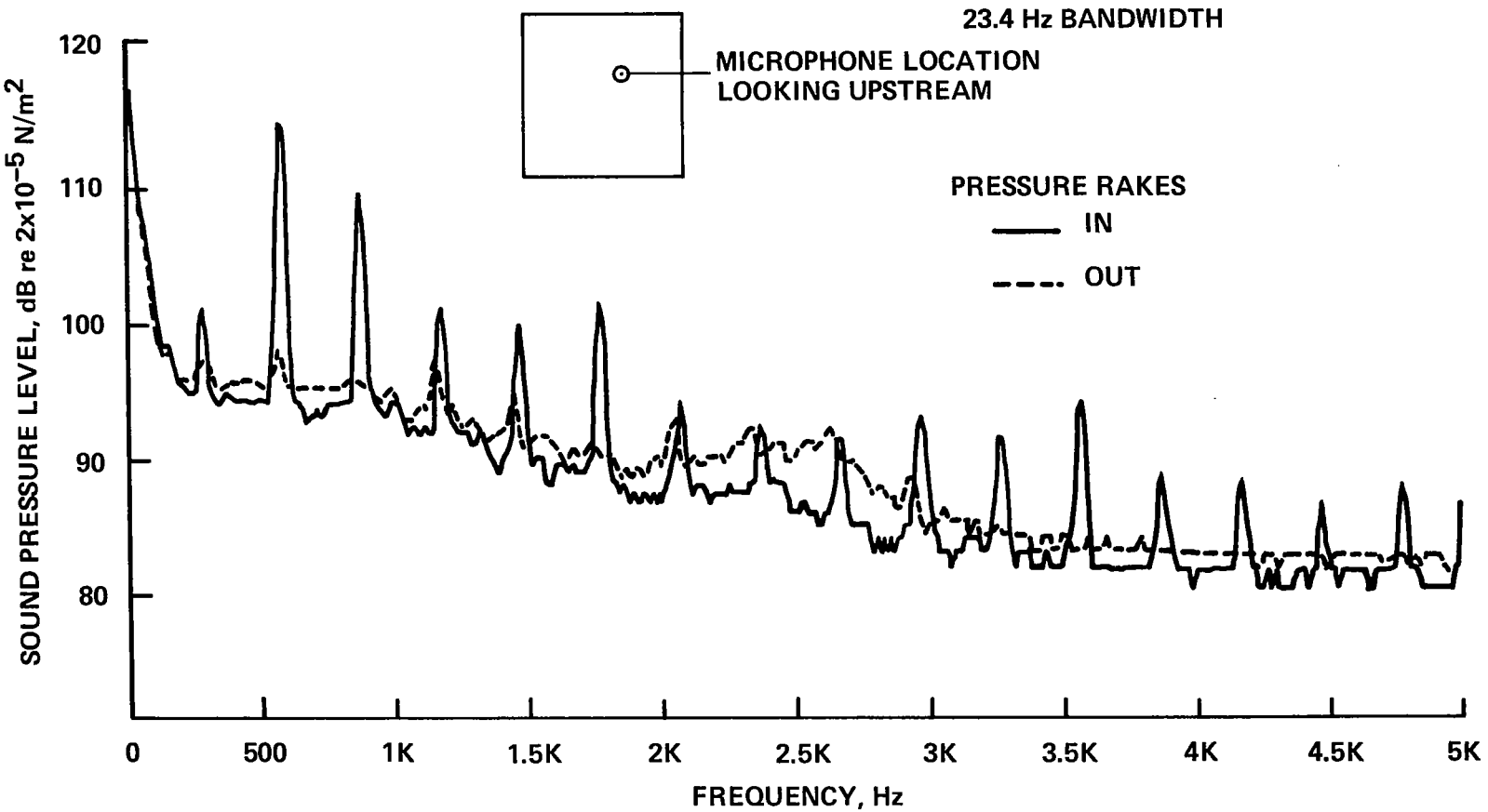

(c) Narrow-band spectra of sound pressure in exhaust.

Figure 15.- Concluded.

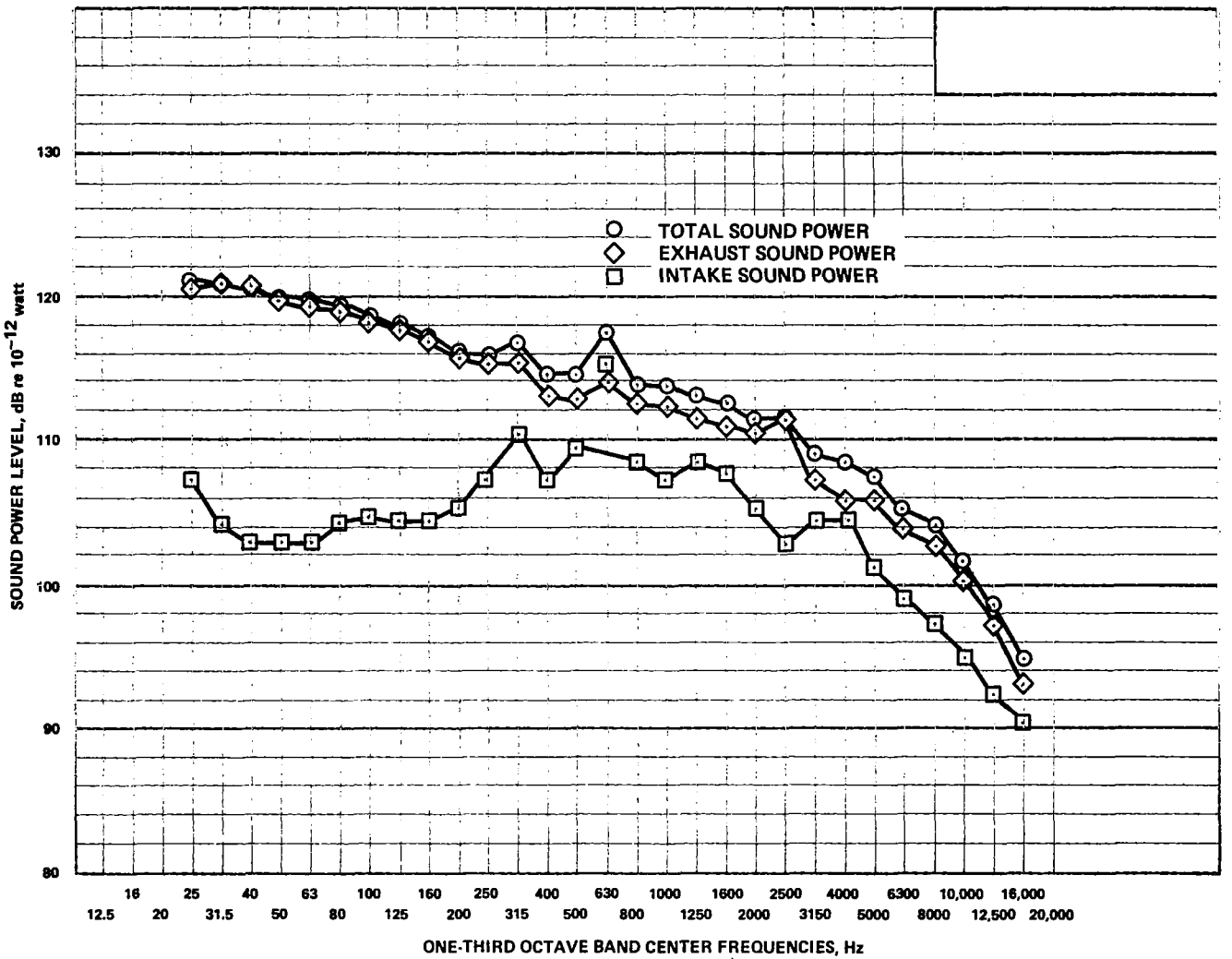

Figure 16.- Upstream and downstream sound power of the low-speed fan, ξ = 40.8°.

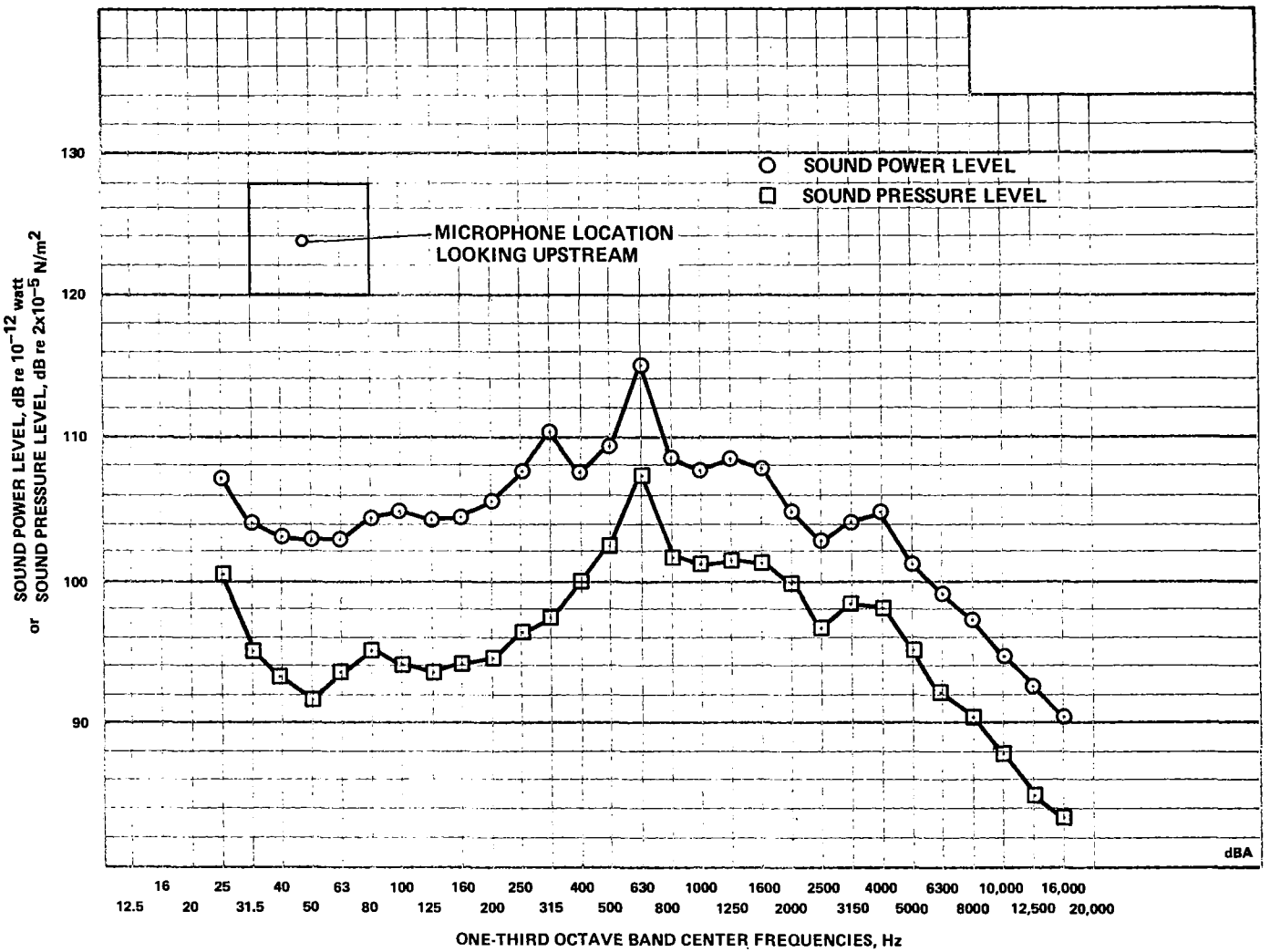

(a) Intake.

Figure 17.- A comparison of low-speed fan sound power levels with typical sound pressure levels, $\xi = 40.8°$.

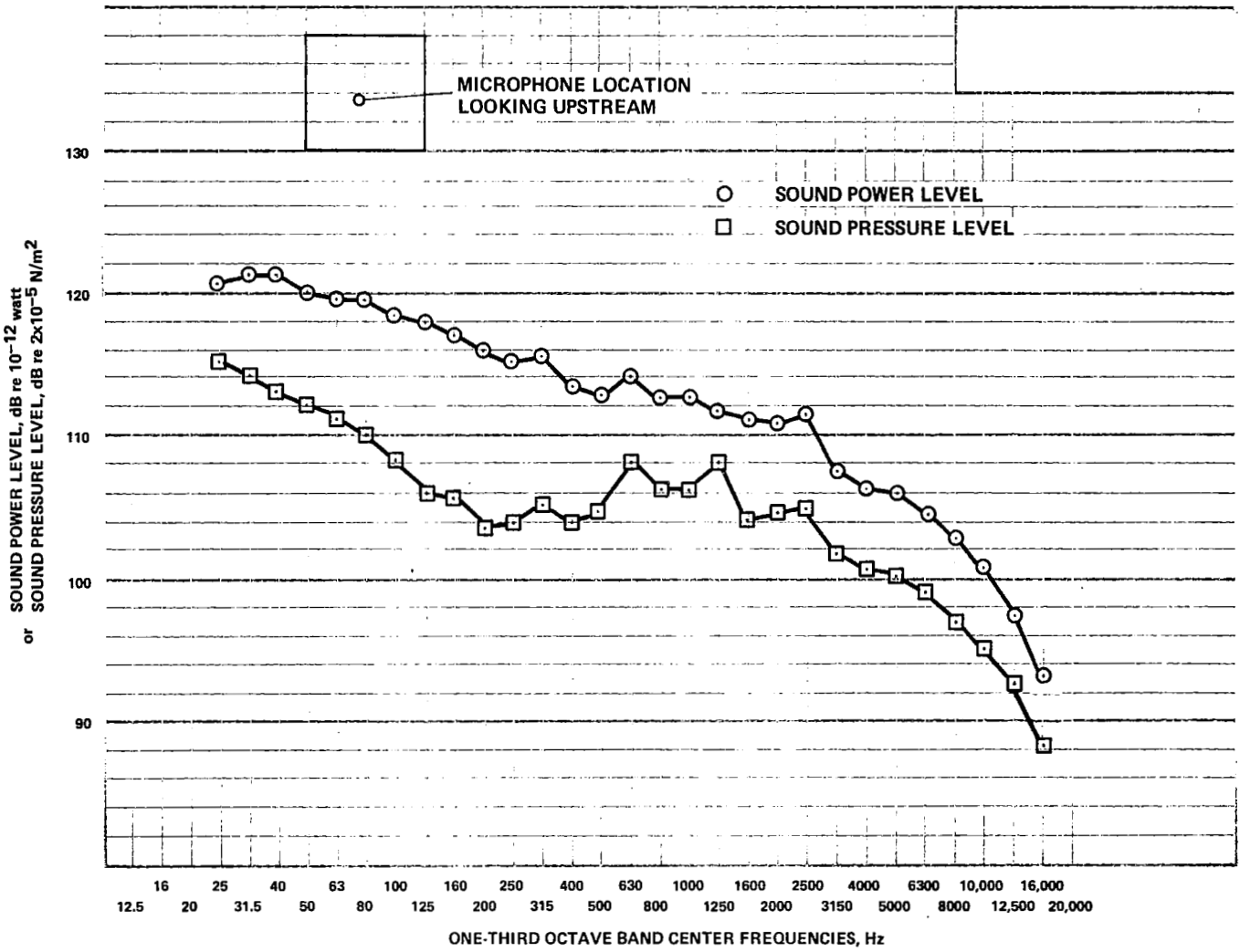

(b) Exhaust.

Figure 17.- Concluded.

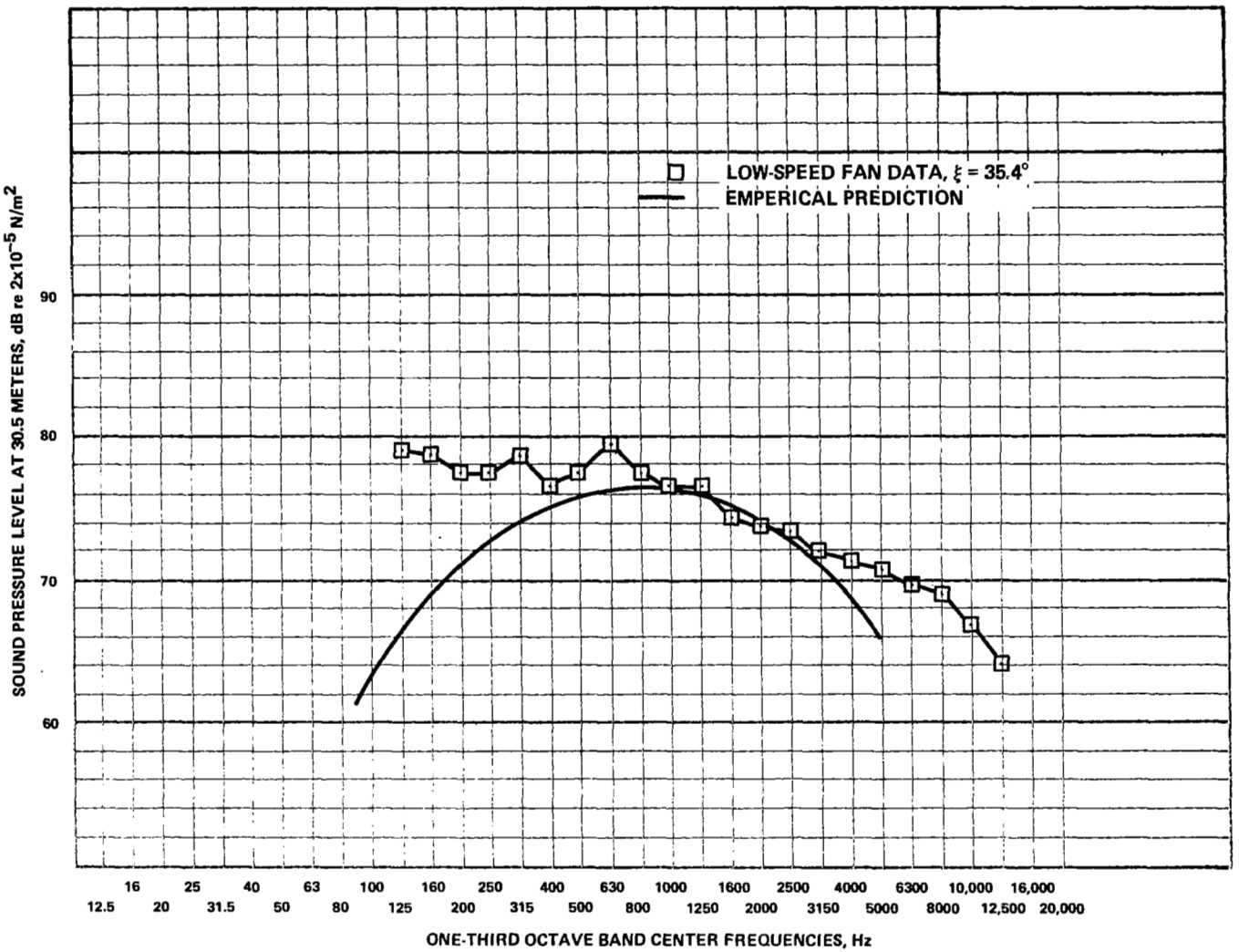

Figure 18.- Estimated low-speed fan sound pressure levels at 30.5 m compared with predicted minimum broadband rotor noise based on method of reference 9.

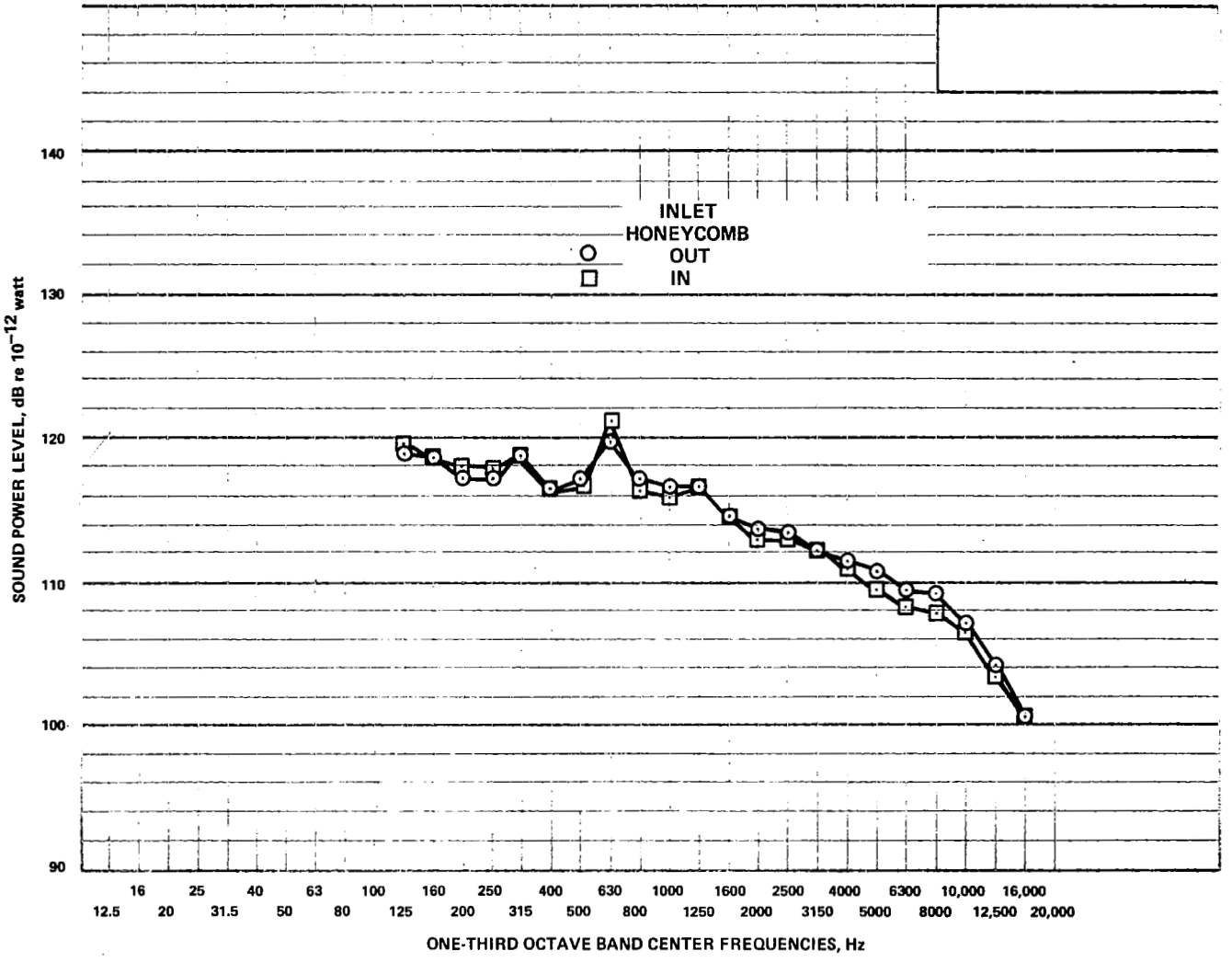

(a) Third-octave spectra of sound power.

Figure 19.- Low-speed fan noise with and without honeycomb in duct inlet, $\xi = 35.4°$.

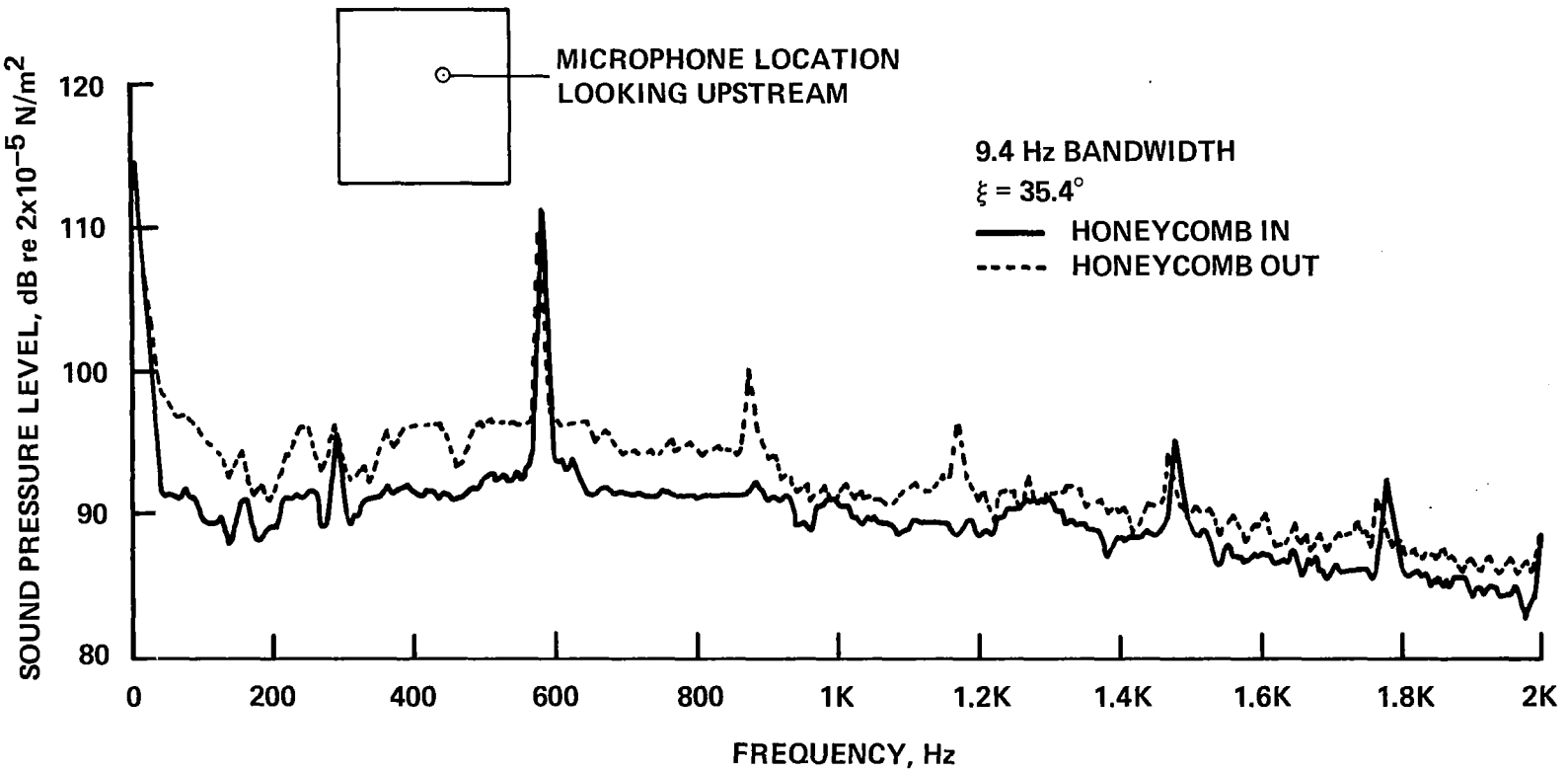

(b) Narrow-band spectra of sound pressures in inlet.

Figure 19.- Continued.

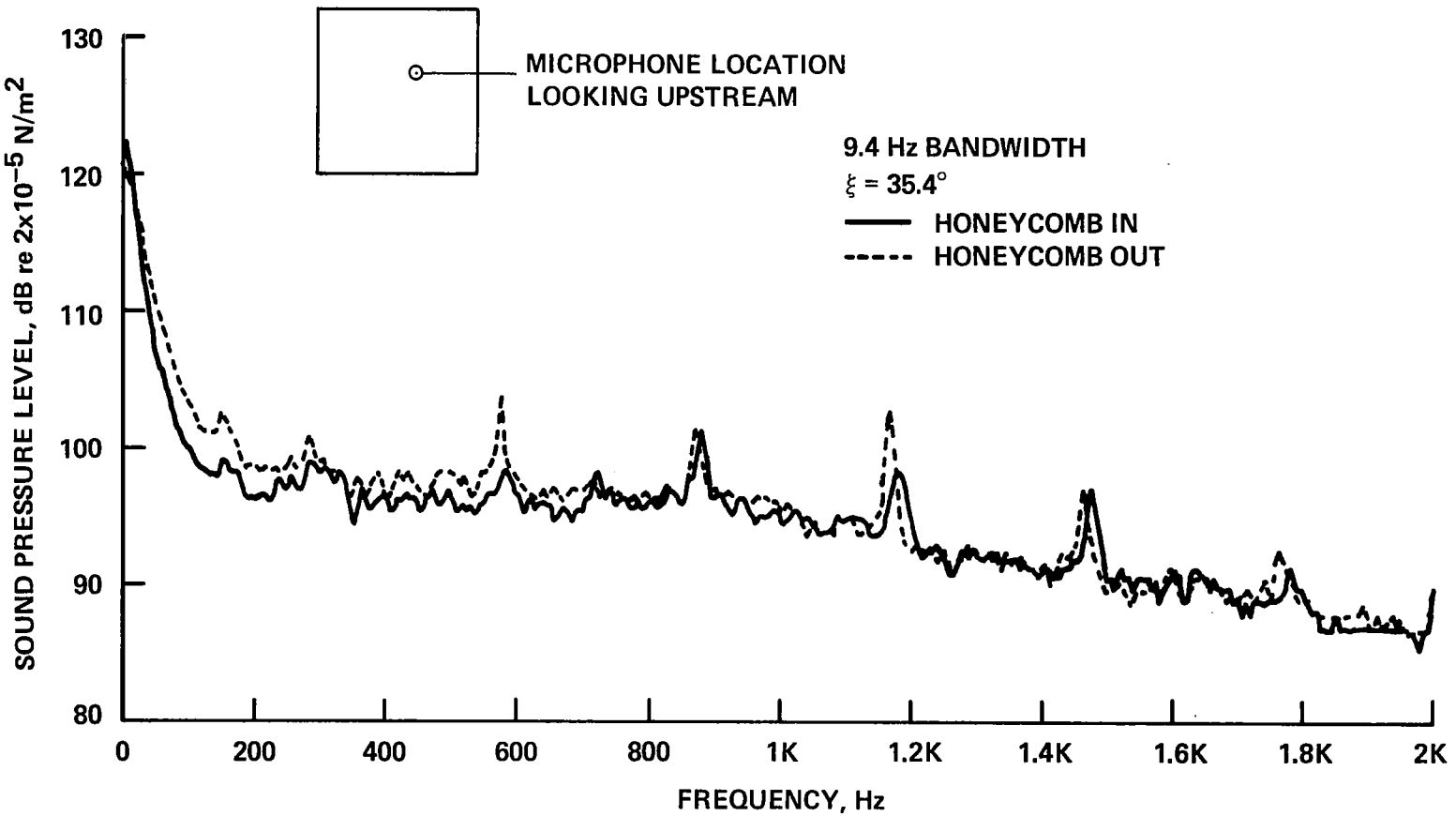

(c) Narrow-band spectra of sound pressures in exhaust.

Figure 19.- Concluded.

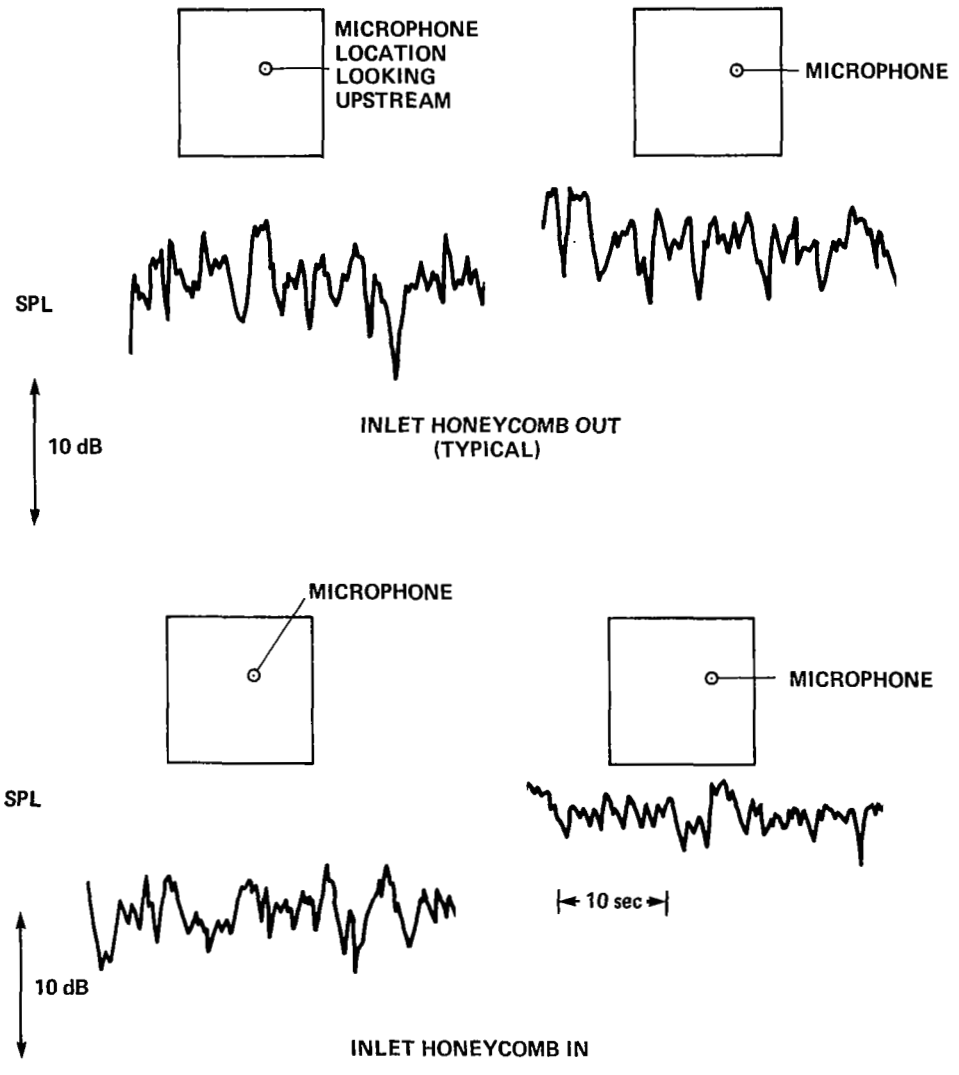

(a) Fundamental frequency f = 295 Hz, inlet microphone 3.

Figure 20.- Time histories of filtered low-speed fan blade-passage noise, honeycomb in and out of inlet, N = 1180 rpm, frequency bandwidth = 10 Hz.

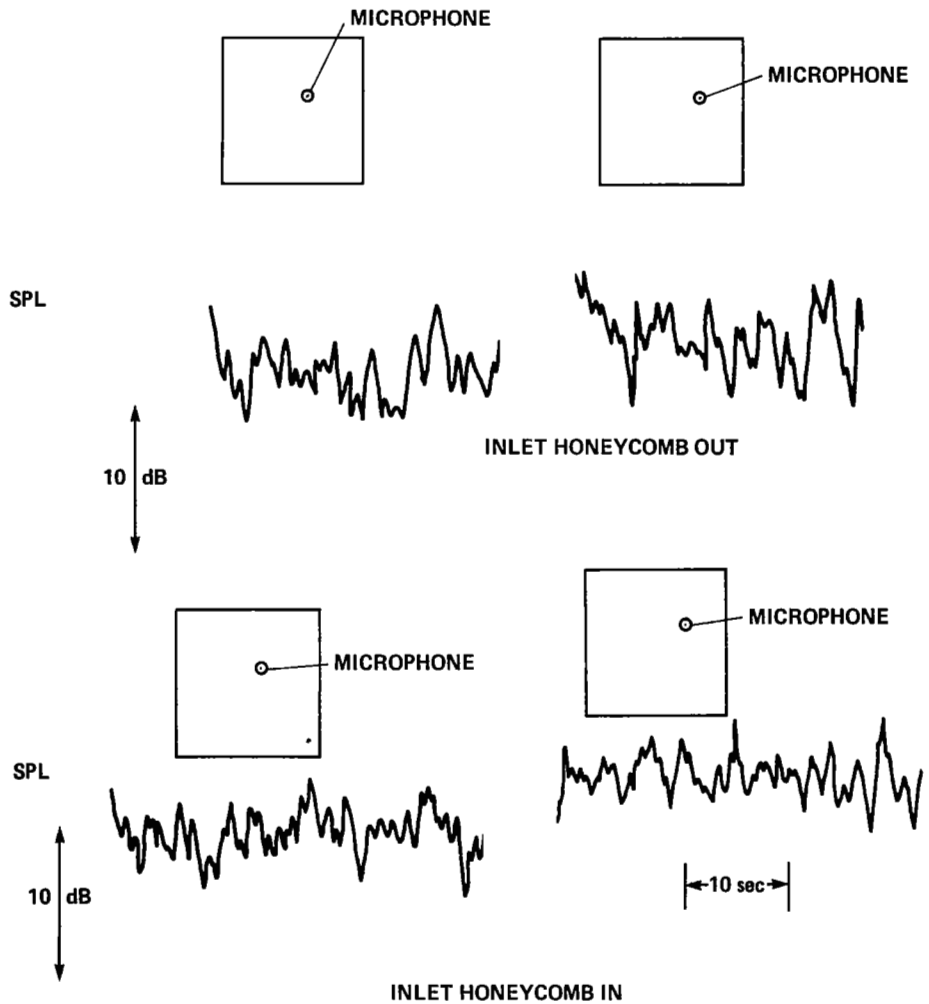

(b) Exhaust microphone 7, f = 295 Hz.

Figure 20.- Continued.

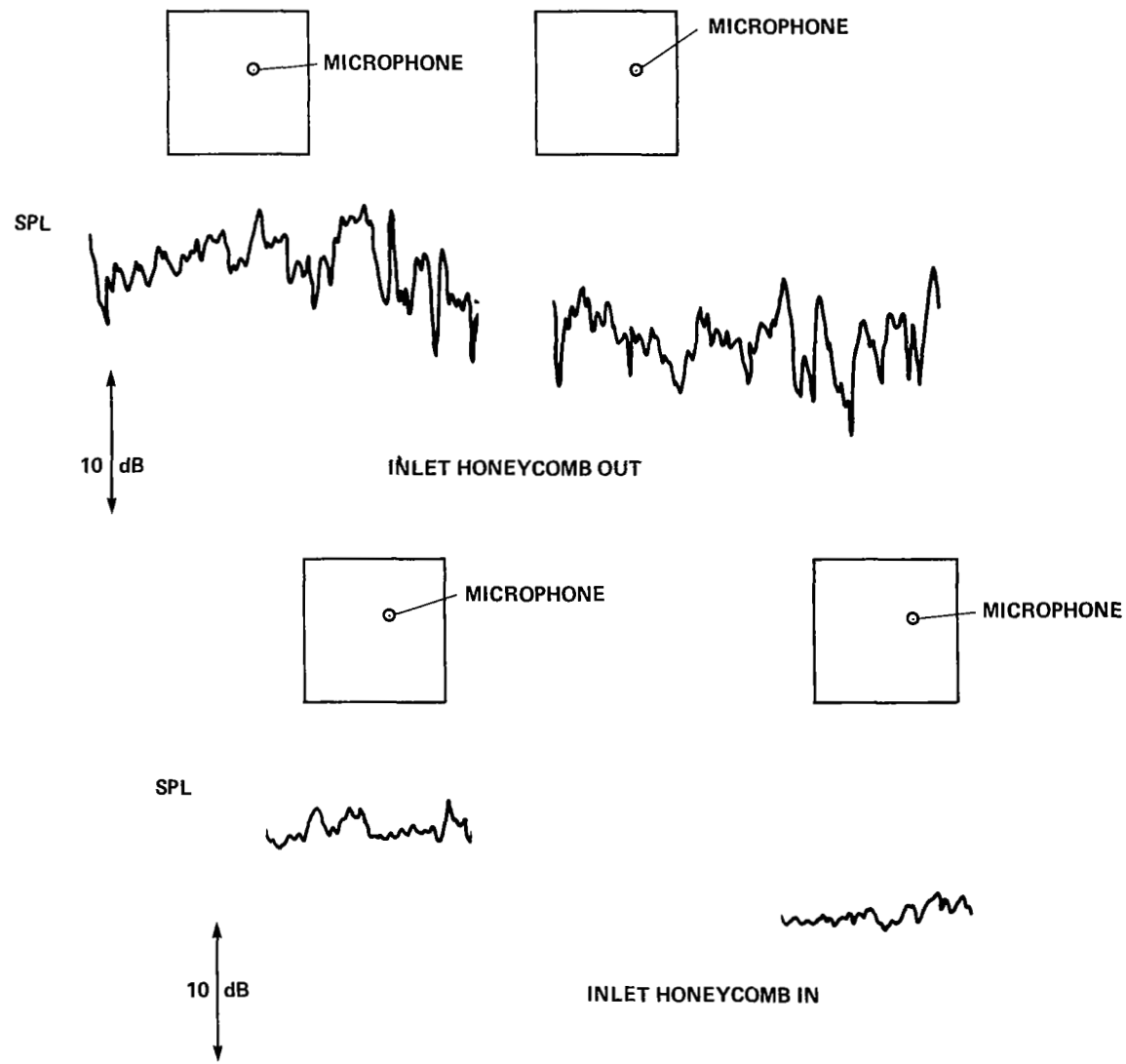

(c) Inlet microphone 3, f = 590 Hz, 2nd harmonic.

Figure 20.- Continued.

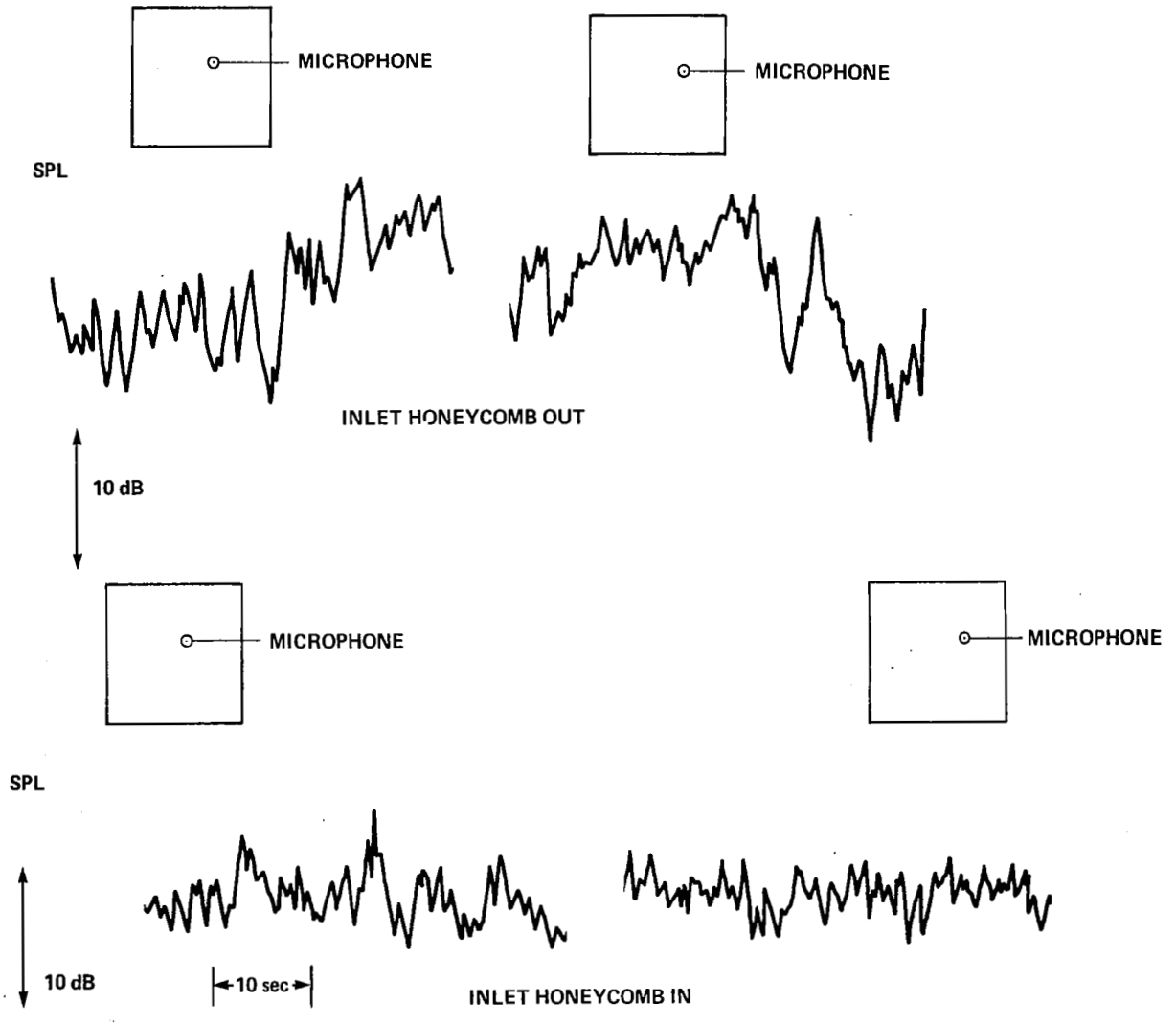

(d) Exhaust microphone 7, f = 590 Hz.

Figure 20.- Continued.

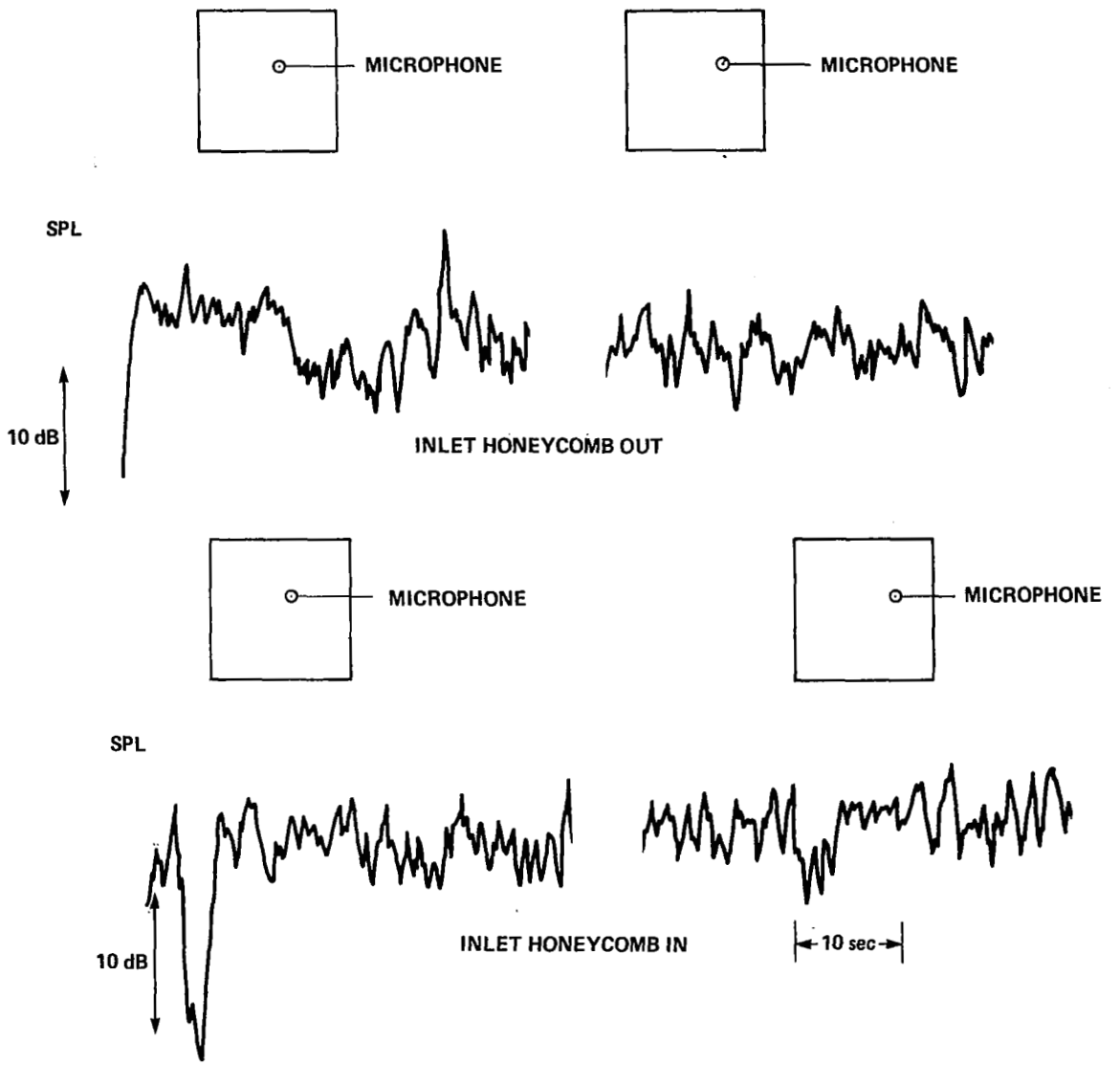

(e) Inlet microphone 3, f = 885 Hz, 3rd harmonic.

Figure 20.- Continued.

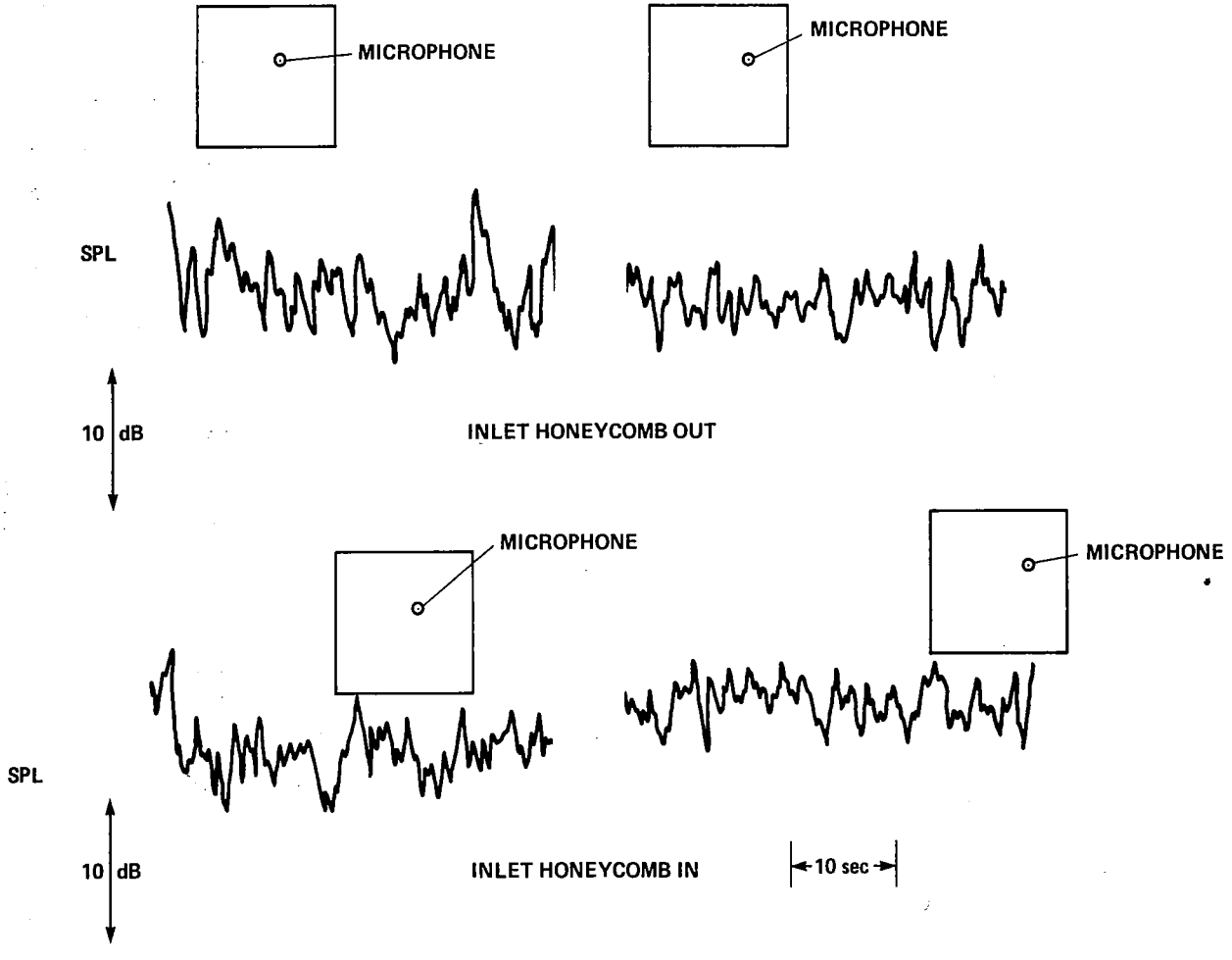

(f) Exhaust microphone 7, f = 885 Hz.

Figure 20.- Concluded.

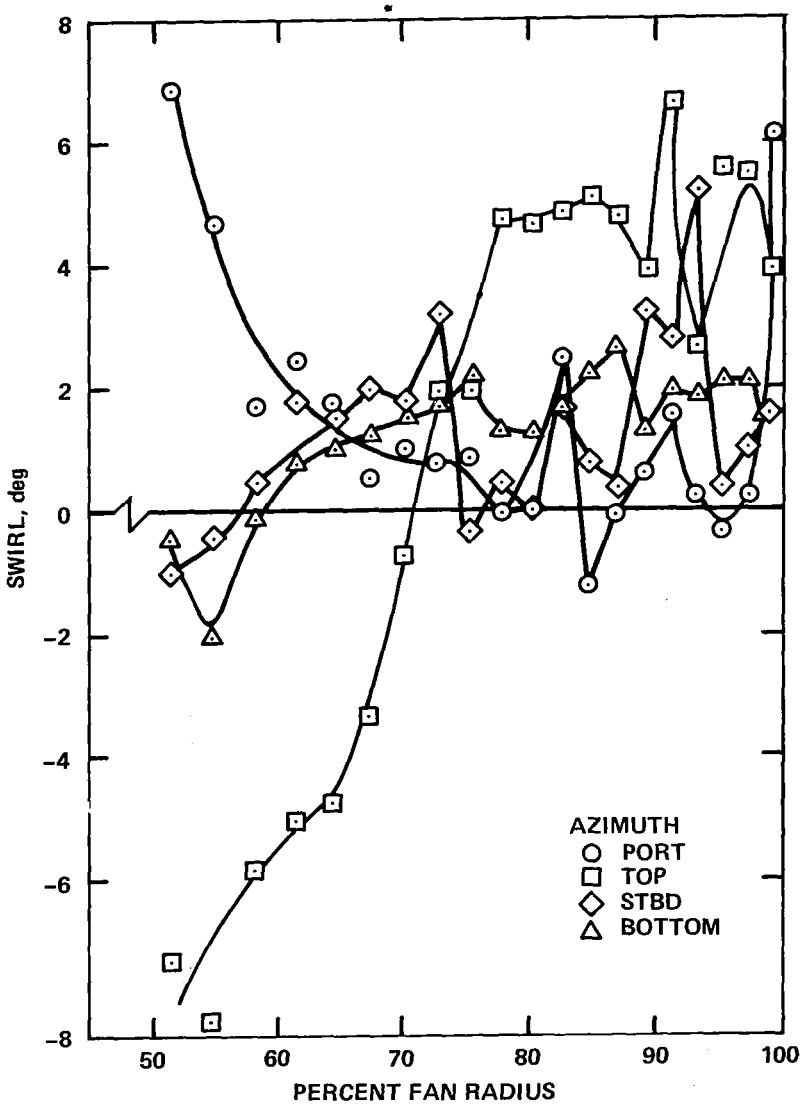

(a) Inlet honeycomb out.

Figure 21.- Steady-state flow swirl 230 mm ahead of low-speed rotor, $\xi = 35.4°$, looking upstream.

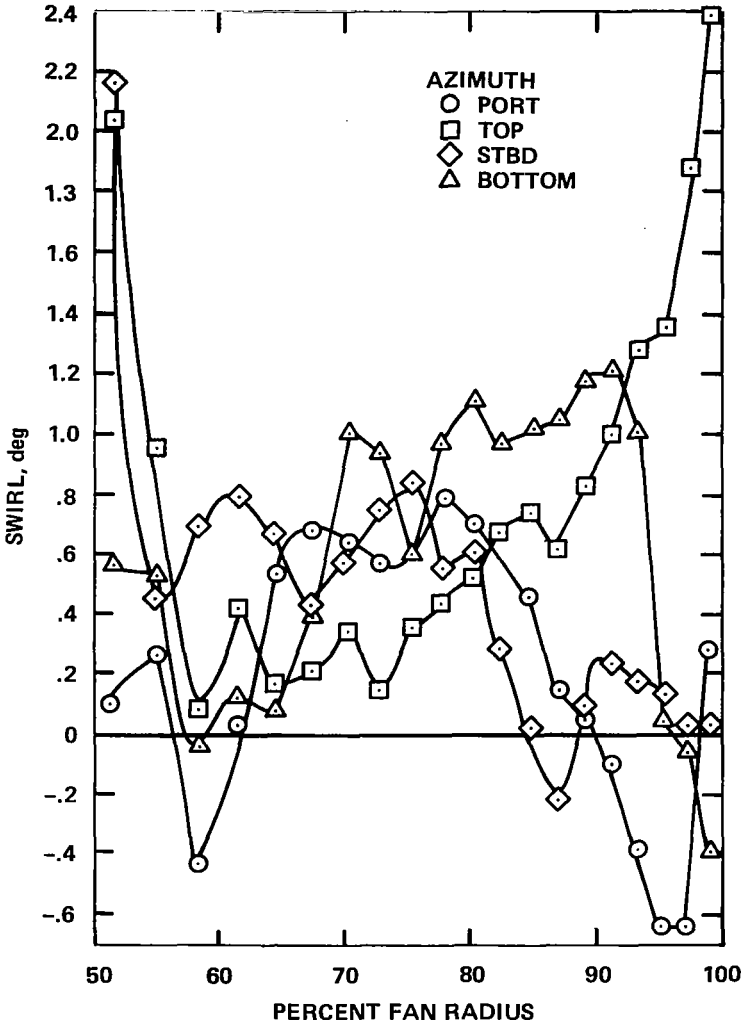

(b) Inlet honeycomb in.

Figure 21.- Concluded.

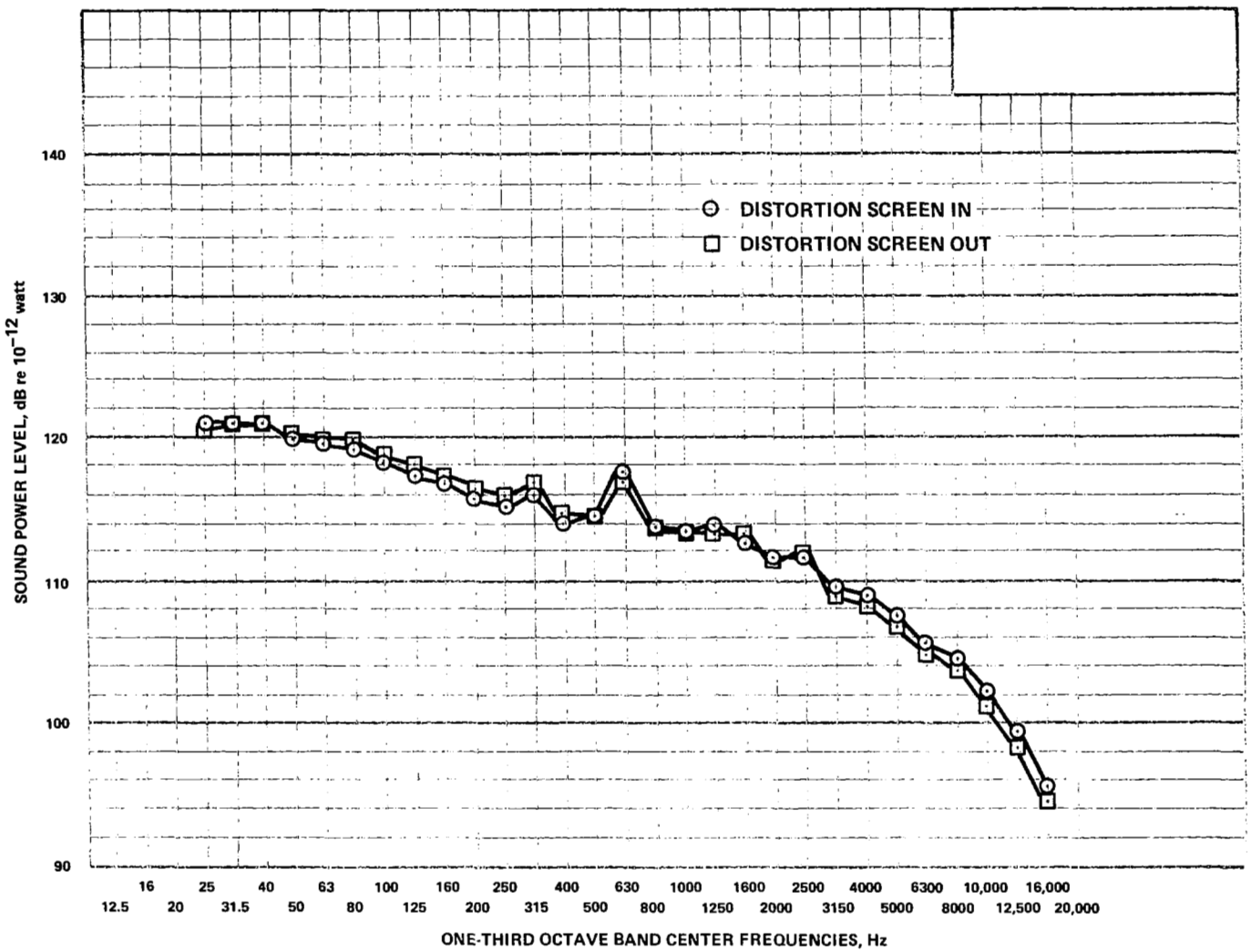

Figure 22.- Effect of distortion screen (fig. 6) on low-speed fan sound power, ξ = 40.8°.

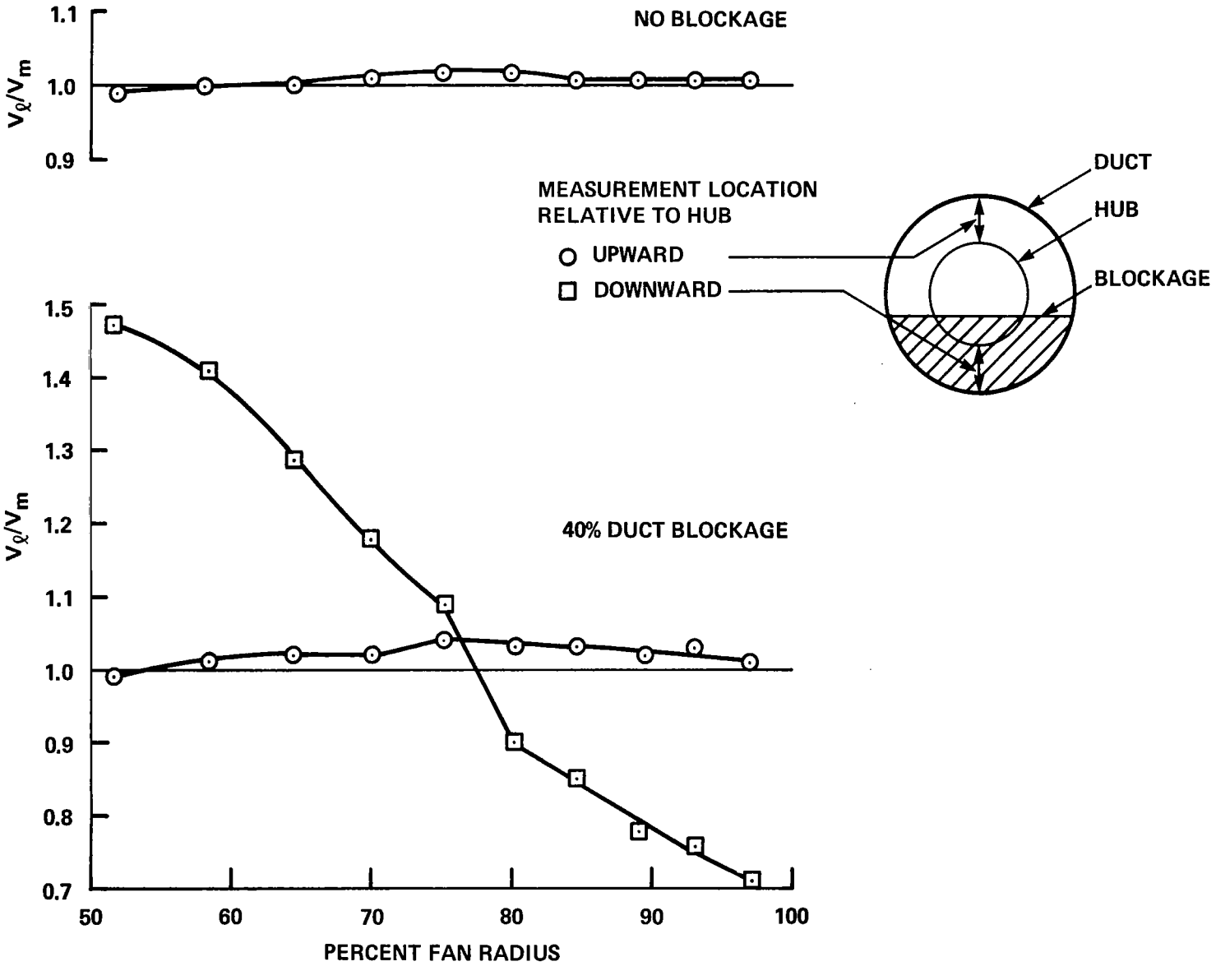

Figure 23.- Inflow velocity distortion due to wooden barrier (fig. 6).

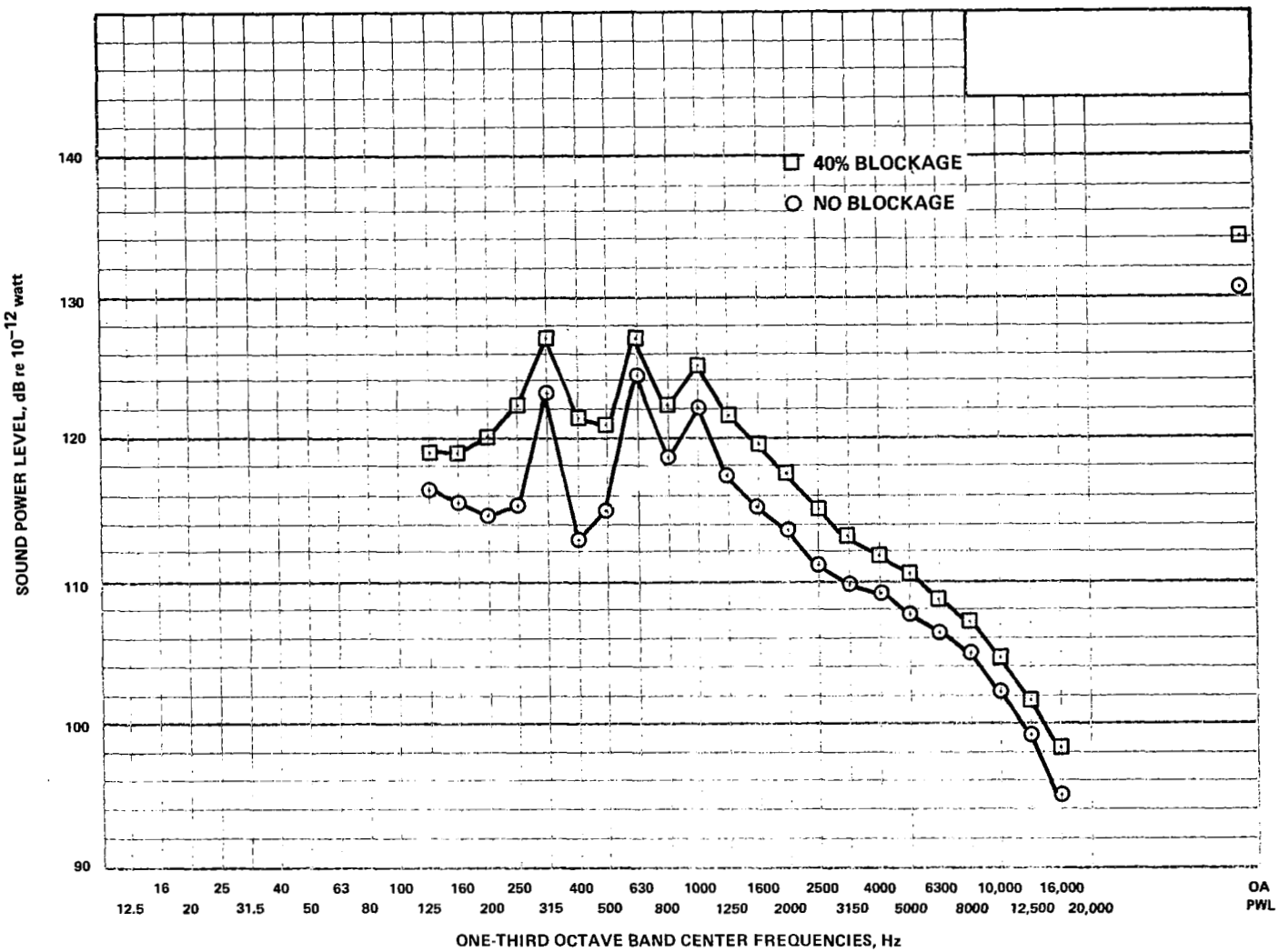

Figure 24.- Effect of flow distortion of figure 23 on low-speed fan sound power, ξ = 40.8°; pressure survey rakes in flow.

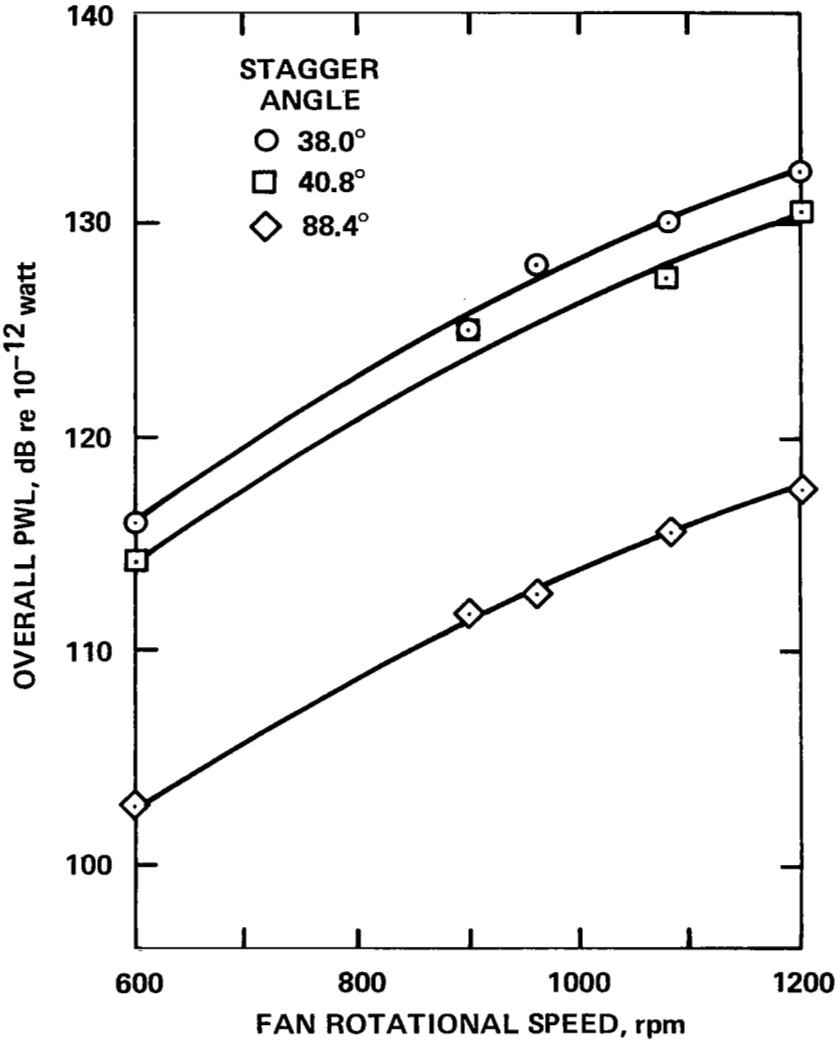

(a) Overall sound power level.

Figure 25.- Variation of low-speed fan noise with rotational speed, pressure survey rakes installed.

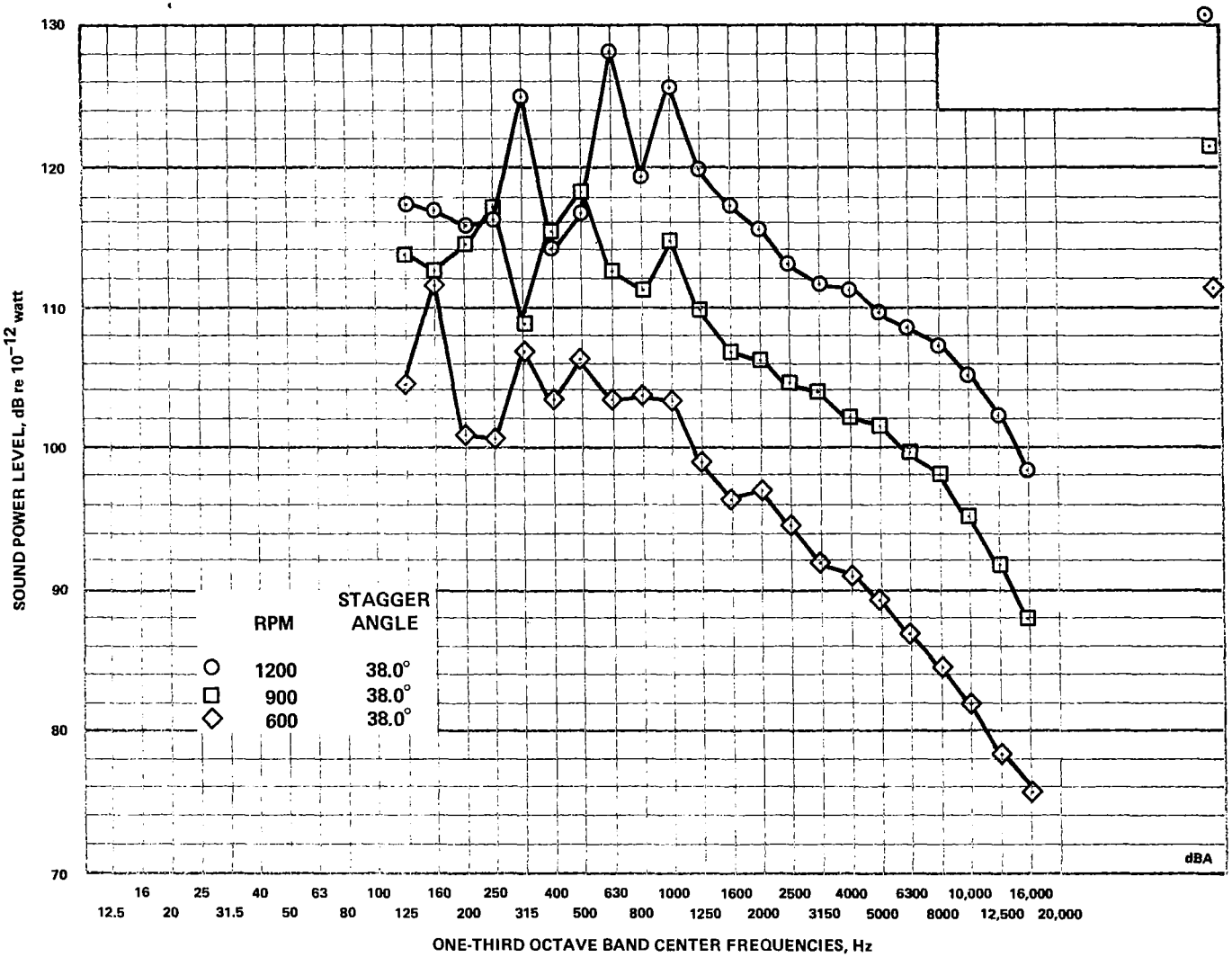

(b) Third-octave spectra of sound power.

Figure 25.- Concluded.

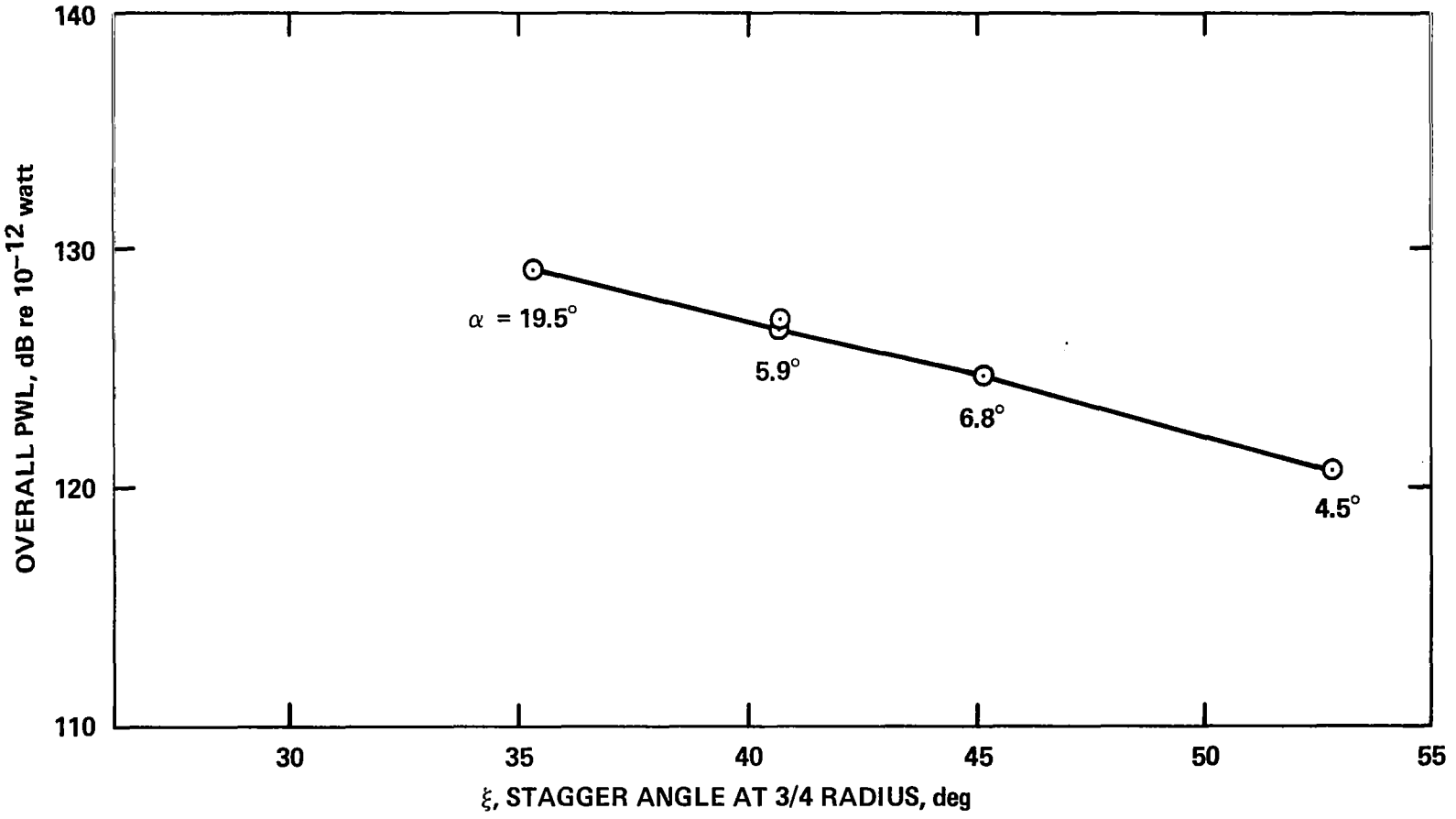

(a) Plotted versus stagger angle; angle-of-attack, α, noted.

Figure 26.- Variation of low-speed fan noise with blade angle, 1200 rpm, variable mass flow rate.

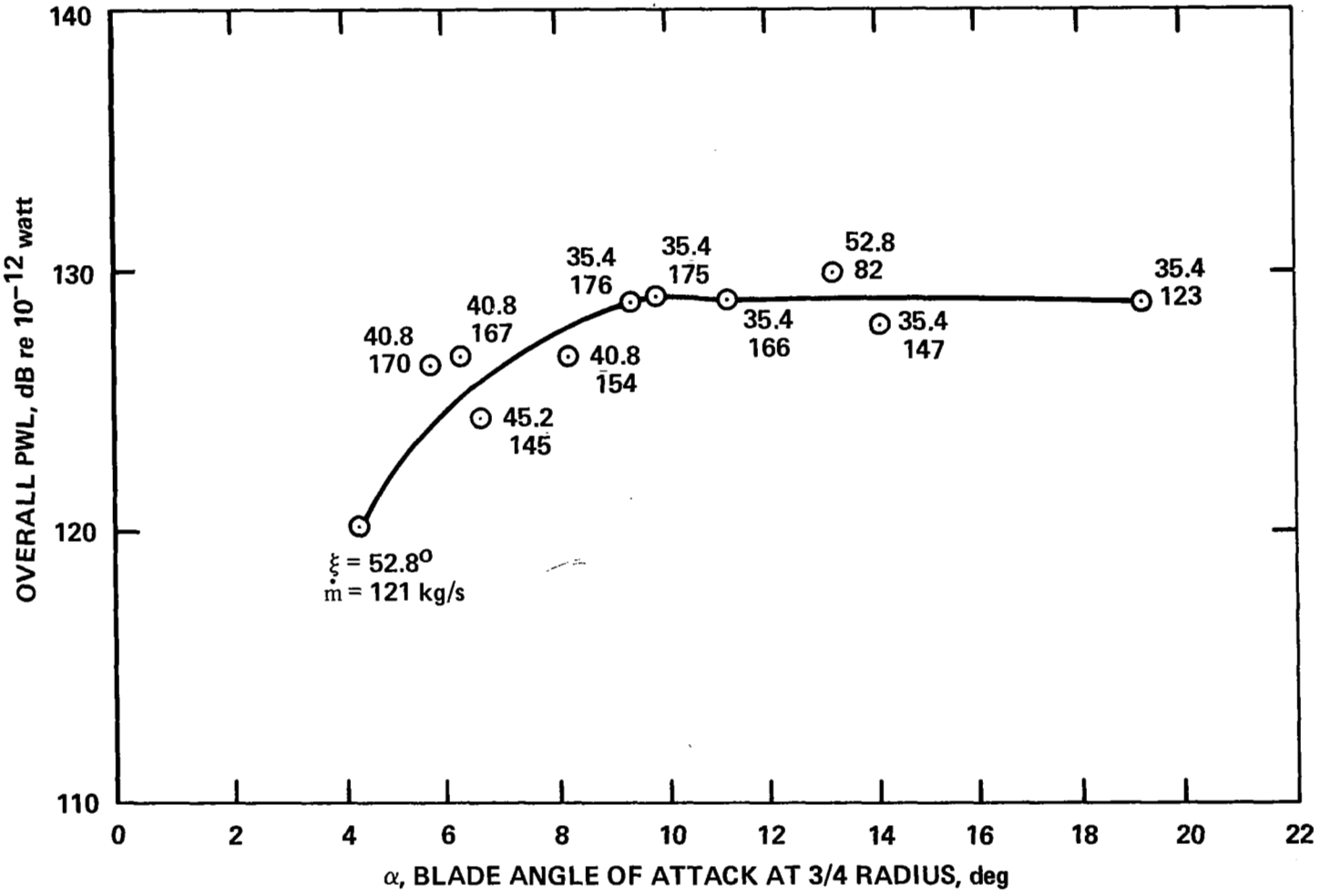

(b) Plotted versus angle of attack.

Figure 26.- Concluded.

1. Report No.	2. Government Accession No.	3. Recipient's Catalog No.
NASA TP-1008		

4. Title and Subtitle	5. Report Date
ACOUSTIC PERFORMANCE OF TWO 1.83-METER-DIAMETER FANS DESIGNED FOR A WIND-TUNNEL DRIVE SYSTEM	August 1977
	6. Performing Organization Code
7. Author(s) Paul T. Soderman and V. Robert Page	8. Performing Organization Report No. A-6888
	10. Work Unit No. 505-06-34-02
9. Performing Organization Name and Address Ames Research Center, NASA and Ames Directorate, USAAMRDL Ames Research Center, Moffett Field, Calif. 94035	11. Contract or Grant No.
	13. Type of Report and Period Covered Technical Paper
12. Sponsoring Agency Name and Address National Aeronautics and Space Administration Washington, D.C. 20546 and U.S. Army Air Mobility R&D Laboratory, Moffett Field, Ca. 94035	14. Sponsoring Agency Code
15. Supplementary Notes	

16. Abstract

A parametric study was made of the noise generated by two 1.83-m (6-ft) diameter fans operating up to a maximum pressure ratio of 1.03. One fan had 15 rotor blades, 23 stator blades, and a maximum rotational speed of 1200 rpm. The other fan had 9 rotor blades, 13 stator blades, and a maximum speed of 2000 rpm. The fans were approximately 1/7-scale models of the 12.2-m (40-ft) diameter fans proposed for repowering the NASA-Ames 40- by 80-Foot Wind Tunnel. The fans were operated individually in a 23.8-m (78-ft) long duct. Sound pressure levels in the duct were used to determine radiated acoustic power as fan speed, blade angle, and mass flow were varied. Results showed that the low-speed fan was slightly quieter than the high-speed fan and, when scaled to full scale, would be 16 dB quieter than the present wind-tunnel fans. The fan noise varied directly with thrust regardless of whether thrust was varied by rotational speed or blade setting for the ranges studied.

17. Key Words (Suggested by Author(s))	18. Distribution Statement
Fan noise Rotor noise Aerodynamic noise Duct acoustics	Unlimited STAR Category - 71

19. Security Classif. (of this report)	20. Security Classif. (of this page)	21. No. of Pages	22. Price*
Unclassified	Unclassified	75	$4.25

*For sale by the National Technical Information Service, Springfield, Virginia 22161

NASA-Langley, 1977 A-6888